4

Multilayer woven fabrics

Abstract: Three-dimensional multilayer woven (MLW) fabrics are textile structures having fibres oriented along the three directions of a unit cell. These fabrics are becoming increasingly important owing to their excellent performance characteristics such as permeability, compressibility, drapeability, ease of handling and ability to conform to complex shapes. The fabrics can be woven with a space between layers (core fabrics) or woven as thick, dense structures. The development of multilayer woven fabrics has shown that these structures need not be interlaced throughout the fabric to have all the advantages of traditional weaving. An attempt is made in this chapter to describe the various structures, manufacturing principles and advantages of multilayer woven fabrics.

Key words: multilayer woven (MLW) fabrics, 3-D woven fabrics, 3-D weaving, structure of MLW fabrics, tensile behaviour of MLW fabrics, shear behaviour of MLW fabrics.

4.1 Introduction to multilayer woven fabrics

Traditional woven fabrics are produced by interlacing two sets of yarn, warp and weft. Plain, twill and satin are the most commonly used structures for composites, which can be produced on either tappet or dobby looms. A number of weft-insertion technologies, including shuttle, rapier, projectile and air-jet, can be used for producing woven preforms. Rapier looms are the most popular type as they can handle a variety of yarns, from very delicate to thick yarns, even metal wires.

Woven fabrics have a number of advantages over unidirectional material. Because of the interlacement, woven composites have better structural integrity and can be handled in the dry form, whereas unidirectional materials cannot be handled before impregnation. Unlike unidirectional prepregs, woven preforms have no shelf-life problems. Woven preforms are highly suitable for RTM processes and also highly formable and hence suitable for drape onto complex shapes.

Although woven fabrics are superior to unidirectional prepregs, there are a number of limitations, including the time involved in preparing the number of layers needed to build up the desired thickness, and possible delamination of the composite due to lack of through-thickness reinforcement. To improve the through-thickness strength, multilayer woven fabrics have

been developed, both on conventional looms and on specialized machines (Potluri *et al.*, 2000).

Three-dimensional multilayer woven fabrics are becoming increasingly important owing to their excellent performance characteristics such as permeability, compressibility, drapeability, ease of handling and ability to conform to complex shapes. They are becoming one of the important forms of reinforcements for composite materials because of their good resistance to delamination over the laminated reinforcements (Chen *et al.*, 1992).

Three-dimensional multilayer woven fabrics are textile structures having fibres oriented along the three directions of a unit cell. A three-dimensional fabric should have three or more yarns in the thickness direction in order to distinguish itself from a planar fibre assembly. These fabrics are composed of several series of warp and filling yarns that form distinct layers, one above the other (Watson, 1955). The fabrics can be woven with a space between layers (core fabrics) or woven as thick, dense structures. In addition to the 3-D features of the macrogeometry, the internal structure of the 3-D multilayer woven fabric is characterized by continuous fibres oriented and integrated in three or more directions. In other words, these fabrics will have more than three yarns in the through-thickness direction and are manufactured with an inherent through-thickness yarn component (Ko, 1989).

The development of multilayer woven fabrics has shown that these structures need not be interlaced throughout the fabric to have all the advantages of traditional weaving. It turns out that the addition of vertical yarns interlaced with the top and bottom horizontal yarns provides the same kind of reinforcement in a 3-D structure that is provided by the over-and-under interlacing of yarns in flat weaving (Mohamed, 1990).

4.2 Advantages of multilayer woven fabrics

Multilayer woven fabrics offer a number of advantages over 2-D structures. Some of the important advantages can be summarized below:

- 3-D woven fabrics exhibit higher through-thickness and interlaminar properties because of their integrated structure in the presence of orthogonal and/or angle interlock constructions.
- These fabrics have complicated geometry and can be made to near-net-shape structures.
- 3-D multilayer woven fabrics can serve as non-crimp reinforcement preforms with the highest fibre volume leading to stronger and lighter structures.
- The ability of 3-D weaving to produce near-net-shape preforms can greatly reduce the cost of a component by reducing material wastage, the need for machining and joining, and the amount of material handled during lay-up.

- 3-D multilayer woven fabrics demonstrate high ballistic impact damage resistance and low-velocity impact damage, which have been a major problem with 2-D laminates in military aircraft structures. These fabrics have *z*-fibres through the part thickness and this feature dramatically improves impact damage tolerance by suppressing delamination.
- High-performance fibres such as carbon, ceramic, aramid, quartz and metal fibres can be woven into multilayer fabrics which can be made up to thicknesses up to one inch (2.54 cm) and widths up to 72 inches (183 cm) conforming to customer-specific complex shapes.
- Multilayer woven fabrics can be given additional strength by insertion in each layer of stuffing yarns, which remain straight and contribute their full strength to that direction. Yarns that interlace between layers as binding yarns contribute partially to the strength of their direction in orthogonal woven fabrics and contribute immensely to the strength in the thickness direction.
- Multilayer woven fabrics are highly conformable to complex mould shapes, providing uniform part thickness and eliminating complicated darting and pin-wheeling. This is because of the absence of interlacing between warp and filling yarns which allows the fabric to bend and internally shear rather easily, without buckling within the in-plane reinforcement.
- 3-D woven fabrics wet out faster in both open and closed moulding, improving quality, reducing moulding times and facilitating migration to vacuum infusion. The structural regularity and internal openness of the fibre architecture, which is strictly defined by the *z*-yarn placement, can explain this effect. Moreover, the *z*-yarns act as capillary channels to transfer resin into the preform interior from the outer surface. The increased permeability translates directly into reduced cycle time, due to faster and easier wet-out.
- Although these structures are typically more expensive than 2-D fabrics and mats, reduction of labour, higher performance and improved process efficiency result in overall cost savings in a variety of applications. When compared on a cost per square metre of finished composite structure, 3-D woven fabric reinforcements consistently outperform traditional 2-D materials.

4.3 Manufacture of multilayer woven fabrics

The conventional 2-D weaving process is carried out employing the mono-directional shedding operation. This enables either a single or a multiple layer warp to be displaced to form only one row-wise shed. Subsequent picking of the weft in the produced single shed results in the interlacing of the corresponding warp type with only one weft. In general it is character-

ized by one filling insertion (pick) per weave cycle or loom rpm, unavoidable crimp, limited thickness and high production speed, whereas 3-D weaving is characterized by multiple filling insertions (picks) per weave cycle or machine rpm, no internal crimp, better performance and greater thickness but lower production speed. A comparison of the traditional 2-D weaving and the 3-D weaving systems is presented in Fig. 4.1.

The principle of the 3-D weaving process is represented in Fig. 4.2. The heart of the 3-D weaving process is the dual-directional shedding operation. Through this operation the multiple layer warp can be displaced to form alternately multiple column-wise and row-wise sheds (Fig. 4.3). Subsequent picking of wefts in the corresponding sheds of the two directions results in the complete interlacing of the multiple layer warp (Z) with the two mutually perpendicular sets of wefts (X and Y).

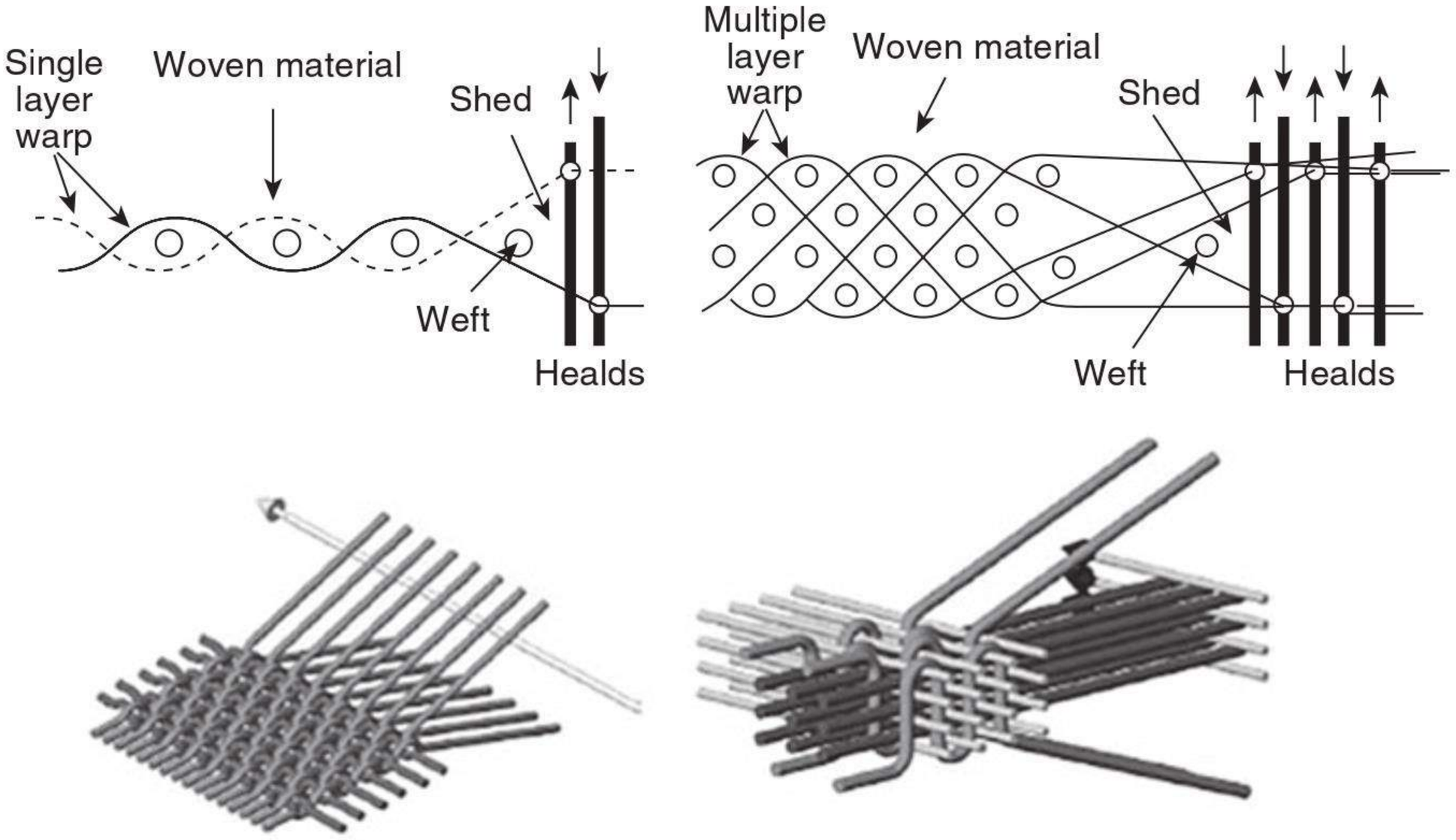

(a) 2-D weaving (b) 3-D weaving

4.1 Comparison of 2-D and 3-D weaving.

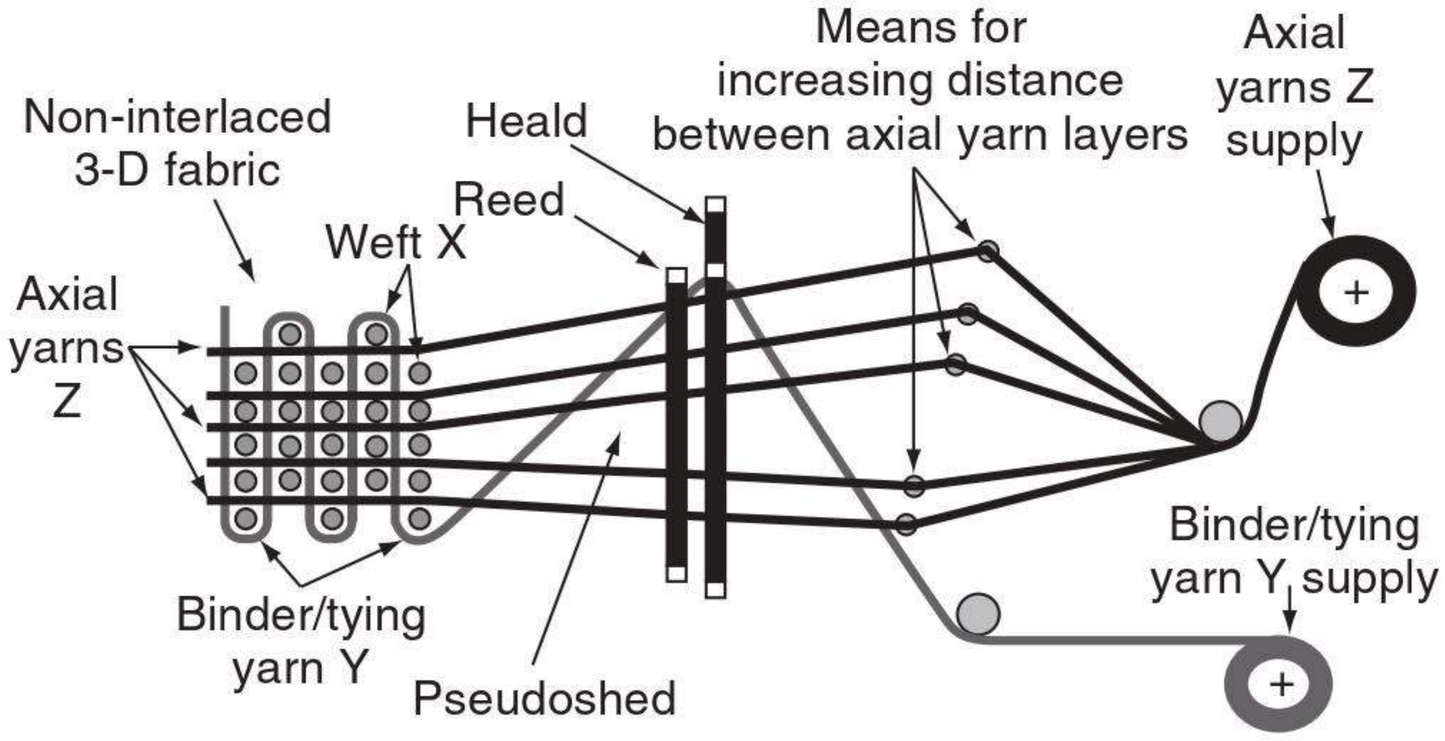

4.2 Principle of 3-D Weaving.

Another point to be noticed in Fig. 4.3 is the alternate formation of the column-wise and row-wise sheds. Accordingly, two mutually perpendicular sets of wefts, the vertical and horizontal sets, will be required. The number of wefts in each set will thus correspond with the number of sheds of the respective directions. As shown, first multiple column-wise sheds are formed into which a corresponding number of vertical wefts are picked. Next, multiple row-wise sheds are formed and a corresponding number of horizontal wefts are picked. Such shedding and picking will result in the interlacing of the multiple layer warp with two orthogonal sets of wefts as shown in Fig. 4.4 and hence an interlaced 3-D fabric, referred to as 3-D woven 3d fabric, will be obtained (Khokar and Peterson, 1998).

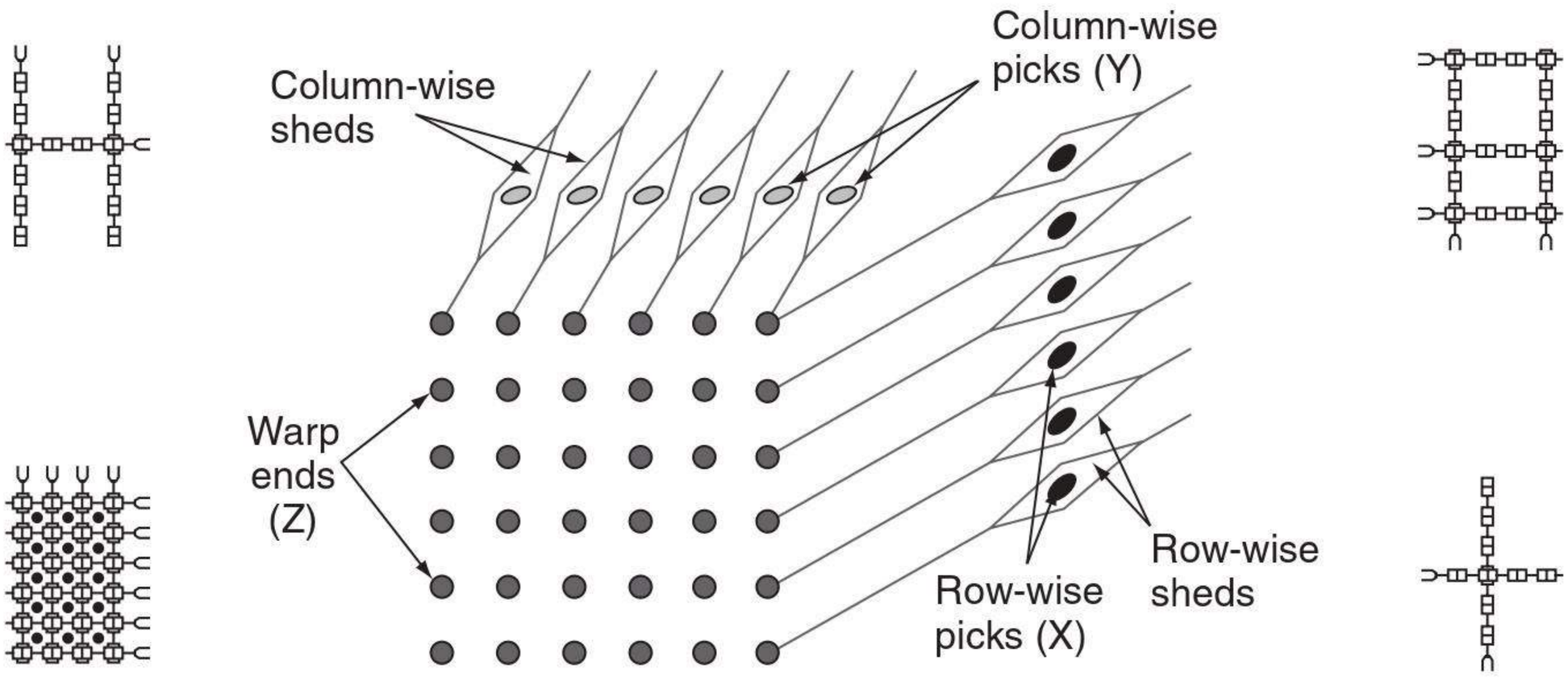

4.3 Principle of dual-directional shedding.

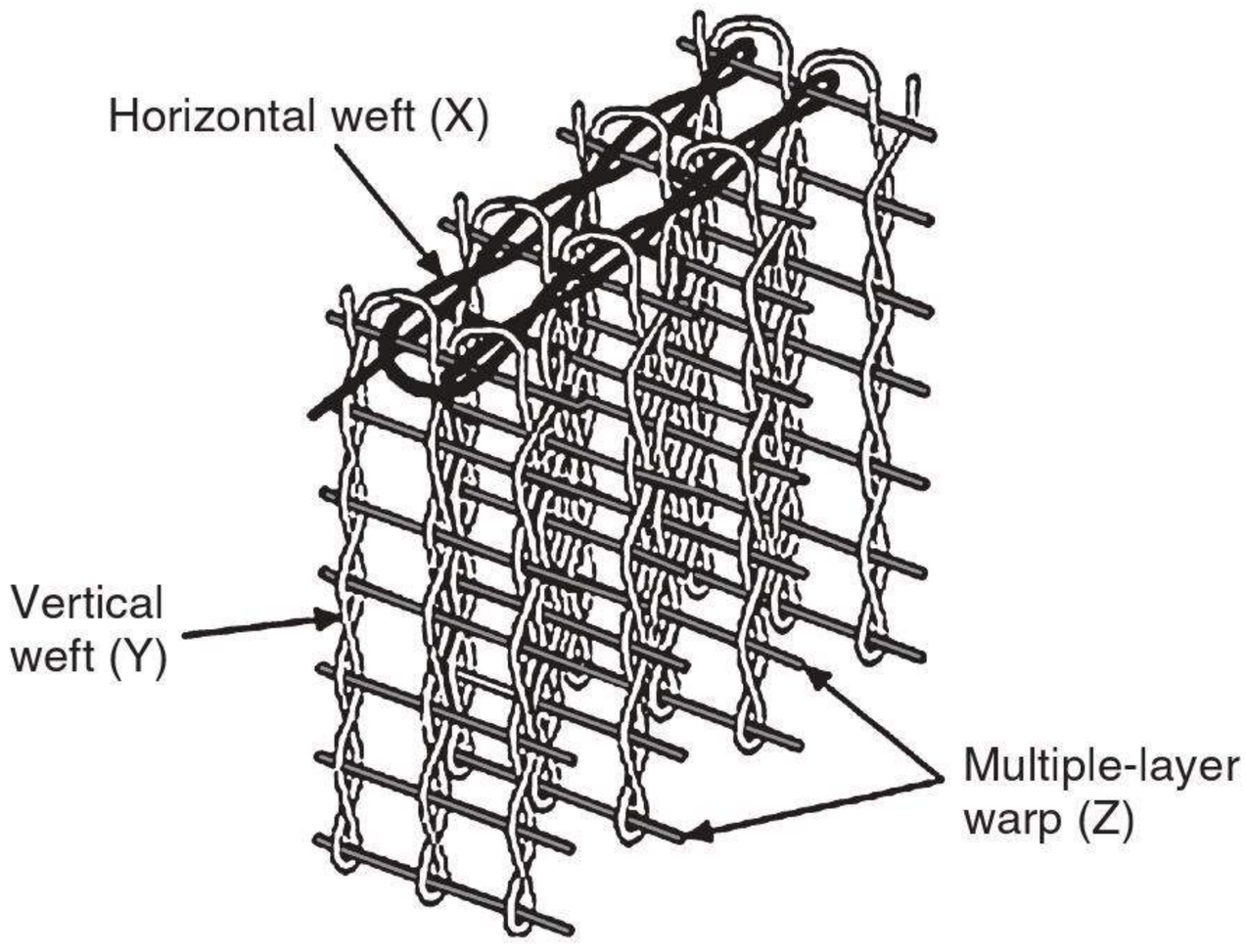

4.4 Interlacing of multiple-layer warp with horizontal and vertical sets of weft.

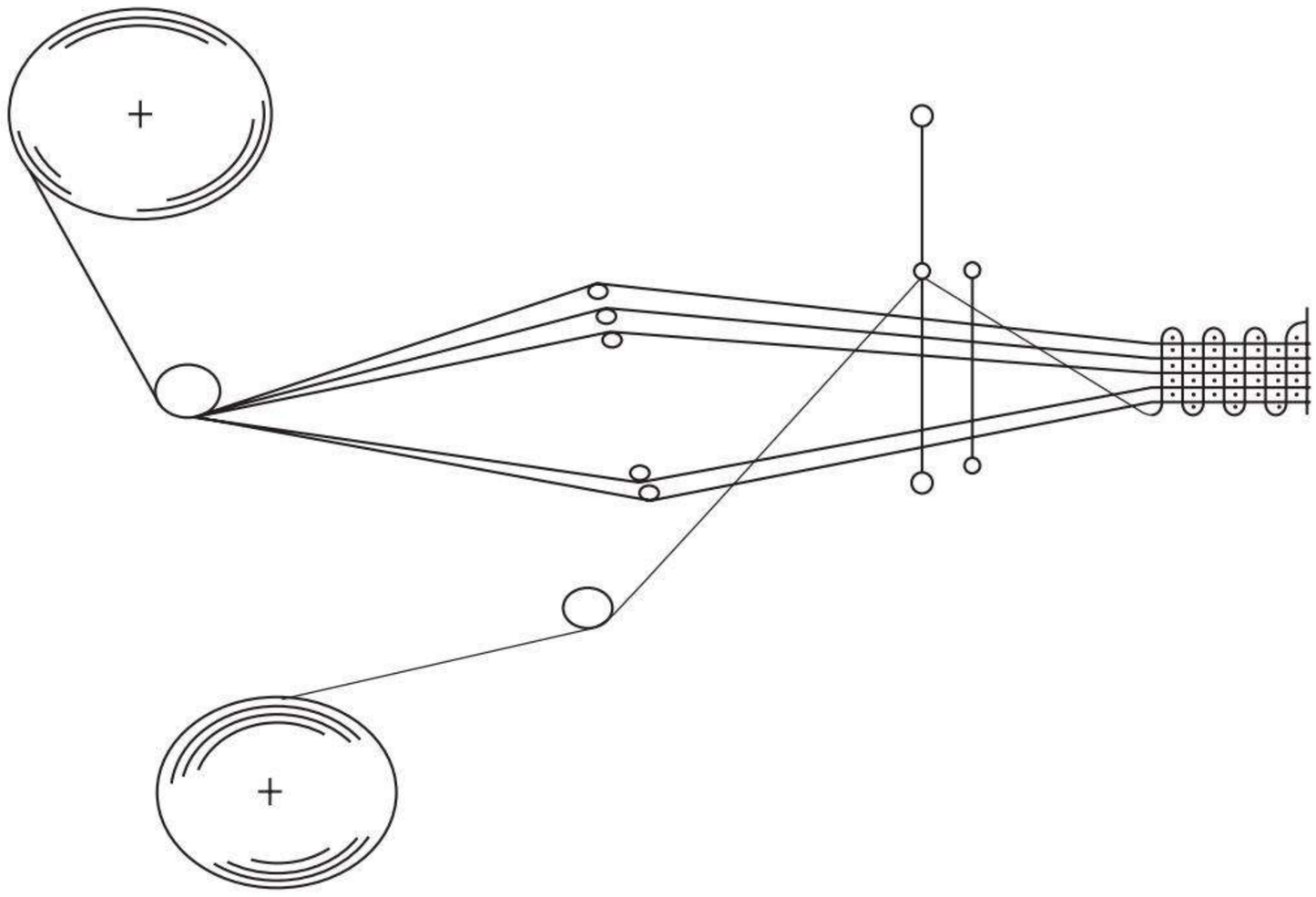

4.5 Multiwarp weaving loom.

Three-dimensional multilayer woven fabrics are produced principally by the multiple warp weaving method, which has long been used for the manufacture of double cloth and triple cloths for bags, webbings and carpets. A typical setup of a multiwarp weaving loom is shown in Fig. 4.5 (Ko, 1989). The number of layers of yarns in the fabric is governed by a special shedding mechanism which controls the height through which the harnesses are lifted. Fabrics with as many as 17 layers have been woven successfully with this method. By the weaving method, various fibre architectures can be produced including solid orthogonal panels, variable thickness solid panels and core structures simulating a box beam, or truss-like structures. Furthermore, by proper manipulation of the warp yarns, as exemplified by the angle interlock structure, the through-thickness yarns can be organized into a diagonal pattern. One limitation of the multiwarp weaving method is the difficulty of introducing yarns in the bias direction as in the triaxial weaving or circular weaving process.

Traditional weaving machines can be adapted well to make multilayer woven fabrics. Mohamed (1990) has described a method of weaving these fabrics with different shapes using a variety of fibres. The special feature of the process is that the multiple weft yarns are inserted simultaneously. The machine was capable of producing continuous thick panel and structural elements with different cross-sections such as T, double-T, I and double-I, with fairly thick walls in all directions. These shapes were made in one step using variety of fibres. A schematic diagram of a loom to produce 3-D multilayer woven fabrics is shown in Fig. 4.6.

Weaving a 3-D woven fabric requires several steps. The steps involved in the actual weaving process are described in Fig. 4.7 (from (a) to (h)). Before weaving begins, two sets of yarns are fed from bobbins and placed in the

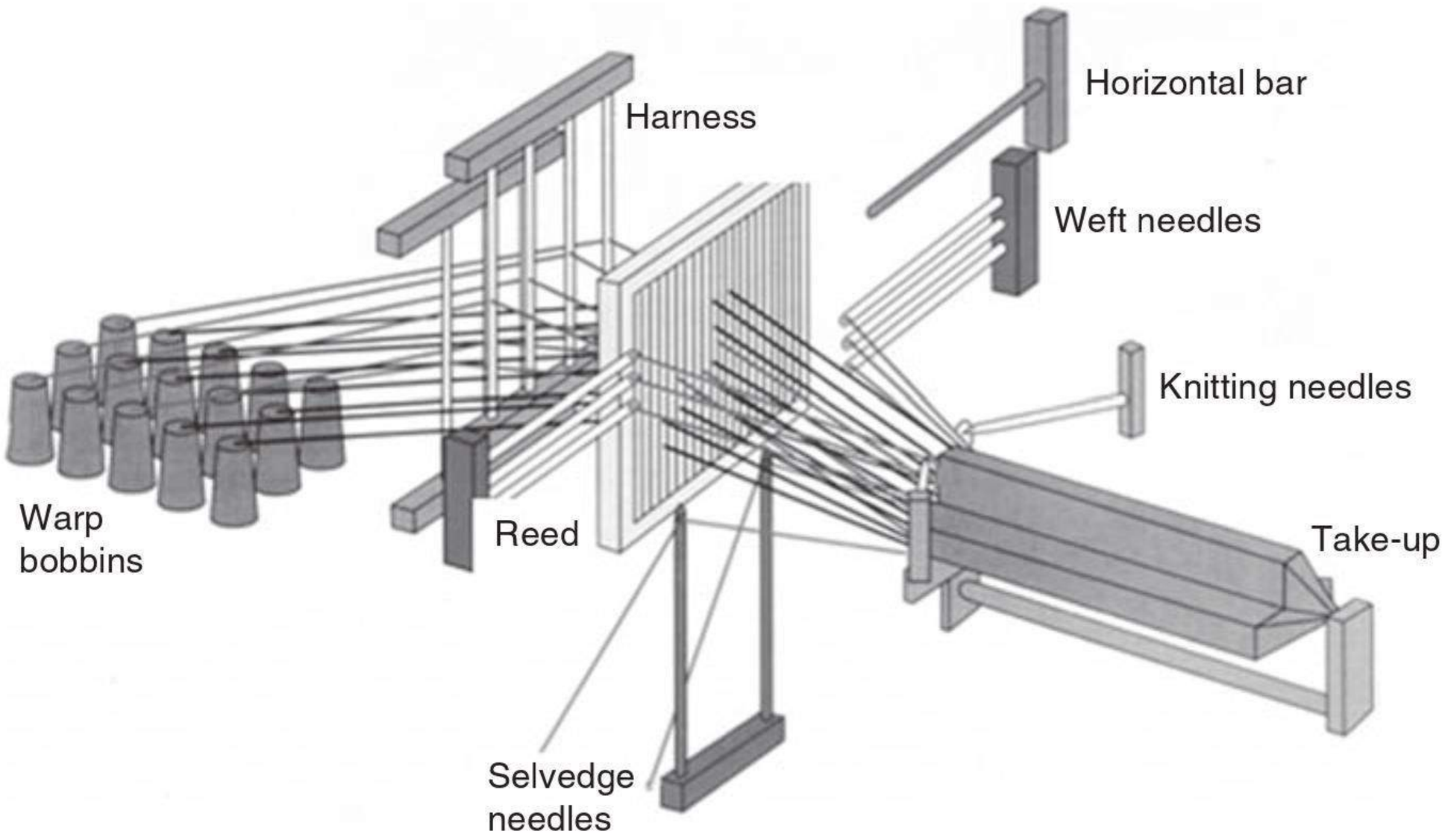

4.6 3-D multilayer weaving system (Mohamed, 1990).

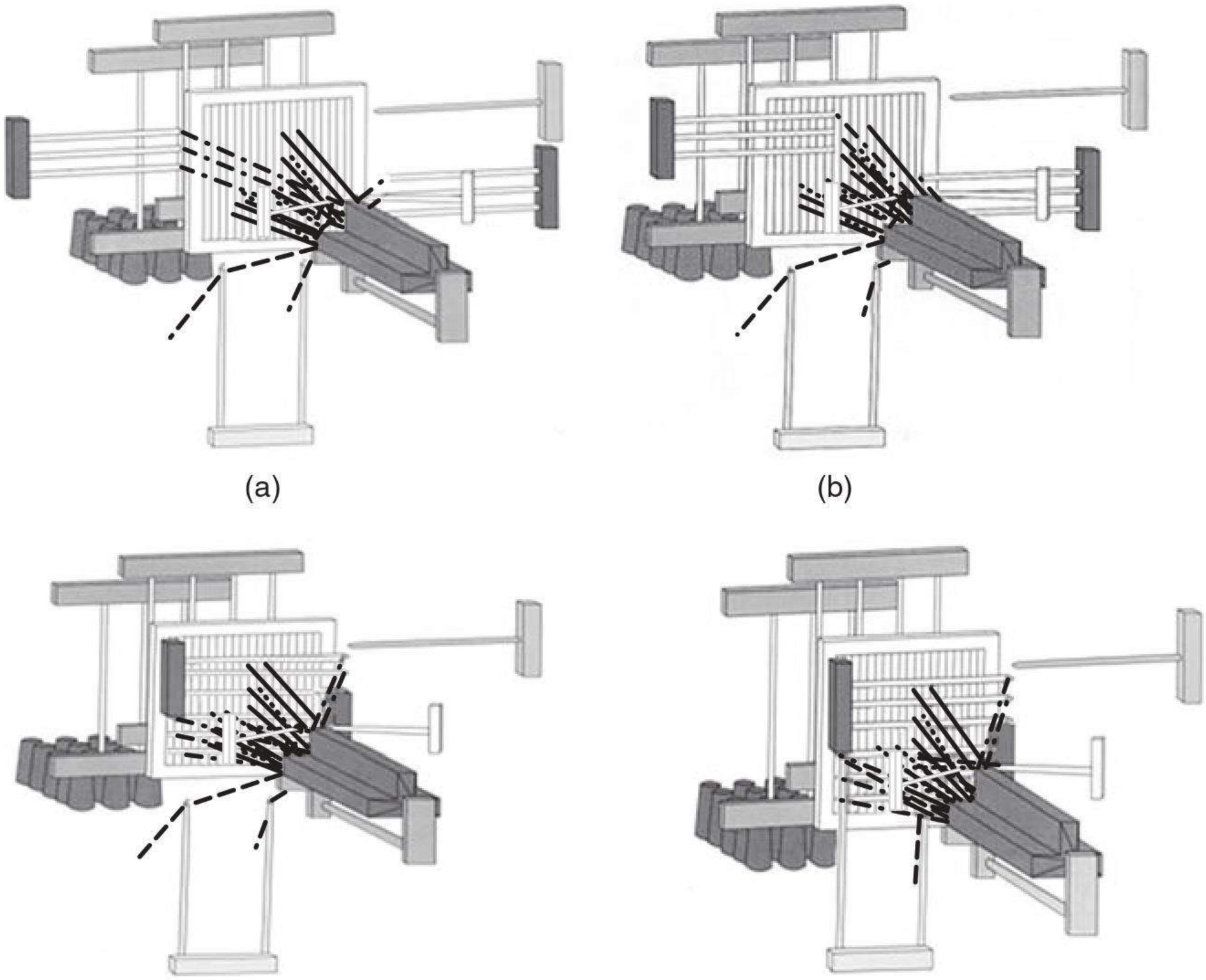

4.7 Stages in the production of multilayer woven fabrics.

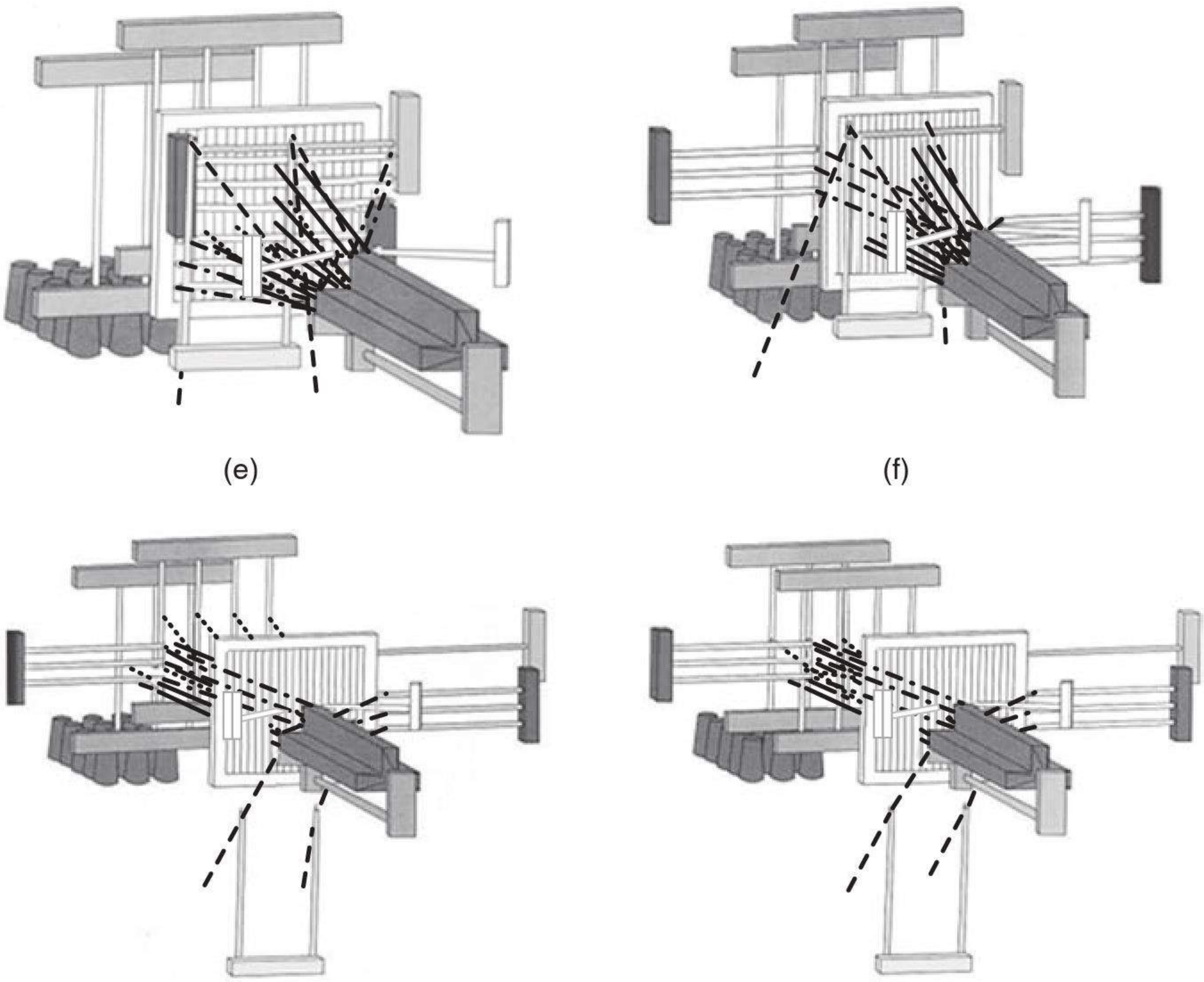

4.7 Continued

lengthwise direction. The first set, the warp yarns (—), will remain stationary during weaving and will become the lengthwise yarns in the finished structure. Harnesses suspend the *z*-yarns (. . . .), the set that will become the vertical yarns, at oblique angles – some from above, some from below. Two additional yarns are used: filling yarns (–··–·), which are inserted from the side by two horizontal sets of needles, and selvedge yarns (----), inserted from below by a pair of vertical needles. Two knitting needles are positioned so that they can knit loops of selvedge yarn together at the corners of the woven beam. Weaving begins as the filling needles move between layers of warp and vertical yarns to insert the filling in a crosswise direction (b, c). Before these needles retract, the vertical selvedge needles move up to catch the filling; a horizontal bar in turn catches the selvedge yarn at the top (d, e). The filling needles retract (f). The pair of knitting needles clasps the two selvedge yarns, allowing the selvedge yarn and crossbar to retract also. The reed – the comb-like device just in front of the harness – moves horizontally to pack the yarns into their finished configurations; during this step, the *z*-

yarns are pushed from their diagonal position into a vertical alignment (g). At the end of the cycle the knitting needles pass the new loop of selvedge yarn through the previous one, and the harnesses switch to reserve the position of the vertical yarns for the next cycle (h).

As in any loom, the 3-D multilayer weaving system begins with a supply arrangement for the lengthwise yarns. This can be either a collection of bobbins on a creel or a set of beams. Two sets of yarns are arranged separately along the length of the loom: the warp (x) yarns and the vertical (z) yarns. The filling (weft) (y) yarn and the yarn that will secure the vertical selvedge edge must be dispensed separately. One of the lengthwise groups of yarns, the warp (x), does not move during the operation of the machine. To form a multilayer structure, the warp yarns are held lengthwise in the machine in a grid pattern matching the cross-sectional arrangement of layers. In a 3-D structure, there are many layers of filling (y) yarns, which must be inserted between the layers of warp yarns in multiples. This is accomplished by inserting the filling across the warp with a vertical row of needles, each needle being perpendicular to the warp and threaded with a length of yarn. To form a simple rectangular block structure, a single set of needles carries filling yarns across all the warp yarns.

A key step in assuring the strength of the finished structure occurs each time the needles cross the warp. A vertical needle, threaded with the yarn that will secure the selvedge, the loops on the vertical edge, is inserted from below the weaving area, coming up to catch the filling yarn that has just been brought across the warp. This selvedge needle holds a loop of each filling yarn at the edge of the warp as the filling needles return to their original positions. Thus a double length of filling is inserted with each cycle. The selvedge needles retract for the next step, but the selvedge yarn – which now holds the filling loops – is clasped and held in its vertical position by a knitting needle. To form a finished corner edge, the loops of selvedge yarns are knitted together as the process continues.

The step that is called beat-up in traditional weaving is used in 3-D weaving to position the vertical (z) yarns. These yarns are threaded through heddles suspended from harness frames (similar to those used in the traditional loom) and are passed through the vertical openings in a reed at angles, crossing on the opposite side of the filling needle. Once every cycle, as the z-yarns are suspended in diagonal positions, the reed moves horizontally to push the filling against the already woven length of fabric. This action pushes the crossed z-yarns into a vertical arrangement. The harnesses holding the z-yarns then move up and down to reverse the positions of the yarns before the process begins again. In this way the vertical yarn that has just been stretched from the bottom to the top of the textile is passed over the topmost filling yarn and held in position to be placed in the opposite direction at the next stage of the weaving.

In summary, 3-D multilayer woven fabrics are fabricated by modifying the conventional weaving mechanisms. Harnesses with multi-eye heddles are used to arrange the warps into three sections in plane form for weaving convenience. The mainframe and flanges are interlaced by a set of warps moving to and fro as a joint. Weft passes through the clear warp sheds separated by multi-eye heddles to form the 3-D woven fabrics in plane form. The differential feeding length between the warp yarns gives rise to extra friction, and therefore hairiness may occur. In order to reduce this friction the warps are passed through the tensioner and weight with ceramic eyes individually between the creel and weaving loom. The thickness of the central portion of the flattened fabrics is different from that of the side portions. Therefore the cloth roller cannot be used to take up the flattened fabrics. The fabric is clipped and pulled by a pair of rollers set in front of the loom as a take-up device.

4.4 General structure and behaviour of multilayer woven fabrics

4.4.1 Structure

In 2-D structures, yarns are laid in a plane and the thickness of the fabric is small compared to its in-plane dimensions. Single layer designs include plain, basket, twill and satin weaves which are used in laminates. Two-dimensional woven fabrics are generally anisotropic, have poor in-plane shear resistance and have less modulus than the fibre materials due to the existence of crimp and crimp interchange. Reducing yarn crimp in the loading direction or using high-modulus yarns improves fabric modulus. To increase isotropy, in-plane shear rigidity and other properties in the bias or diagonal direction, triaxial woven fabrics have been developed in which three yarn systems interlace at 60° angles.

Unlike in 2-D fabrics, in 3-D woven fabric structures the thickness or z-direction dimension is considerable relative to the x and y dimensions. Fibres or yarns are intertwined, interlaced or intermeshed in the x (longitudinal), y (cross) and z (vertical) directions. For 3-D structures, there may be an endless number of possibilities for yarn spacing in a 3-D space (Adanur, 1995). In practice, there are enormous variations in multiple layer textile structures. A structure can be of different layers, each layer may have different weaves, the yarns from different layers may be arranged in different orders, and so on (Chen *et al.*, 1992).

As illustrated in Fig. 4.8 (Pastore and Cai, 1990), there are four basic components to a generalized 3-D woven fabric geometry: warp, web, fill and surface weave yarns. Warp yarns are the system of yarns which run in the machine direction and have no crimp. These are also called 'stuffer' yarns

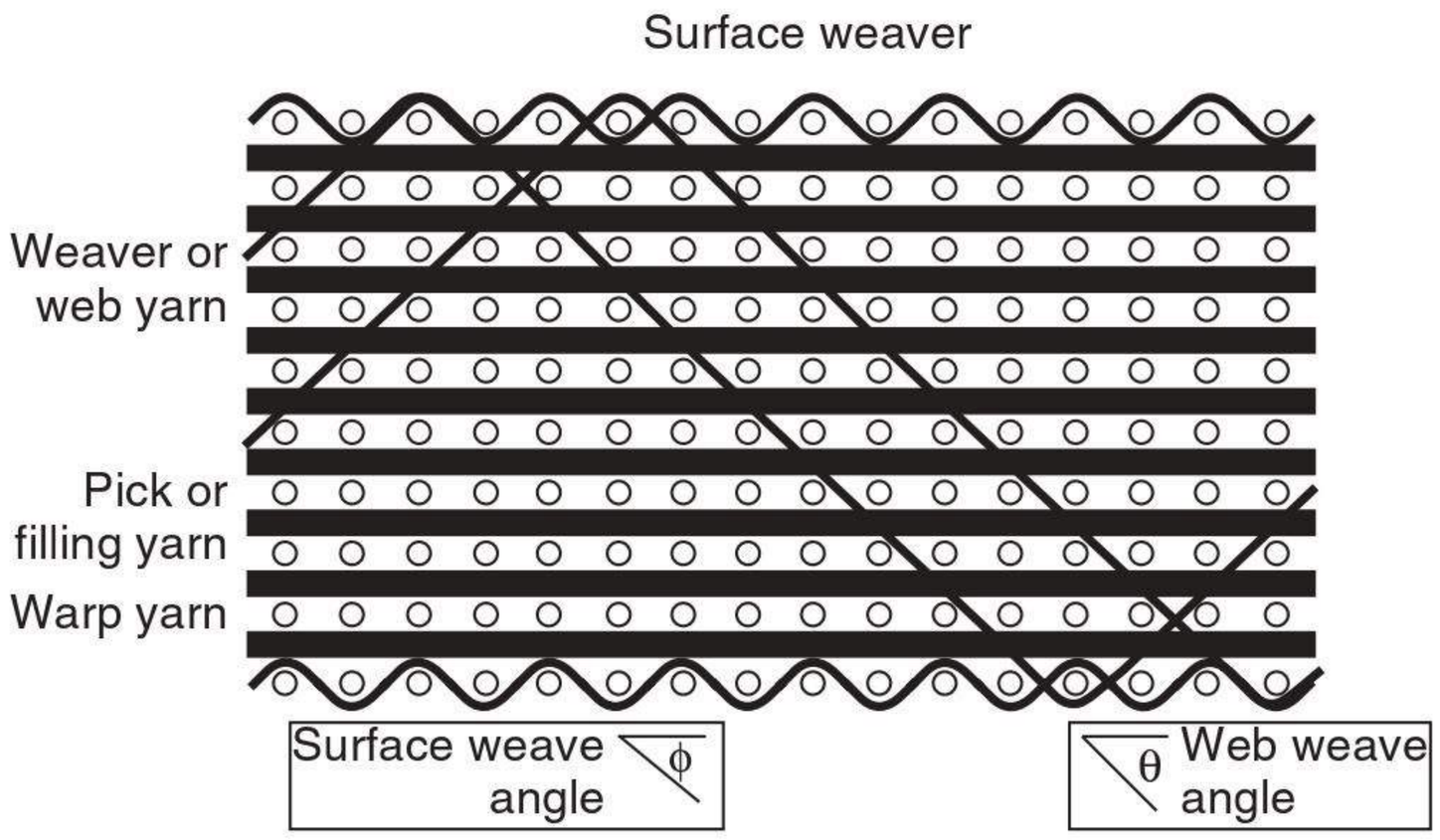

4.8 Schematic illustration of generalized 3-D woven fabric projected to the *x*–*z* (fabric length–thickness) plane.

or 'longitudinals'. Because of their very low crimp, these yarns provide the primary strength and stiffness in the longitudinal (x) direction of the material. Web yarns run in the machine direction and provide the interlacing necessary for fabric integrity. These yarns contain crimp in the through-thickness direction, providing the z-directional properties of the system. These yarns are sometimes called 'weavers'. The 'weave angle' of the web yarns refers to the angle of orientation of the web yarn with respect to the warp direction. Fill yarns are perpendicular to the machine direction and interlace with the web yarns. These yarns are sometimes called 'picks'. These yarns also possess crimp in the through-thickness direction, but this crimp is negligible compared to that of the warp yarns for these fabric systems. These yarns provide the transverse (y) directional properties of the composite system. Surface weave yarns run in the machine direction and form what is essentially a 2-D weave on the surface of the fabric. Surface weave yarns are incorporated into the structure when the web yarns are insufficient to provide a smooth surface on the face and back of the cloth. These yarns experience crimp in the through-thickness direction. When surface weave yarns are employed in the fabric, there are two yarns for every warp plane of the fabric. This system of yarns contributes the least to the mechanical properties of the composite.

Pattern design of three-dimensional multilayer woven fabrics

Three-dimensional woven structures can be classified into angle interlock and orthogonal interlock binding according to the orientation of binders, or through-thickness and layer-to-layer binding if the penetration depth of binders is concerned. Combination of the definitions can evolve four basic binding possibilities, i.e., angle interlock/through-thickness binding (A/T),

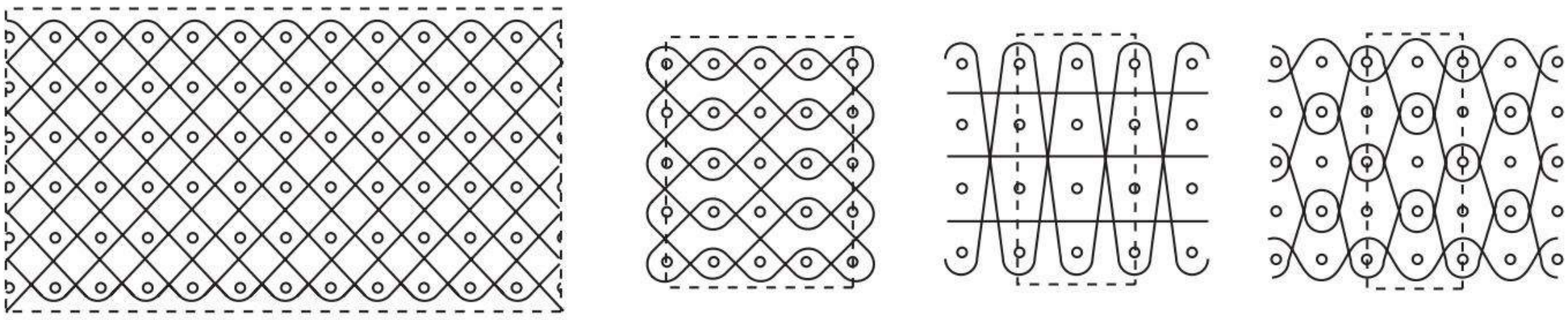

(a) A/T binding (b) A/L binding (c) O/T binding (d) O/L binding

4.9 3-D woven structures with various binding patterns.

angle interlock/layer-to-layer binding (A/L), orthogonal interlock/through-thickness binding (O/T) and orthogonal interlock/layer-to-layer binding (O/L). These four binding patterns, for which the unit cell is enclosed by a dotted rectangle, are shown in Fig. 4.9.

Binding patterns are of prime importance in determining the fibre architecture of 3-D woven preforms and in analysing the performance of woven composites. Other conditions being the same, an orthogonal interlock binding can provide a greater fibre volume fraction than an angle interlock binding, particularly in the thickness direction. This provides a possible way to modify the performance of woven composites by selecting a suitable binding pattern with respect to the orientation of binders. On the other hand, woven preforms with an angle interlock binding possess better pliability and distortion capability than those with an orthogonal binding. It is therefore appropriate to select angle interlock binding for producing woven composites with complex configurations (Yi and Ding, 2004). In addition, a layer-to-layer binding can also offer a greater fibre volume fraction than its counterpart of a through-thickness binding because of the overlapping arrangement of binders in the thickness direction. Therefore, the design of penetration depth of binders could provide another way to improve the performance of woven composites.

Weave instruction in cross-sections of weft

After the binding pattern of a 3-D woven structure is determined, a method of instructions to drive the weaving machine should be given in order to clearly illustrate the geometrical arrangement of the constituent yarns and consequently to guide the drawing and denting processes. To demonstrate the method, a typical 3-D woven pattern as shown in Fig. 4.10(a) is used. No doubt, the 3-D woven structure can be presented by means of the traditional design method for a compound structure (Goerner, 1989). However, this seems to be over-complex for the 3-D woven structures, particularly when the number of fabric layers is beyond the common range.

The three lengthwise-arranged yarns including binder, stuffer and surface warp are jointly called warp yarns for convenience. They are numbered

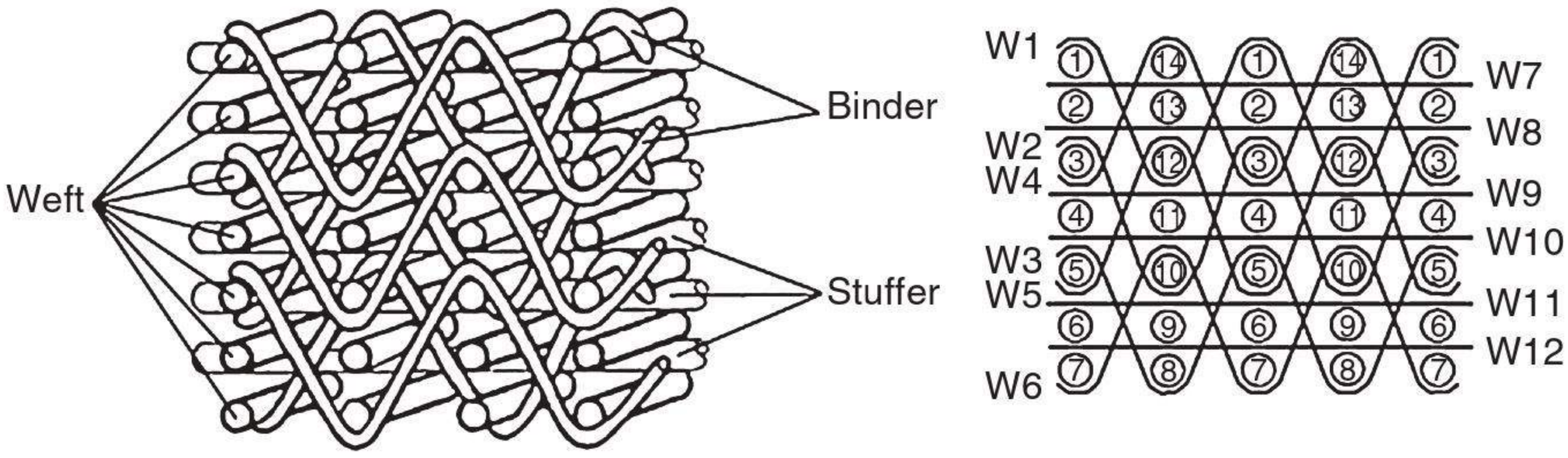

(a) Yarn architecture of 3-D woven fabric (b) Cross-section of weft

4.10 Schematic diagram of a typical 3-D woven structure.

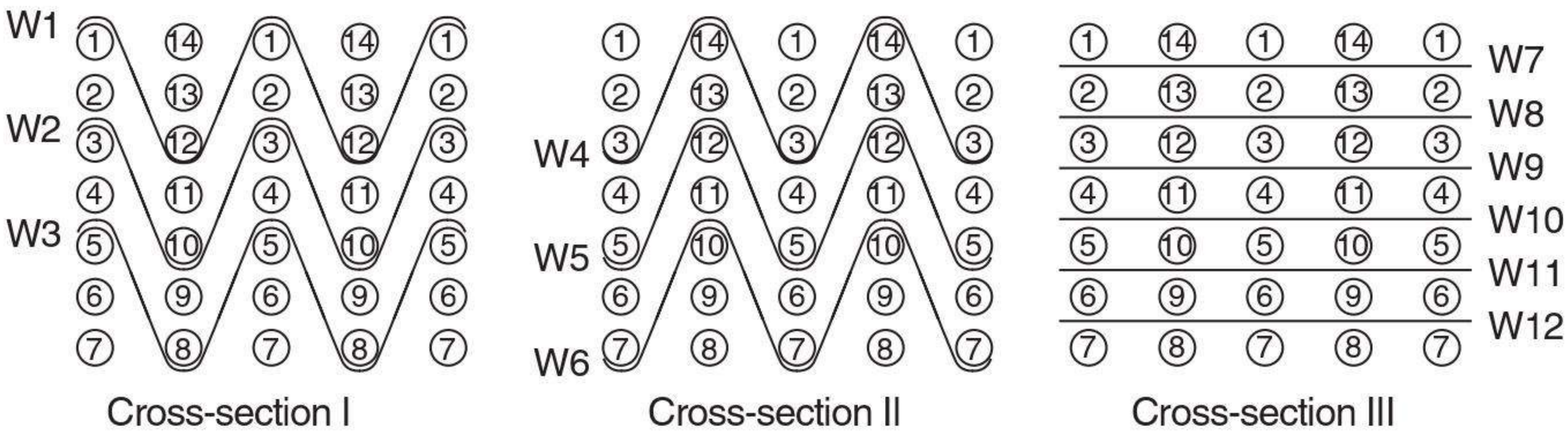

4.11 Binder and stuffer in a dent.

consecutively corresponding to the harness frames. Similarly, the wefts are numbered to illustrate the picking sequence, as shown in Fig. 4.10(b). To ensure a steady working condition of harness frames, wefts should be numbered in descending order from the top to the bottom along a weft column, then in ascending order from the bottom to the top along the next column, and so on.

To avoid severe yarn-to-yarn friction within a dent of reed, the warp yarns that are not interlaced on a cross-section of weft are grouped and drawn in a dent. From this point of view, for the woven structure shown in Fig. 4.10, three cross-sections with corresponding warp yarns are identified, as shown in Fig. 4.11.

It can be seen from Fig. 4.11 that the warp yarns in each cross-section are arranged in parallel and do not exchange their positions in the vertical direction during the weaving process. Once they are drawn in a dent, no friction between them will occur. For this particular structure, there are 12 warp yarns within a weave repeat, including six binders divided into two groups and six stuffers. Consequently, three dents are required with the denting program 3–3–6. Binders W1–W3 are inserted in the first dent, binders W4–W6 in the second dent and stuffers W7–W12 in the third one. It follows that if the straight draw method is used, the weave instruction can easily be obtained. For 3-D structures other than the one described, the proposed method can still be used.

Two of the most common architectures of 3-D woven fabrics used in most applications are the orthogonal and layer interlock weaves, which are illustrated in Fig. 4.12(a) and (b). The important difference between these two weaves is the weave pattern of the through-thickness binder yarn.

The angle interlock woven fabrics consist of three sets of yarns. The stuffers (warp yarns) and warp weavers are oriented along the longitudinal direction, i.e., along the loom feed direction. The fillers (weft yarns) are oriented transverse to the loom feed direction, and are inserted between layers of stuffers. The stuffers and fillers form an orthogonal array. The warp weavers traverse through the thickness of the weave, and interlock with filler layers. The warp weavers crisscross the weave thickness at off-axis

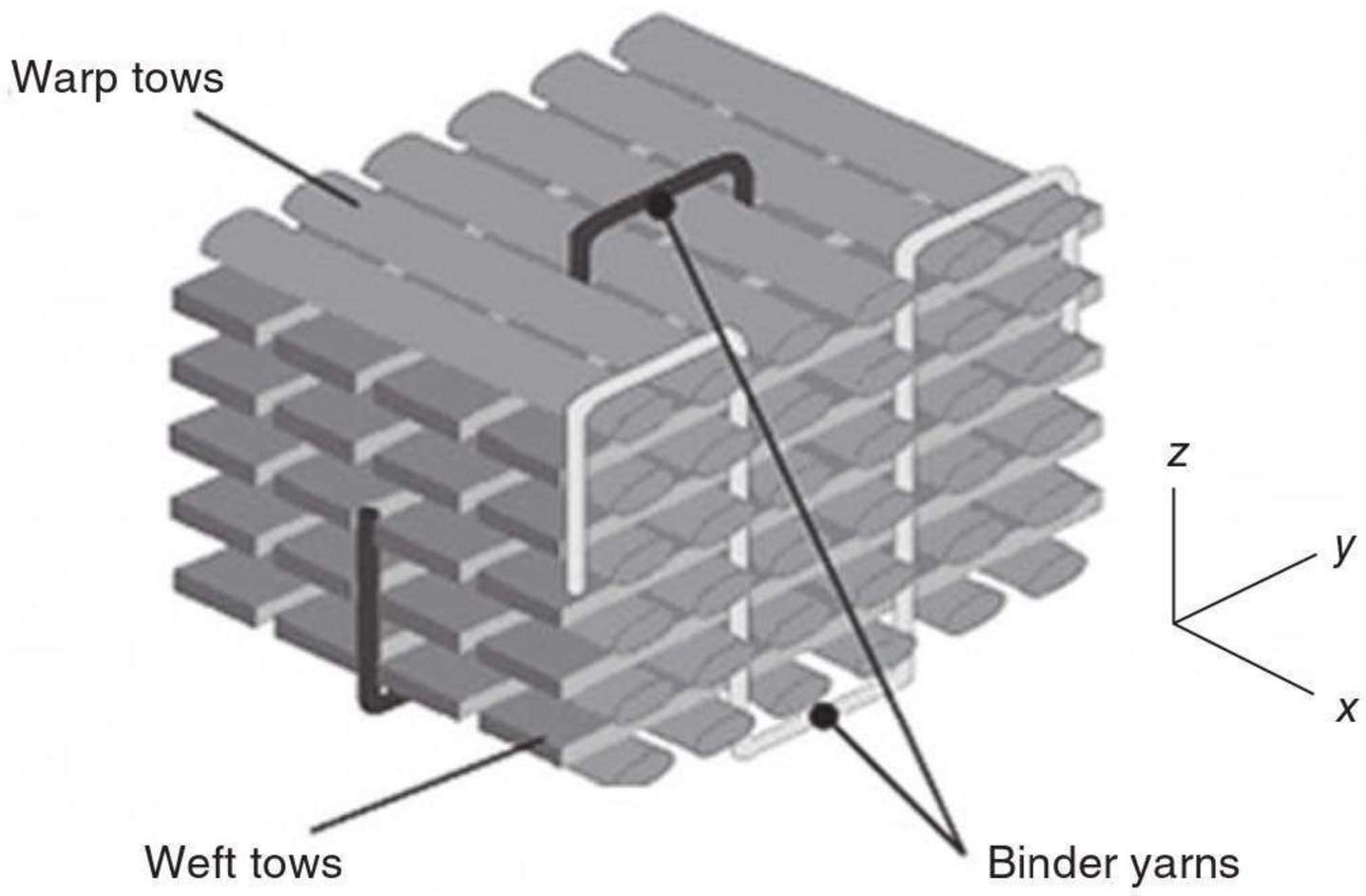

(a) Orthogonal

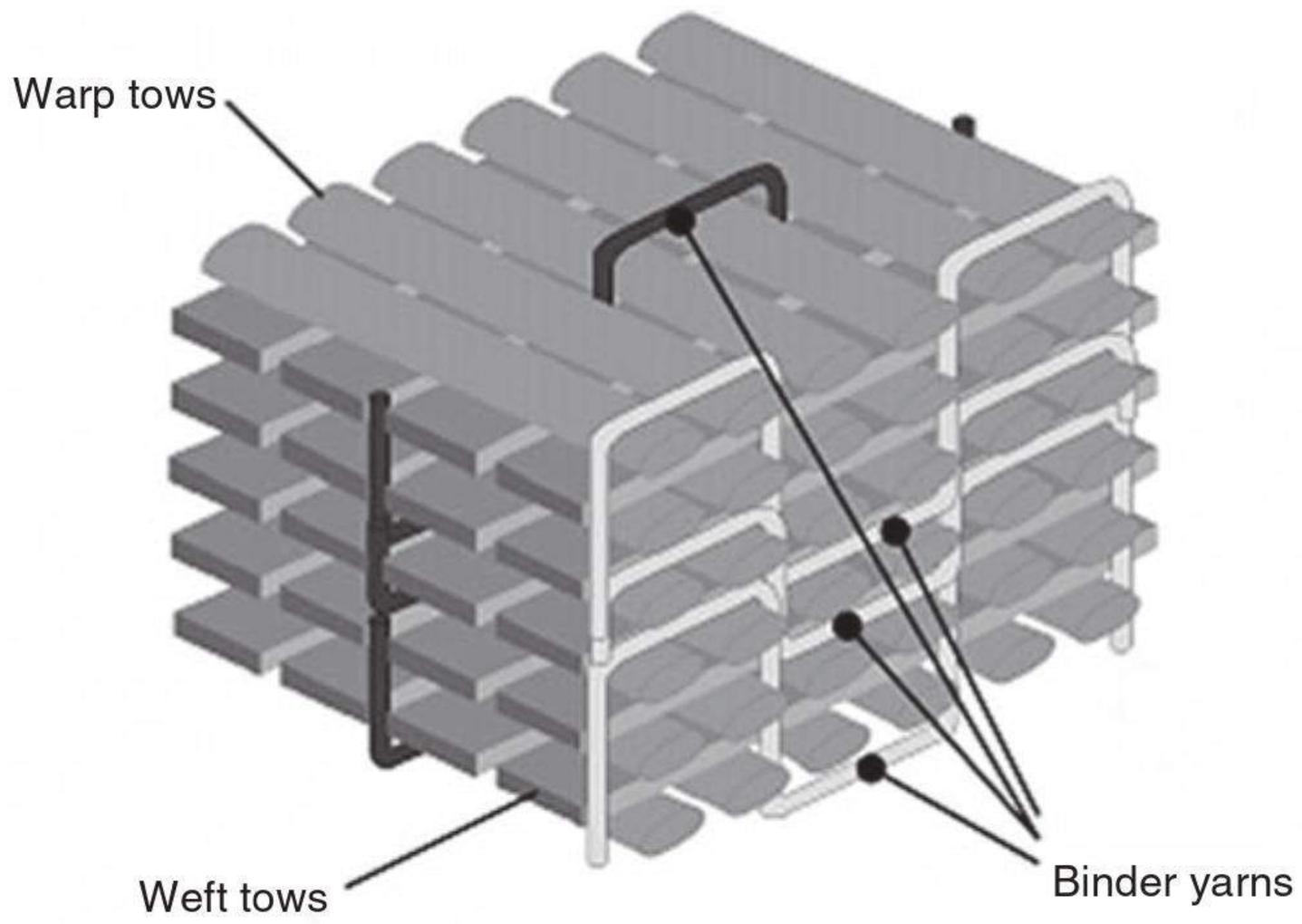

(b) Layer-interlock

4.12 3-D woven structures.

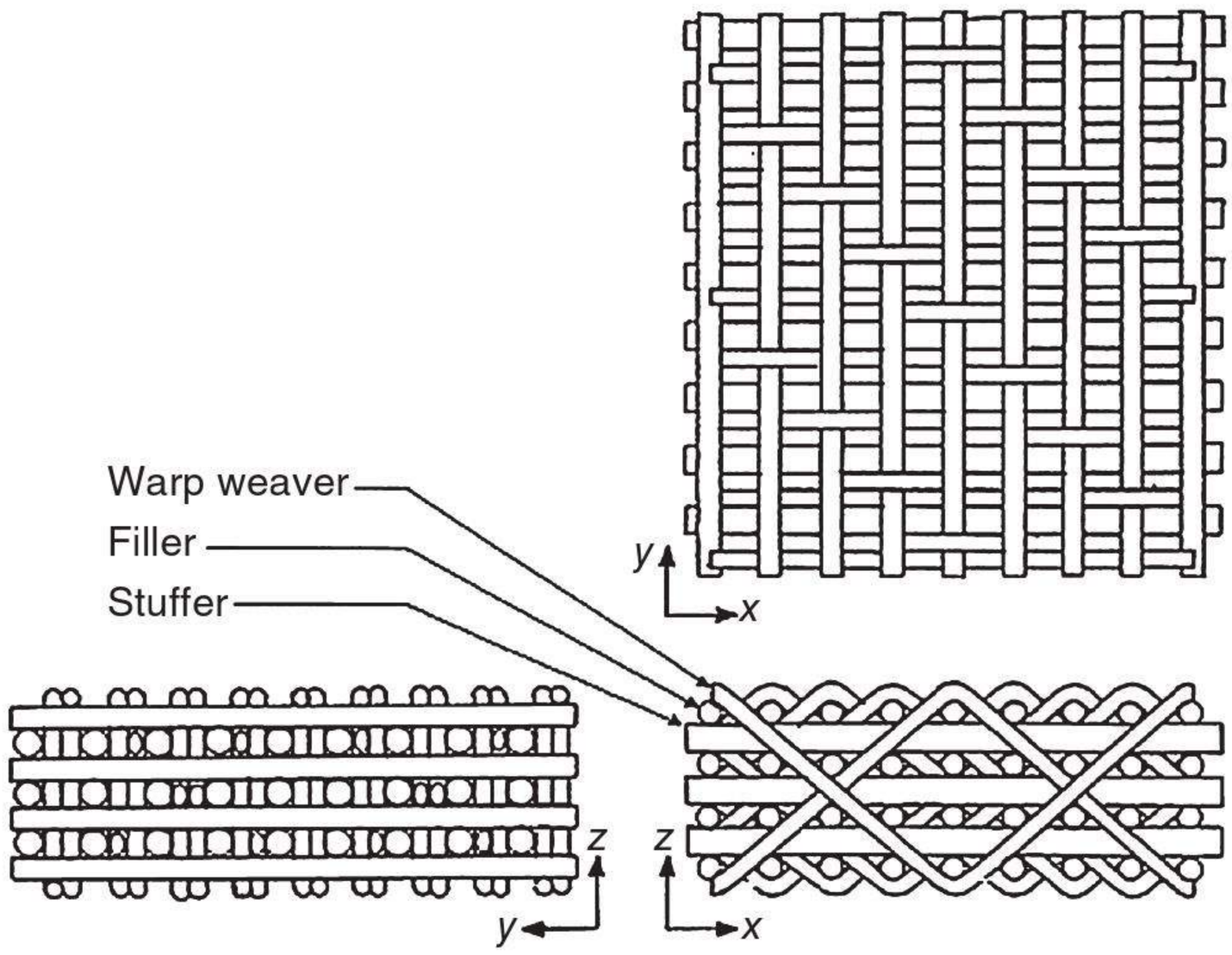

(c) Schematic representation of a 3-D through-thickness angle interlock woven structure

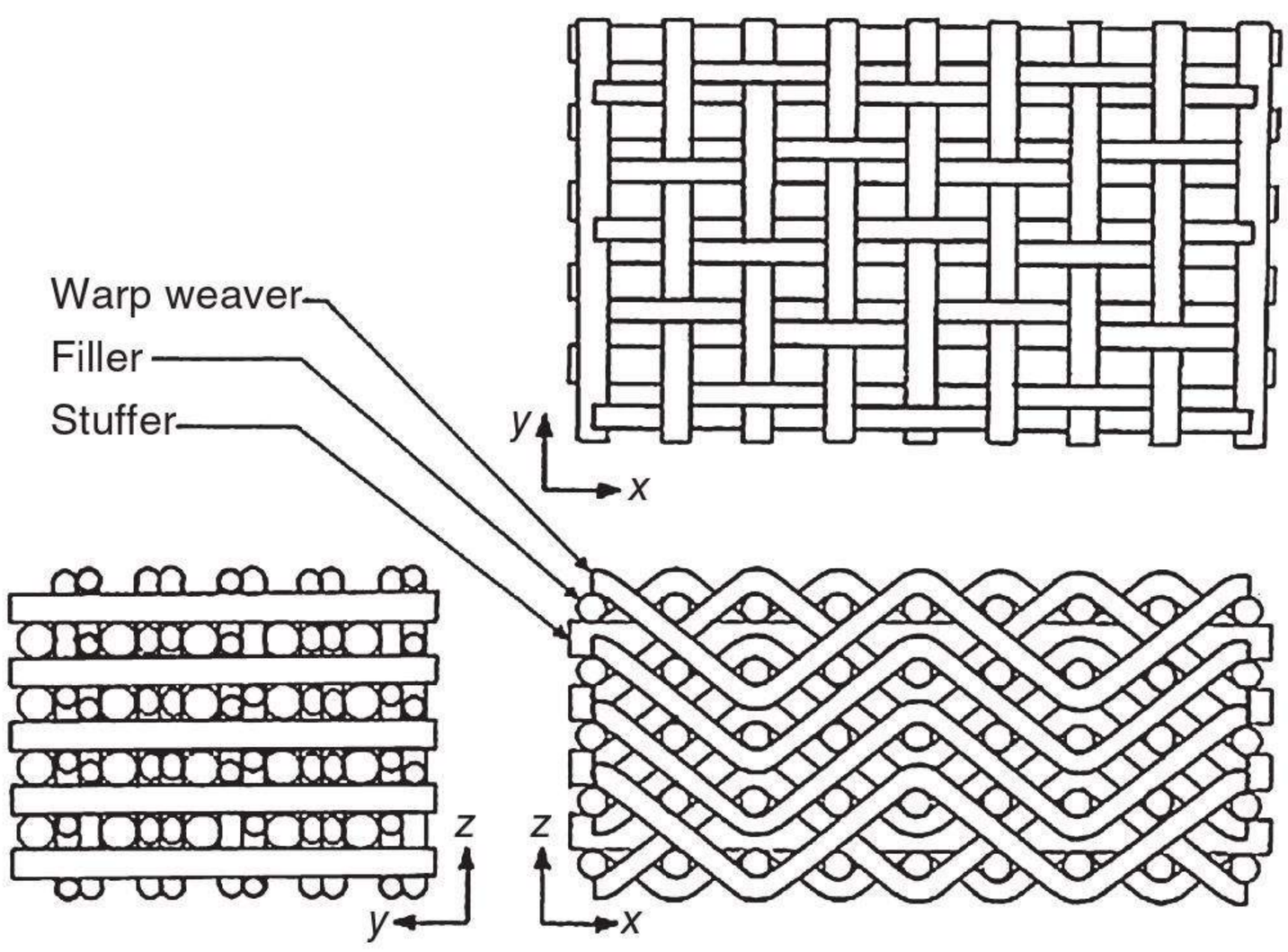

(d) Schematic representation of a 3-D layer-to-layer angle interlock woven structure

4.12 Continued

angles. Different weave geometrical parameters are yarn size, yarn spacing, yarn distribution, interlock lengths and depths. There are two main types of angle interlock preforms: through-thickness angle interlock weave (TTAW) and layer-to-layer angle interlock weave (LLAW).

The TTAW is a multilayered preform in which warp weavers travel from one surface of the preform to the other, holding together all the layers of the preform. The LLAW is a multilayered preform in which warp weavers travel from one layer to the adjacent layer, and back. A set of warp weaves together hold all the layers of the preform.

The schematic arrangements of TTAW and LLAW with ideal geometry are shown in Fig. 4.12(c) and (d). Here, the in-plane yarns, i.e., stuffers and fillers, are straight and the warp weavers are segmentwise straight. Once the preform has been formed, it is densified to form the final composite structure. Densification is the process of surrounding all the fibres/yarns within the preform structure with a resin, leading to a solid composite structure consisting of preform reinforcement and resin. Normally, using the 3-D preforms and resin transfer moulding, 3-D composites are made. Typically, the preform is formed thicker than the mould opening to ensure pressure on the preform during densification. However, such a compressive force applied to the preform necessarily results in some distortion of the yarns within the composite. The thickness of the composite would be less than the nominal thickness of the preform. Even before densification, the yarns within a preform would be wavy (Naik *et al.*, 2002).

4.4.2 Mechanical behaviour of multilayer woven fabrics and composites

Multilayer woven (MLW) fabrics are composed of warp, weft and sometimes binding yarns. The yarn stiffness in one set during weaving will influence the bending behaviour of the yarn in the other sets. When two yarns from two sets meet to interlace, it is the flexible one that bends more. Furthermore, the path of the yarn in the fabric is another factor which controls the yarn bending character. There is a variety of choices of 3-D fabric construction. It is important to understand the mechanical properties of MLW fabrics in terms of tensile, compressive and shear behaviour as these properties will have a direct bearing on the final characteristics of the composite produced. Although a very limited literature exists on the mechanical behaviour of MLW preforms, many researchers have attempted to study the effect of the mechanical behaviour of different varieties of MLW fabrics on the final performance of the composites.

Tensile behaviour

In a study on the tensile behaviour of 3-D woven composites by using different fabric structures, Gu and Zhili (2002) reported the tensile properties of four different types of 3-D woven fabrics and their effect on the tensile properties of composites. The 3-D woven structures analyzed for their tensile behaviour are presented in Fig. 4.13.

The tensile strength results for MLW preforms are presented in Table 4.1. The tensile strength values of orthogonal structures with and without layer-to-layer binding are comparable, and those of angle interlock and modified angle interlock are also comparable, although the difference between the

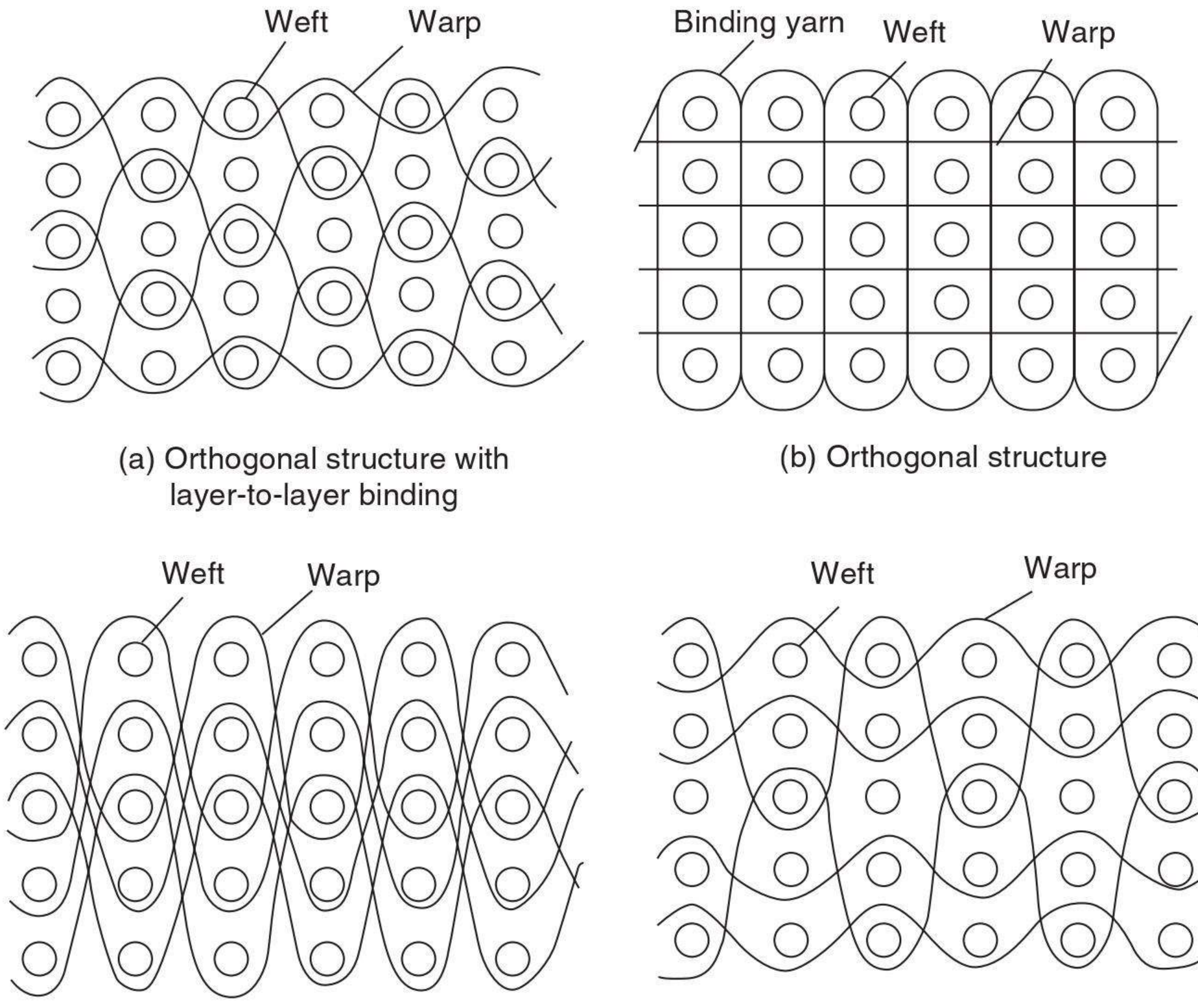

(a) Orthogonal structure with layer-to-layer binding

(b) Orthogonal structure

(c) Angle interlock structure

(d) Modified angle interlock structure

4.13 3-D woven structures.

Table 4.1 Tensile strength results for MLW preforms

Type of fabric	Tensile strength (kN)			Average (kN)
Orthogonal structure with layer-to-layer binding	2.20	1.90	2.00	2.03
Orthogonal structure	2.75	2.70	2.80	2.75
Angle interlock structure	2.50	2.60	2.60	2.57
Modified angle interlock structure	2.95	2.80	3.00	2.92

Source: adapted from Gu and Zhili, 2002.

first two samples is significantly larger. The difference may be attributed to the totally different warp passages in these two samples. All the warp ends in sample 1 are in a binding state, those on the top and bottom being bent slightly, the others to a large extent. The strength values of samples 3 and 4 also exhibit a large difference and this may again be attributed to the bending behaviour of the yarn in the fabric. These differences in the strength

values of different fabrics do affect the performance of the final composite for a specific application.

The high strain rate (HSR) stress–strain behaviour of 3-D Kevlar woven hybrid composites using an epoxy resin system under fill, warp and through-thickness loading is presented in Figs 4.14 to 4.16. A representative quasi-static stress–strain curve is plotted in the same figures. The quasi-static behaviour is almost linear up to the ultimate stress level for this loading.

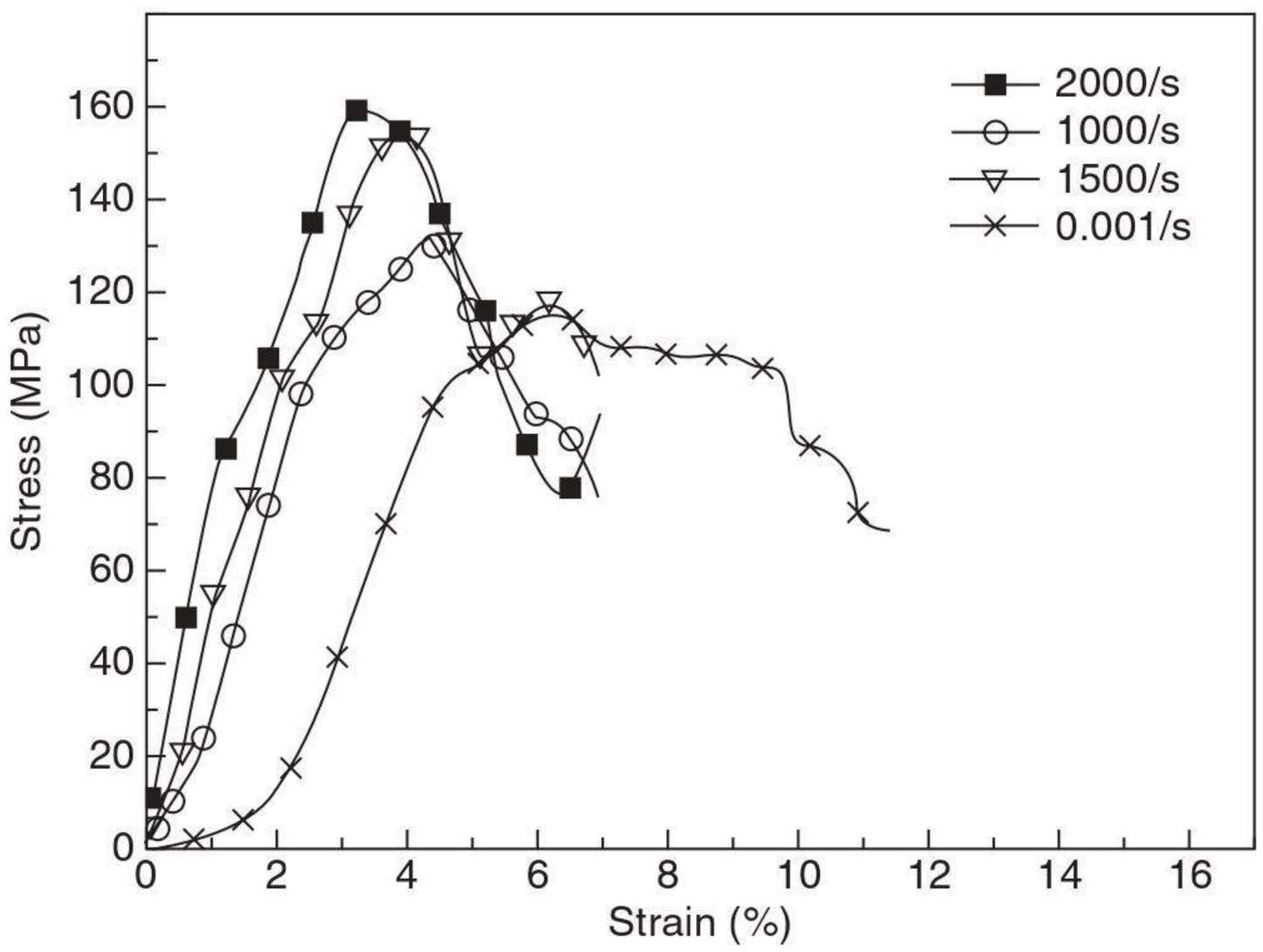

4.14 Stress–strain curves of 3-D woven composites at various strain rates in the in-plane warp direction (adapted from Guo *et al.*, 2007).

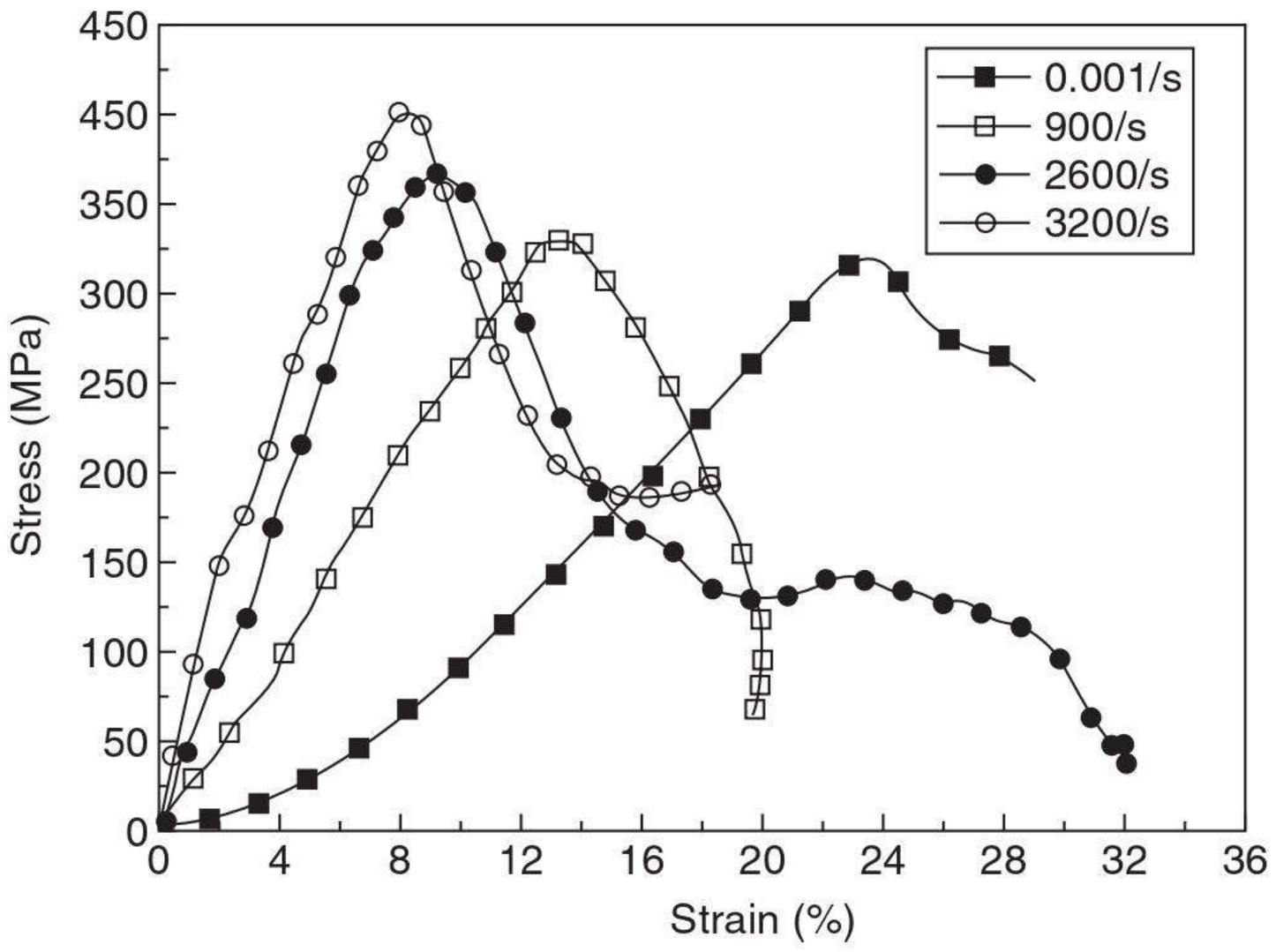

4.15 Stress–strain curves of 3-D woven composites at various strain rates in the in-plane fill direction (adapted from Guo *et al.*, 2007).

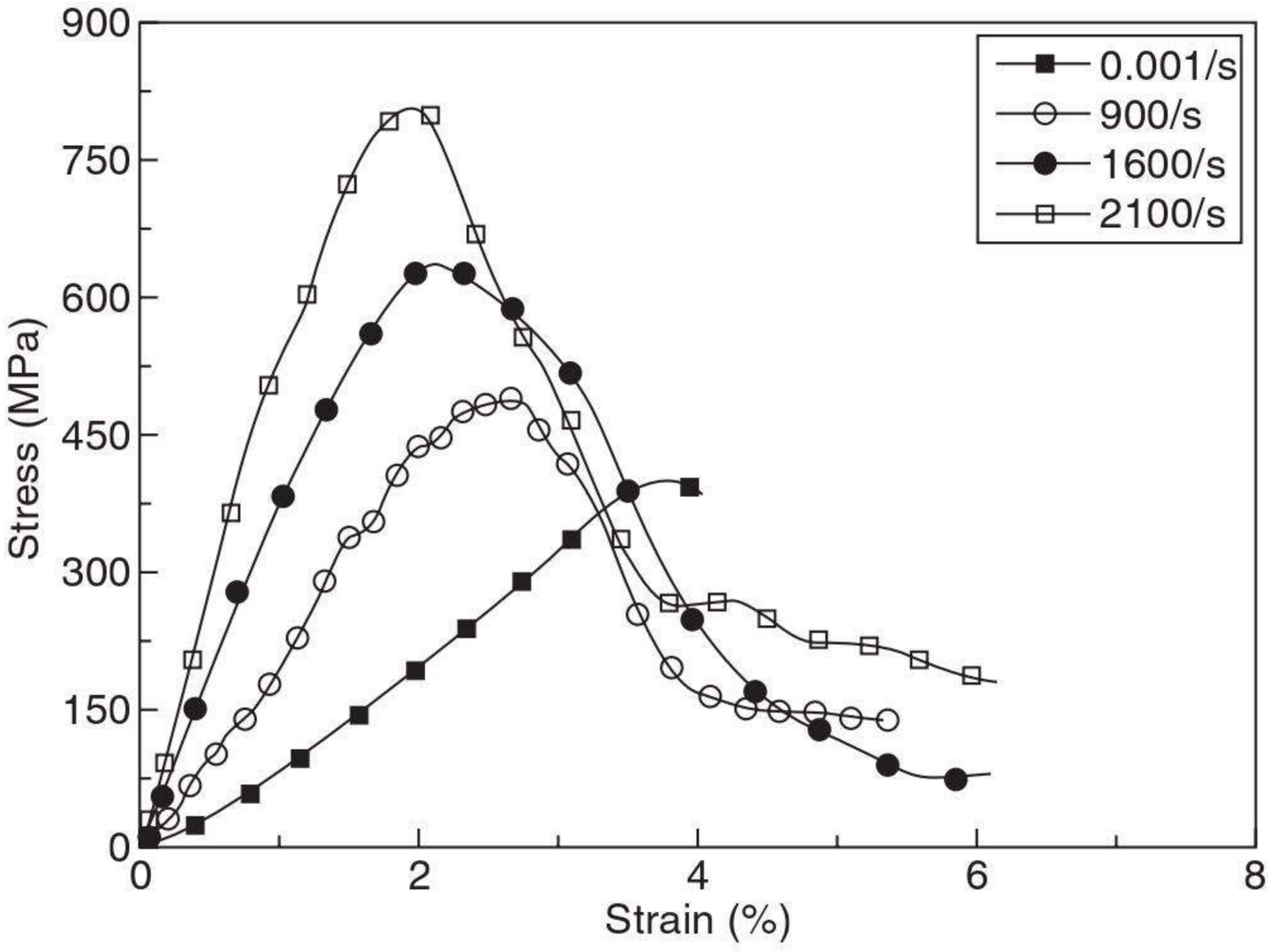

4.16 Stress–strain curves of 3-D woven composites at various strain rates in the through-thickness direction (adapted from Guo *et al.*, 2007).

Similar to quasi-static tests, all the HSR specimens showed some linear behaviour at lower loads (Guo *et al.*, 2007). As the propagating stress pulses further load the specimens, they show progressive non-linear behaviour in the stress–strain response. The non-linear behaviour of the material is dominated by matrix cracks and confirmed by visual inspection and microscopy after the test. In the fill or warp direction, the first region in the stress–strain curve was the elastic region, which extended from the beginning. The elastic region was related to the strain rate. It was found that with the increase of strain rate the elastic region decreased. The first significantly non-linear behaviour occurred after the elastic region as a result of microbuckling and some matrix microcracking. Around peak load, delaminations and formation of kink bands lead to a sequence of load drops. In the out-of-plane direction, there existed an elastic region and non-linear behaviour, but it was different from that in the in-plane direction because the loading pressed in the longitudinal direction, not in the transverse direction. Because there are some z-yarns in the out-of-plane direction, the elastic behaviour was affected by the z-yarns and the other yarns. In any region, there existed some relative damage modes.

Shear behaviour

Three-dimensional orthogonal woven fabric composites have high in-plane tensile stiffness and strength in the warp and weft directions because there is no crimp in the warp and weft yarns in the in-plane direction. Furthermore,

the composites exhibit higher interlaminar shear strength than the laminates because the *z*-direction tows exist in the through-thickness direction. Some researchers have studied the high-strain-rate response of 3-D textile structure composites under compressive and tensile loading (Hosur *et al.*, 2003; Sun *et al.*, 2005a, b, c). The shear stress–strain curve, shear failure stress and shear failure strain in quasi-static and high-strain-rate loading conditions were compared. The shear deformation and failure mode of the composite in quasi-static conditions and at high strain rates were observed to demonstrate the failure mode at different strain rates.

The shear stress–strain curves of 3-D orthogonal woven composites at various strain rates in the warp and weft directions are respectively shown in Figs 4.17 and 4.18. Figure 4.17 shows that the shear failure stress is nearly invariable with increasing shear strain rate. However, the failure strain decreased with increasing shear strain rate. The shear stiffness at different shear strain rates is increased with increasing strain rate. It can be seen from Fig. 4.18 that the shear failure stress of 3-D orthogonal woven composites increased with increasing shear strain rate, and the shear failure strain decreased with increasing shear strain rate. Further, the shear stiffness of 3-D orthogonal woven composites increased with increasing strain rate. The shear failure stress, shear failure strain and shear stiffness are listed in Tables 4.2 and 4.3 for warp and weft direction shear, respectively (Baozhong Sun and Bohong Gu, 2006).

Figure 4.19 depicts the shear failure stress of 3-D orthogonal woven composites at various strain rates in the warp and weft directions of loading.

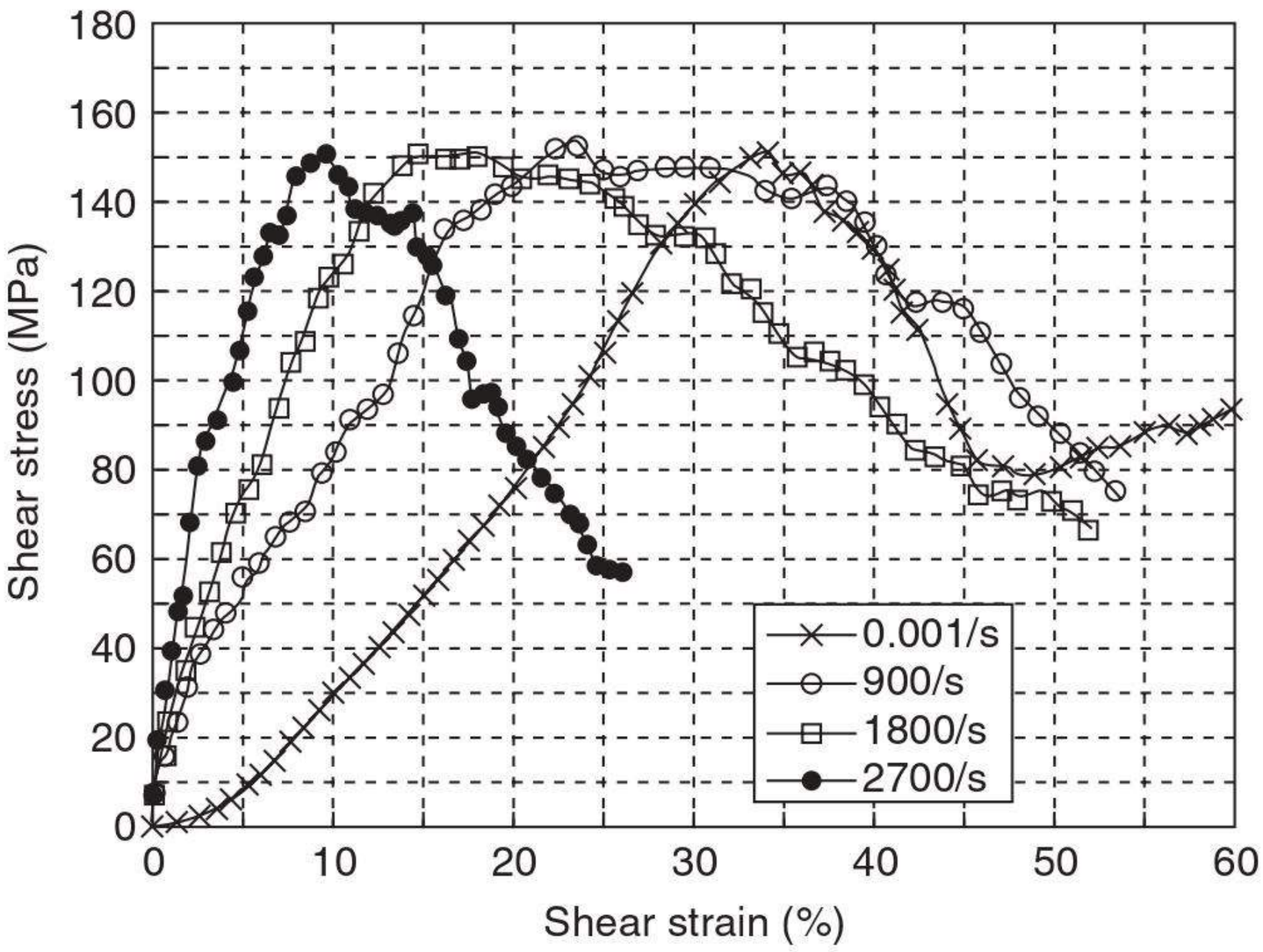

4.17 Stress–strain curves of 3-D orthogonal woven composites at various strain rates in the warp direction (adapted from Baozhong Sun and Bohong Gu, 2006).

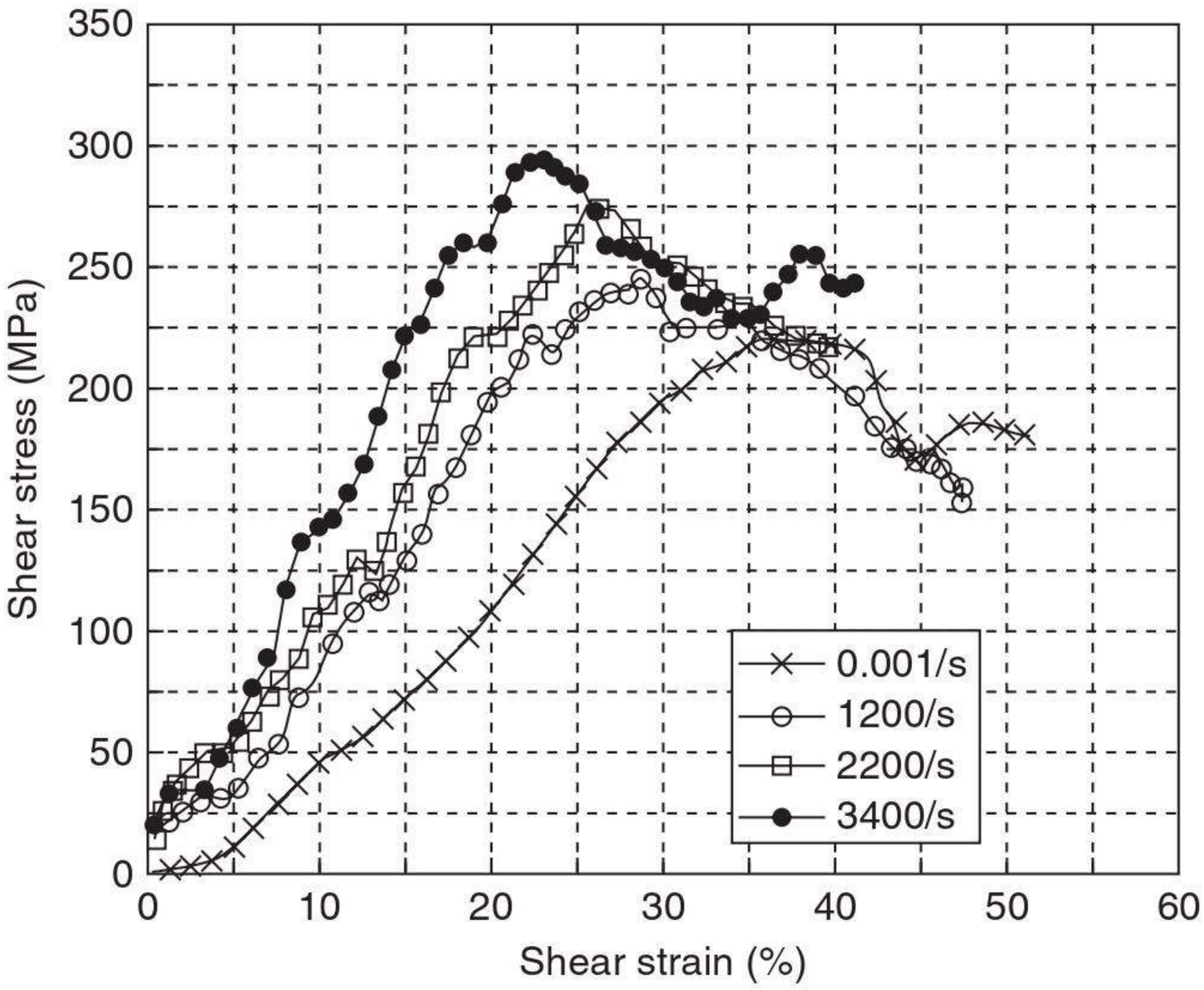

4.18 Stress–strain curves of 3-D orthogonal woven composites at various strain rates in the weft direction (adapted from Baozhong Sun and Bohong Gu, 2006).

Table 4.2 Mechanical properties of 3-D orthogonal woven composites at various strain rates in the warp direction

Shear strain (s^{-1})	Shear stiffness (GPa)	Shear failure (MPa)	Failure strain (%)
0.001	0.376	151.00	33.71
900	0.81	152.19	22.01
1800	1.27	152.00	13.64
2700	2.01	151.00	9.64

Source: adapted from Baozhong Sun and Bohong Gu, 2006.

Table 4.3 Mechanical properties of 3-D orthogonal woven composites at various strain rates in the weft-direction

Shear strain (s^{-1})	Shear stiffness (GPa)	Shear failure (MPa)	Failure strain (%)
0.001	0.630	220.02	36.01
1200	0.83	246.01	27.11
2200	1.12	270.98	23.96
3400	1.33	294.02	22.00

Source: adapted from Baozhong Sun and Bohong Gu, 2006.

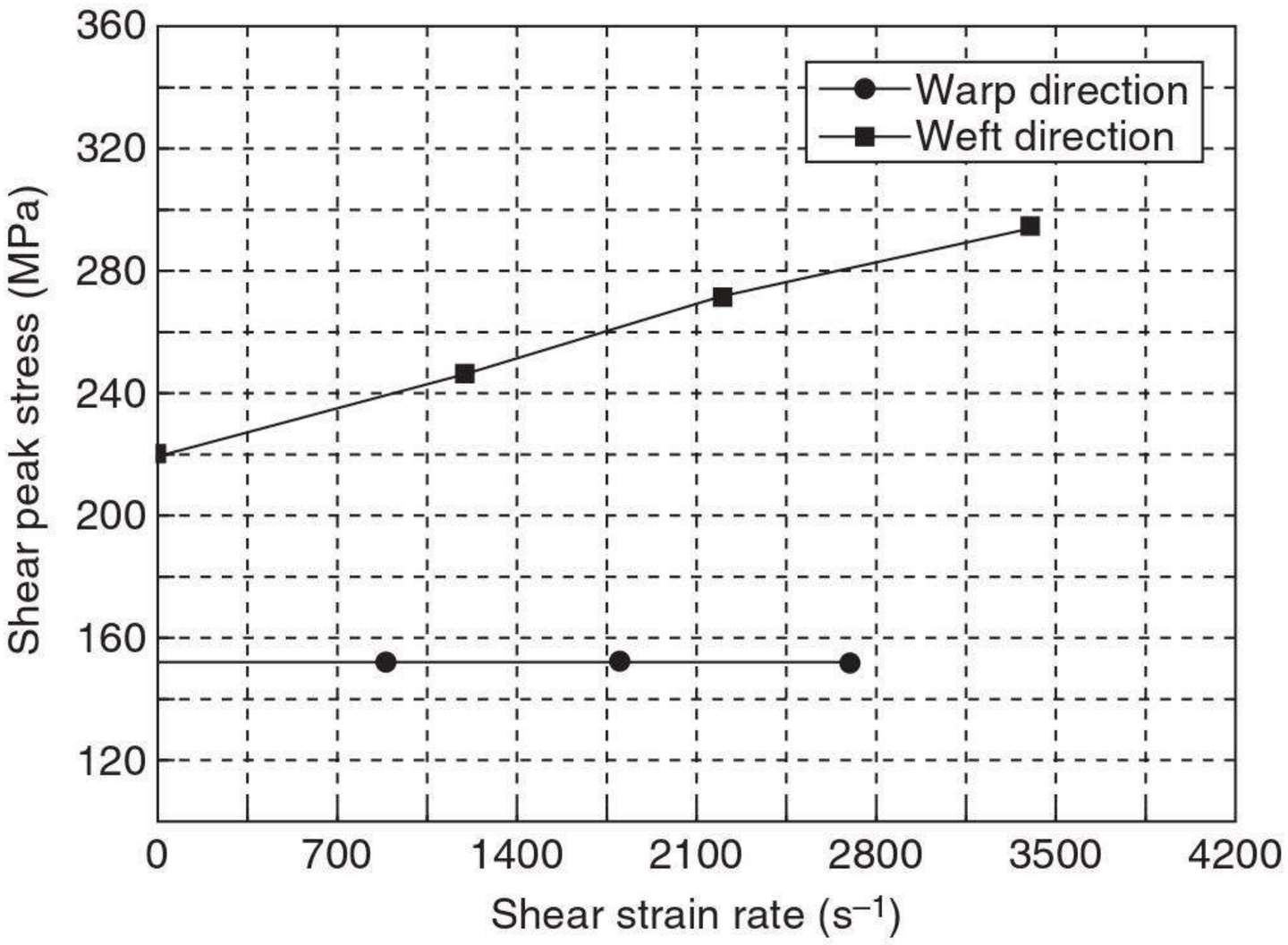

4.19 Shear failure stress of 3-D orthogonal woven composites in the warp and weft directions at various strain rates (adapted from Baozhong Sun and Bohong Gu, 2006).

From Fig. 4.19, the shear failure stress of 3-D orthogonal woven composites in the warp direction loading is nearly invariable with increasing shear strain rate. However, the shear failure stress in the weft direction loading increased with increasing shear strain rate.

The failure strain of the 3-D orthogonal woven composites in the warp and weft directions at various strain rates is shown in Fig. 4.20. The failure strain in the two directions decreases non-linearly with an increase in strain rate. Furthermore, the failure strain in the warp direction at higher strain rates decreases more rapidly compared with that in the weft direction. This shows that the failure strain in warp-direction loading is more rate-sensitive than that in weft-direction loading. From Fig. 4.20, the 3-D woven composites have larger shear failure strain in weft-direction loading than in warp-direction loading. This shows that the failure strains for loading in both the warp and weft directions are different at the same strain rate because different fibres are used for the warp and weft directions, respectively.

Figure 4.21 depicts the shear stiffness of 3-D orthogonal woven composites in two directions at various strain rates. The shear stiffness linearly increases with the strain rate in both the warp and weft directions. The shear stiffness of 3-D orthogonal woven composites in the weft direction is greater than that in the warp direction under quasi-static loading. This shows that the shear stiffness is more sensitive to shear strain rate in warp-direction loading than in weft-direction loading.

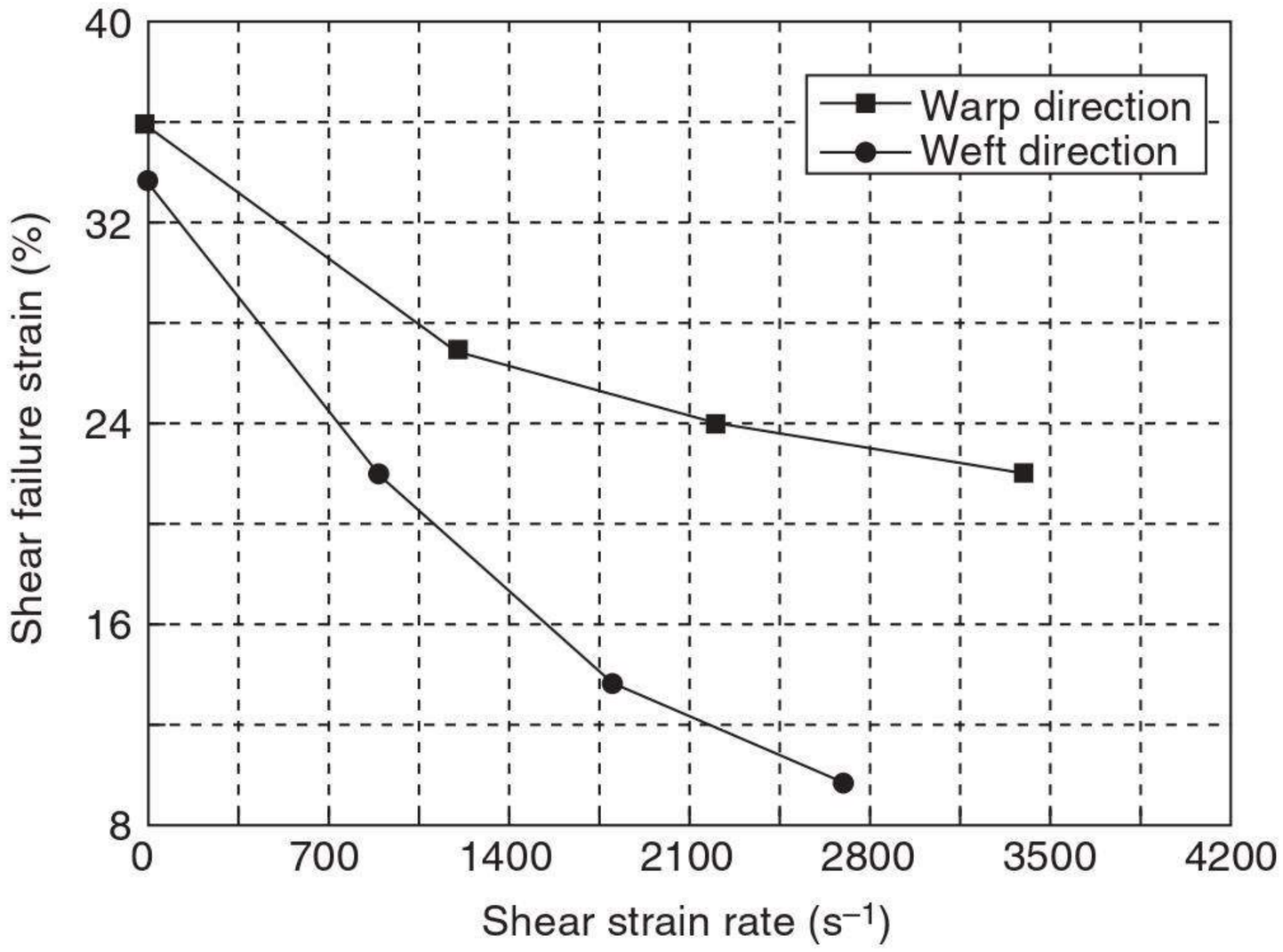

4.20 Shear failure strain of 3-D orthogonal woven composites in the warp and weft directions at various strain rates (adapted from Baozhong Sun and Bohong Gu, 2006).

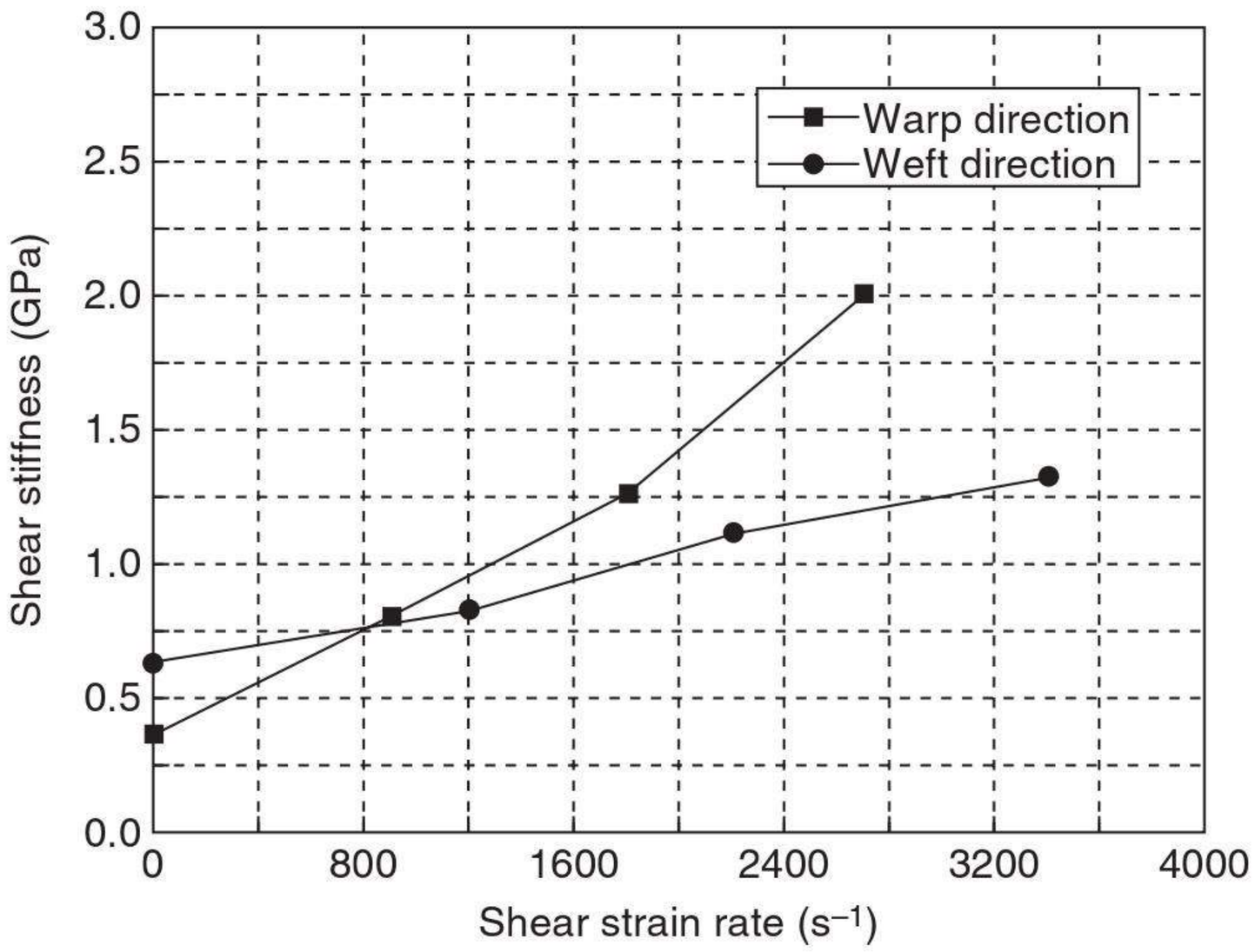

4.21 Shear stiffness of 3-D orthogonal woven composites in the warp and weft directions at various strain rates (adapted from Baozhong Sun and Bohong Gu, 2006).

Compressive behaviour

In order to understand the compressive behaviour of 3-D woven fabrics, researchers have attempted to study their effect on the properties of the final composites. In a study on the effect of fabric structure on the mechanical behaviour of 3-D woven composites, Youjiang Wang and Dongming

Table 4.4 Compression and flexural properties of 3-D woven composites

Type of fabric	Compression		Flexure	
	E (GPa) (CV%)	σ (MPa) (CV%)	E (GPa) (CV%)	σ (MPa) (CV%)
3-D woven	20.6 (3.1)	425 (5.4)	12.4 (7.2)	507 (5.6)
3-D woven (twisted yarn)	13.7 (4.8)	337 (7.7)	14.6 (3.4)	418 (4.2)

Zhao (2006) studied the compressive behaviour of 3-D woven fabrics and of 3-D woven fabrics with twisted yarns. Compressive properties such as modulus and strength were measured on the composites produced from these fabrics.

The measured compressive moduli for both composites were found to be lower than their respective tensile values (Table 4.4). This is attributed to the effect of fibre crimping, similar to the case when a bundle of wires are twisted together and then subjected to tensile and compressive loads; however, the compressive strengths for these composites are generally close to the corresponding tensile strengths. It was noticed that the specimens essentially failed in shear, with local yarn buckling and kink band formation. Such compressive failure modes are distinguished from those for composites reinforced with 2-D plain weave fabrics, in which failure associated with large-scale delamination and buckling is often observed. The bonding effect of the through-thickness yarns substantially decreased the possibility of delamination and limited the size of the failure zone.

4.5 Applications of multilayer woven fabrics

Multiple-layer woven textile fabrics are becoming one of the most important forms of reinforcement for composite materials because of their good resistance to delamination over the laminated reinforcements. Because of the 3-D integrated fibre assemblage, such structures are less prone to delamination and can offer high impact resistance.

- Multilayer woven fabrics are being used in a number of applications as composite reinforcements for defence, marine, automotive, aerospace and transportation industries. They also find applications in geotechnical engineering, the biomedical field and as protective clothing.
- In automotives, multilayer woven composites are used as drive shafts, side rails, doors, cross-members, oil pans, suspension arms, leaf springs,

wheels, quarter panels, trunk decks, hoods, hinges, transmission support, bumpers, seat frames and wheels.

- In the defence industry, 3-D woven fabric composites are ideal materials for lightweight mobile, easily transportable vehicles for tactical shelters, ballistic combat and logistic applications. They are ideal materials for aircraft and aerospace applications where high strength-to-weight ratio is required. For example, the strength of glass fibre composite is five times that of aluminium.
- In addition to structural body composites, composites are also used for interior parts such as overhead luggage compartments, sidewalls, ceilings, floors, galleys, partitions, cargo liners, etc.
- In aerospace applications, 40% of the composites are used for military applications. The applications include the wing box, forward fuselage, horizontal stabilizer, elevators, rudder, over-wing surfaces, etc.
- Three-dimensional multilayer woven fabric composites are used in space structures such as missiles, rockets and satellites. Space structures require low weight, high stiffness, a low coefficient of thermal expansion and dimensional stability, which are the main properties offered by the 3-D fabrics. The application areas of 3-D woven composites in missile systems include rocket motor cases, nozzles, skirts and interstage structures, control surfaces and guidance structural components. Structural components used in space include trusses, platforms, shells, pressure vessels and tanks.
- In the marine industry, 3-D multilayer woven fabrics are used for applications such as hull structures, fairwaters, sonar domes, antennas, floats, buoys, masts, spars, deckhouses, etc. They are also used in mine warfare vessels, tankers, trawlers, ferries, sonar domes, submarines, powerboats, racing yachts, pleasure boats, luxury yachts and laminated sailboats.
- In the medical field, multilayer woven fabrics are being used for manufacturing stents, prostheses, artificial joints and organs, implants, scaffolds, etc.
- The use of 3-D multilayer woven fabrics is also increasing in sporting goods. In particular, the graphite–boron and Kevlar–epoxy composites are used in golf carts, surf boards, hang-glider frames, javelins, hockey sticks, sail planes, sail shafts, fishing rods, snow and water skis, bows, arrows, tennis rackets, pole-vaulting poles, skateboards, bats, helmets, bicycle frames, canoes, catamarans, oars, paddles, etc.
- Other applications for multilayer woven fabrics include narrow-width webbing products where strength or abrasion resistance are desired: belting products for conveyors, dryers and paper machine clothing; filtration products; ballistic materials; ablatives; constant-thickness structural composites in which damage tolerance or through-thickness

mechanical properties are essential; and biomedical applications that utilize the high compression strength afforded by the z-fibres. In all cases there are driving technical reasons that make the 3-D woven structure more desirable than a fabricated 2-D fabric alternative.

Recently, these materials have been finding increased usage in more commercial applications, particularly in marine structures and industrial components that are very cost sensitive. Due to the availability of heavyweight fabrics/reinforcements, and the subsequent reduction in lay-up labour, 3-D fabrics can reduce the cost of the finished composite structure.

4.6 Summary

This chapter summarizes the structure, manufacture and properties of multilayer woven fabrics. Three-dimensional multilayer woven (MLW) fabrics are becoming increasingly important owing to their excellent performance: permeability, compressibility, drapeability, ease of handling and ability to conform to complex shapes. Three-dimensional multilayer woven fabrics are textile structures having fibres oriented along the three directions of a unit cell. A 3-D fabric should have three or more yarns in the thickness direction in order to distinguish itself from a planar fibre assembly. Compared with 2-D woven fabrics, multilayer woven fabrics exhibit higher through-thickness and interlaminar properties because of their integrated structure in the presence of orthogonal and/or angle interlock constructions. They offer better processability and eliminate delamination of fabrics. These 3-D woven preforms with various architectures can be fabricated using different weaving methods. Multiwarp weaving methods are used for weaving orthogonal and/or angle interlocked multilayer woven fabrics.

MLW fabrics are finding wide application in composites, sports and the aerospace industry because of their superior properties compared to 2-D woven fabrics. Three-dimensional MLW fabric preforms offer many advantages over both 2-D fabrics and other categories of 3-D preforms. Other categories of 3-D preforms require extensive modifications to existing equipment or new equipment, whereas multilayer woven fabrics can be produced using existing textile manufacturing techniques on conventional equipment with few modifications.

Three-dimensional (3-D) orthogonal woven fabric composites have high in-plane tensile stiffness and strength in the warp and weft directions because there is no crimp in the warp and weft yarns in the in-plane direction. Furthermore, the composites have higher interlaminar shear strength than the laminates because the z-direction tows exist in the through-thickness direction.

4.7 References

Adanur S (1995), Textile structural composites, in *Wellington Sears Handbook of Industrial Textiles,* Technomic Publishing, Lancaster, PA, 231–271.

Baozhong Sun and Bohong Gu (2006), Shear behavior of 3D orthogonal woven fabric composites under high strain rates, *Journal of Reinforced Plastics and Composites*, **25**, 17, 1833–1845.

Chen X, Knox R T, McKenna D F and Mather R R (1992), Simulation of multiple layer woven textile structures for composite reinforcements, *Proc. First Int. Conf. on Intelligent Systems Engineering (Conf. Publ. No. 360)*, Edinburgh, UK, 104–110.

Goerner D (1989), Double, treble and four ply cloths, in *Woven Structure and Design, Part 2 Compound Structures,* BTTG Wira House, Leeds, UK, 16–58.

Gu H and Zhili Z (2002), Tensile behaviour of 3D woven composites by using different fabric structures, *Materials and Design*, **23**, 671–674.

Guo X, Li W, Gu B and Qiu Y (2007), Effect of strain rate on compression loading of 3D woven composites in three directions, *Pigment and Resin Technology*, **36**, 1, 39–43.

Hosur M V, Adya M, Vaidya U K, Mayer A and Jeelani S (2003), Effect of stitching and weave architecture on the high strain rate compression response of affordable woven carbon/epoxy composites, *Composite Structures*, **59**, 4, 507–523.

Khokar N and Peterson E (1998), 3D fabrics through the 'true' 3D-weaving process, *World Textile Congress on Industrial, Technical and High Performance Textiles,* University of Huddersfield, UK, 15–16 July, 175–181.

Ko F K (1989), Three-dimensional fabrics for composites, in *Textile Structural Composites* (ed. Tsu-Wei Chou and Frank K. Ko), Elsevier, New York, 129–171.

Mohamed M H (1990), Three-dimensional textiles, *American Scientist*, **78**, 6, 530–541.

Naik N K, Azad N M and Durga Prasad P (2002), Stress and failure analysis of 3D angle interlock woven composites, *Journal of Composite Materials*, **36**, 93–123.

Pastore C M and Cai Y J (1990), Applications of computer aided geometric modeling for textile structural composites, *Proc. 2nd Int. Conf. on Computer Aided Design in Composite Material Technology*, Brussels, Belgium, 25–27 April.

Potluri P, Porat I and Sharma S (2000), Three-dimensional weaving and moulding of textile composites, *Textiles Magazine*, Issue 4, 14–17.

Sun B Z, Gu B H and Ding X (2005a), Compressive behavior of 3D angle-interlock woven fabric composites at various strain rates, *Polymer Testing*, **24**, 4, 447–454.

Sun B Z, Yang L and Gu B H (2005b), Strain rate effect on four-step three-dimensional braided composite compressive behavior, *AIAA Journal*, **43**, 5, 994–999.

Sun B Z, Liu F and Gu B Z (2005c), Influence of strain rate on the uniaxial tensile behavior of 4-step 3D braided composites, *Composites, Part A*, **36**, 11, 1477–1485.

Watson W (1955), *Advanced Textile Design* (3rd edn), London: Longmans, Green.

Yi H L and Ding X (2004), Conventional approach on manufacturing 3D woven preforms used for composites, *Journal of Industrial Textiles*, **34**, 1, July, 39–50.

Youjiang Wang and Dongming Zhao (2006), Effect of fabric structures on the mechanical properties of 3-D textile composites, *Journal of Industrial Textiles*, **35**, 3, January, 239–256.

5

Tensile properties of multiaxial warp-knitted fabrics

Abstract: With the increasing application of multiaxial warp-knitted (MWK) reinforced composites in the automotive and other industries, the need to determine their mechanical properties, especially the tensile-extension behaviour, impact on the energy absorption capacity and damage tolerance properties, is becoming more and more important to ensure the stability and safety of the designed structures. The tensile properties of an MWK structure in a particular direction are governed by those of the yarns inserted in that direction. Many researchers have studied MWK fabrics, but very few have attempted to model their mechanical properties. In this chapter, a macroscopic modelling approach dealing with fabric structure under uniaxial tensile deformation is described to give an understanding of the tensile properties of MWK fabrics.

Key words: multiaxial warp-knitted (MWK) fabrics, tensile behaviour of MWK fabrics, modelling uniaxial tensile deformation, stress–strain relationship.

5.1 Introduction

Multiaxial warp-knitted (MWK) fabrics were formerly developed as substrates for flexible coated fabrics. They have an important role in the field of industrial applications due to their outstanding mechanical properties. At the beginning of the 1990s, MWK fabrics entered the field of rigid structural composites to produce aerospace-quality components, marine parts and automotive frames. As one of the 3-D composite preforms, MWK fabrics are attracting more and more interest due to their low production costs, high production efficiency, structural integrity, flexibility in design, high tear resistance and improved through-thickness strength. In addition to their good ease of handling and production economics, MWK structures also provide conformability to complex shapes, flexibility in the principal yarn directions and improved through-thickness strength.

Nowadays, MWK structures have a wide range of applications – from geotextiles, pneumatic materials and construction materials to automobiles, aerospace-quality components as well as vessel-body parts due to their desired mechanical properties, flexibity in design and low production cost (Kaufmann, 1991). In MWK structures, all the layers of insertion yarns are placed in perfect order and show the uniformity of the non-crimped

parallel yarns. While the insertion yarns play a principal role in the plane reinforcement, the stitch yarns can provide the through-thickness reinforcement, and therefore produce a significant increase in damage tolerance, structural integrity and out-of-plane strength.

With the increasing application of MWK-reinforced composites in automotive and other industries, the need to determine their mechanical properties – especially their tensile-extension behaviour, impact on energy absorption capacity and damage tolerance properties – is becoming increasingly important in order to ensure the stability and safety of the designed structures.

MWK structures can be produced in a single knitting process. In addition to good ease of handling and production economics, MWK structures also conform to complex shapes and are flexible in the principal yarn directions. The mechanical properties of MWK structural composites, especially out-of-plane strength and impact behaviour, may be superior to those of conventional woven laminated composites due to the elimination of fibre crimp in the insertion yarns and to the presence of the through-thickness reinforcing stitch loops.

5.2 Tensile behaviour of multiaxial warp-knitted fabrics

Recent textile and composite literature reflects the growing interest in the strength properties of MWK-reinforced composite materials. The tensile performance of MWK fabrics has also been a much-discussed topic within the published literature. As MWK fabrics have more complex geometric architectures than woven and braided fabrics, most of the investigation has focused upon the general tensile properties (Dexter and Hasko, 1996). Only limited attention has been given to modelling the strength properties and knitting parameters of MWK fabrics, such as loop lengths, shapes and densities, that will allow a more detailed and quantitative analysis. However, a number of researchers have been working on this area and they have produced some meaningful results and conclusions.

Typical MWK fabrics have a complex structure in three dimensions to improve damage tolerance and reliability. All layers of the insertion yarns in a MWK structure are placed in an expected order and show the uniformity of the non-crimped parallel yarns. The insertion yarns play a principal role in the plane layer and with the increase of binding points, the symmetry of binding distribution and the increase of stitch yarn linear densities, the properties of MWK structures can be greatly improved. Therefore, MWK structure can provide a significant increase in damage tolerance, structural integrity and out-of-plane strength of the reinforced structure (Ko *et al.*, 1980, 1982, 1985, 1986).

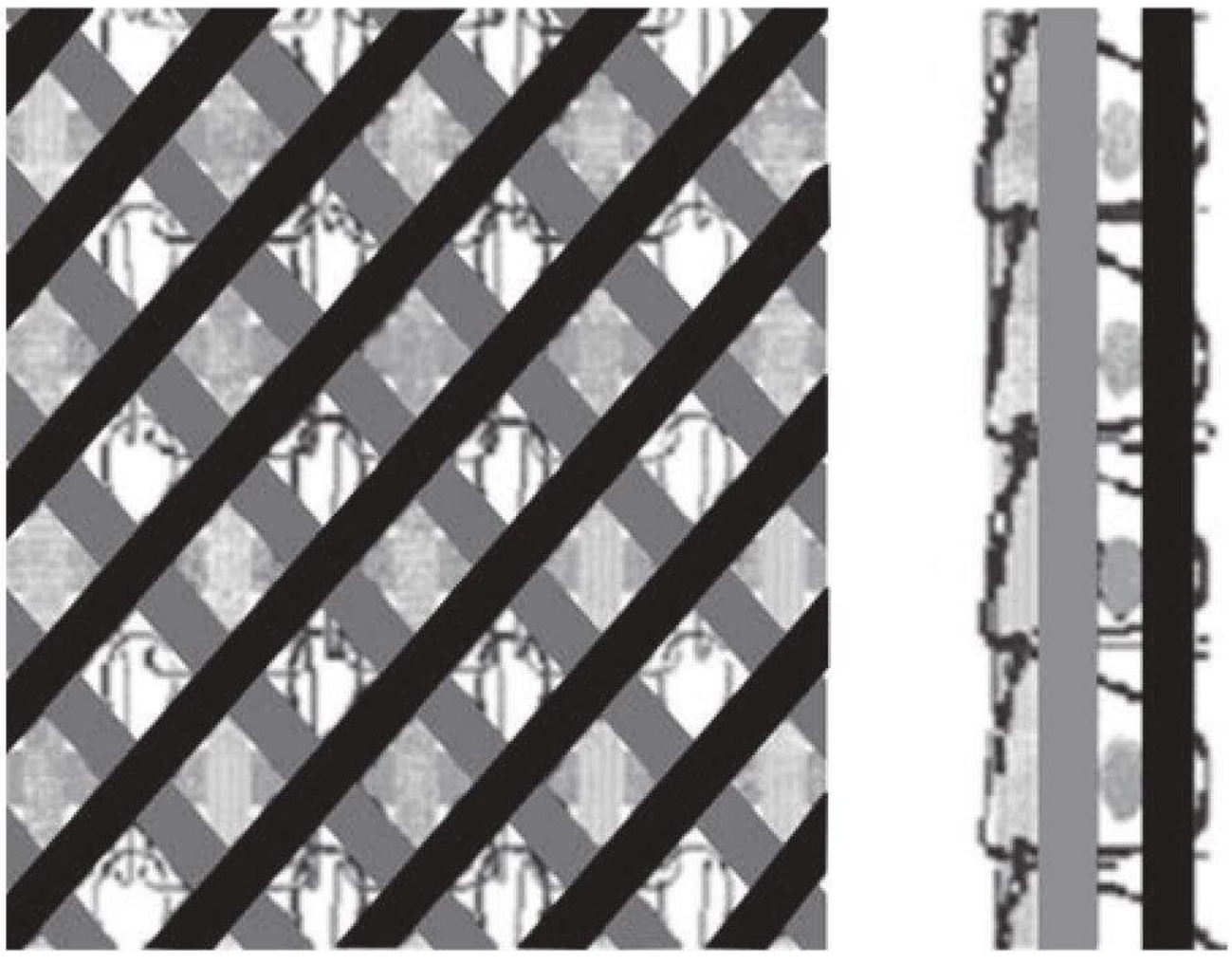

(a) Common MWK structure

(b) Improved MWK structure

5.1 An improved MWK structure with double-loop pillar stitch.

Zhou Rongxing *et al.* (2004) studied the tensile properties of MWK structures produced with different basic stitches for composite reinforcement. In order to compare these structures, an experimental study of the tensile properties of MWK structures was carried out (as per Chinese National Standard GB7689.6-89 and GB/T7690-1989 respectively) using tricot stitch and double-loop stitch, as shown in Fig. 5.1. The results demonstrated that double-loop pillar stitches have better mechanical properties. The in-plane mechanical properties of an MWK structure in a test direction mainly depend on the properties of the insertion yarns in that direction. The tensile properties were better in the wale direction than in other directions, and the properties in the diagonal were the poorest. In addition, the authors deduced that the basic stitch has an obvious influence on the mechanical properties of the MWK structure.

Chen Nanliang (2002) has investigated the effect of the materials and structures of warp-knitted ground on the tensile strength of the composite reinforced with MWK fabrics. He reported that the material has a great influence on tensile strength: the tensile property of glass fibre used as warp-knitted ground is much better than that of polyester fibre in both the horizontal and vertical testing directions. In addition, different testing directions have different and varied effects on tensile properties. In the horizontal testing direction, the tensile property shows no obvious difference when using different warp-knitted binding stitches, i.e. plain tricot ground and cord stitch. In the vertical testing direction, however, tensile strength with a cord stitch ground is apparently better than with tricot.

Shen Wei (2002) tested and compared the tensile property of biaxial warp-knitted fabric with that of plain weave fabric in a study that is very meaningful for the understanding of the tensile characteristics of MWK fabrics. In this research, the relationship between the tensile strength of biaxial warp-knitted fabric and the density of the yarns was studied by means of regression analysis, and some characteristics and advantages of the biaxial warp-knitted fabric were also explored. It was observed that the tensile behaviour of biaxial warp-knitted fabric and plain woven fabric will show very different tensile strength curves. The potential of the yarn's tensile resistance can contribute more to the whole fabric's tensile performance, especially insertion yarns with high modulus. The tensile strength of biaxial warp-knitted fabric has a linear relationship with the insertion yarns along the tensile stress direction and the density of the insertion yarns with high tensile resistance. The tensile potential of yarns in biaxial warp-knitted fabric can be used more efficiently than in plain woven fabric, and insertion methods will cause different utilization of the yarn's strength.

The tensile behaviour of MWK fabrics has been demonstrated by Chen Nanliang and co-workers (2001, 2002). Their tests confirmed that the tensile stress, strain and elastic modulus of MWK fabric were superior to those of woven fabrics and that the tensile property depends on the structural parameters, such as the insertion methods of the binding yarns and the yarn's strength and density in the test direction. These conclusions are in agreement with the work of Shen Wei (2002). Although Shen Wei's conclusions were based on the testing of biaxial warp-knitted fabrics, the principle – especially the tensile mechanism – is very similar. In addition, Chen Nanliang suggested that existing test methods for tensile properties cannot at present meet the testing requirement for the diagonal yarn's exact contribution to the tensile properties of the whole fabric.

The interweave crimp of woven fabric is a factor influencing the tensile stiffness and strength of woven fabric, and its reinforced composites, because of the interlacement of warp and weft yarns. Contrary to the construction of woven fabrics, in a multiaxial, multilayer warp-knitted (MMWK) fabric the warp (0°), weft (90°) and bias ($\pm\theta$) yarns are held together by a chain or tricot stitch yarn through the thickness direction. There are no crimps of the warp, weft and bias yarns in MMWK fabrics. Hence, tensile stiffness and tensile strength will reach a maximum value compared with other kinds of fabrics. MMWK fabric-reinforced composites, like unidirectional composites, also have high values of tensile stiffness and strength along warp, weft and bias directions.

The deformation behaviour of MWK fabric has been studied under bending, tension, shear and friction, and the research revealed that biaxial and quadraxial fabrics demonstrated fairly isotropic behaviour in bending, tension and friction, but they displayed anisotropic deformation behaviour in shearing under low load (Lomov *et al.*, 2003). In a study of MWK fabrics,

the tensile extension properties and deformation mechanisms of multiaxial non-crimp fabrics have been investigated (Kong *et al.*, 2004). This study evaluated the extension properties of a variety of biaxial and triaxial fabrics, consisting of continuous E-glass yarns stitched together with 0.14 mm diameter polyester thread. The results may be summarized as follows.

Figure 5.2 represents curves of load against gross longitudinal strain for the biaxial fabrics. The curves show a gradual rise in the load resistance until a strain of 0.15, above which the resistance to bias deformation increases rapidly for biaxial fabric type I. However, both types of biaxial fabric show a lower resistance to bias extension than plain woven fabric. Figure 5.3 shows the load–strain curves for the triaxial fabrics that were warp knitted with different line tensions on the stitch thread. It can be seen that the resistance to bias loading of the triaxial fabric increases with the line tension of the stitches, although in all cases the deformation load resistance was lower than for woven fabric.

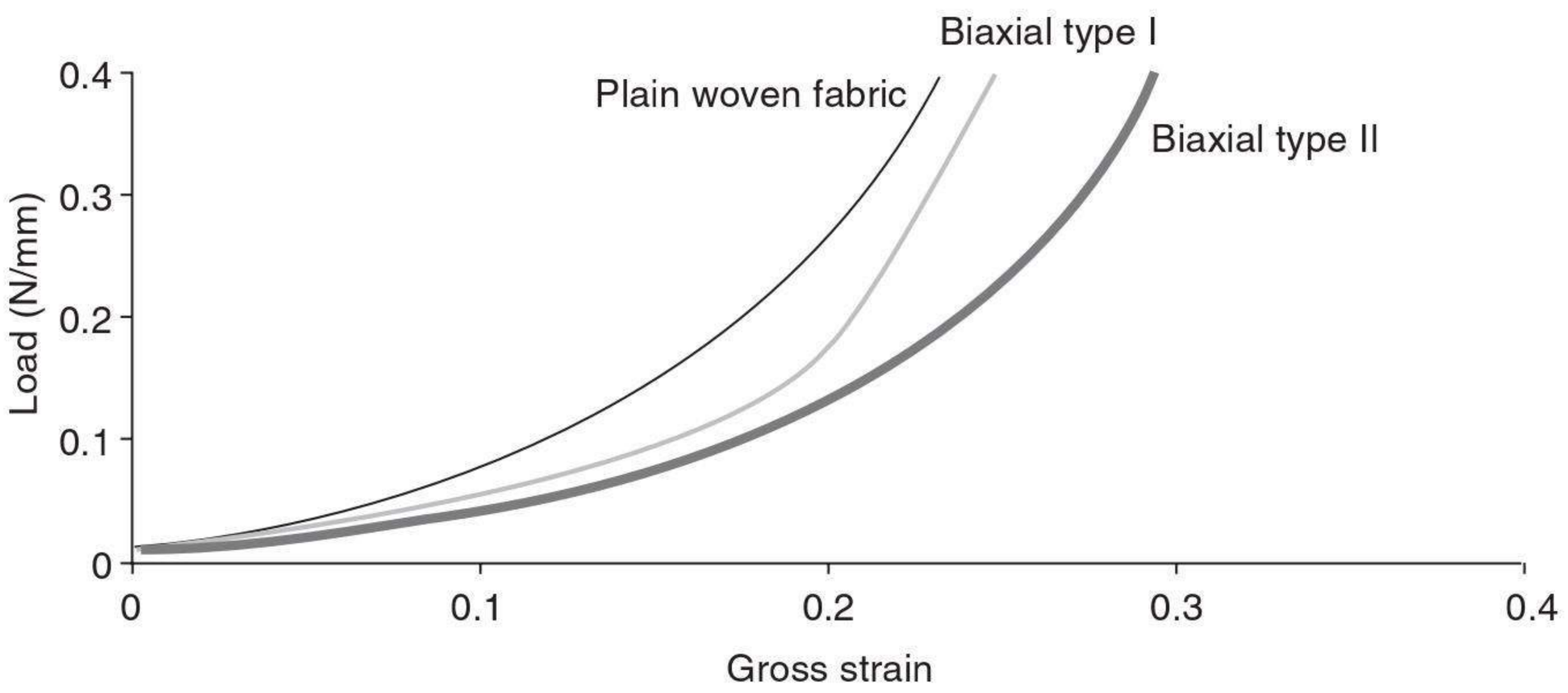

5.2 Gross bias extension curves for biaxial and plain woven fabrics.

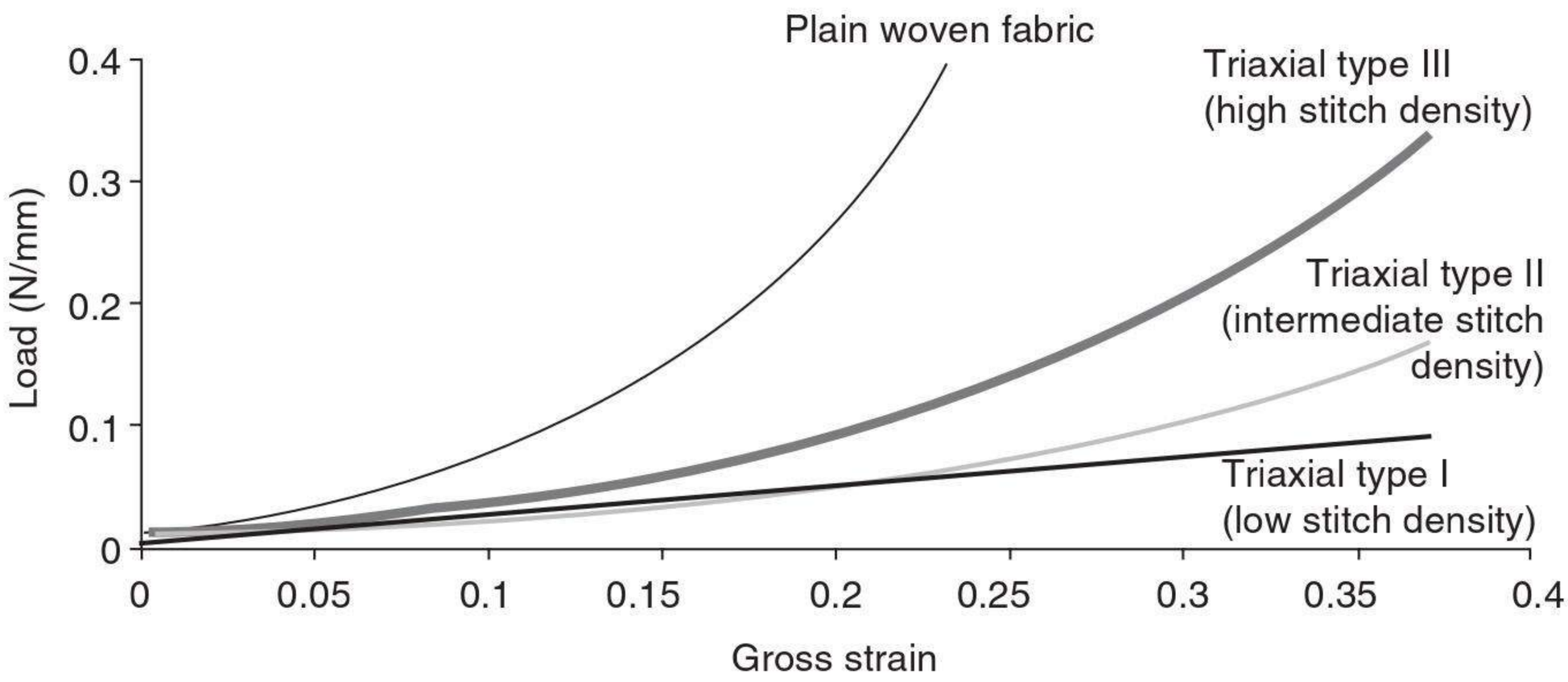

5.3 Bias extension curves for triaxial-type fabrics with different stitch-line tensions and for plain woven fabric.

In another interesting study (Pattyn *et al.*, 1999), the tensile extension properties of MWK fabrics and multilayered, multiaxial stitched preforms were compared. It was observed from the results that both types of fabrics exhibited a high in-plane performance. For stitched multiaxial fabrics, the elastic behaviour is more or less isotropic, while the strength behaviour is anisotropic (more pronounced for carbon). For glass-epoxy, the elastic performance is slightly better for the stitched multiaxial than for the regular MWK fabric, and there was no difference for carbon-epoxy. The results for strength and elongation properties are presented in Tables 5.1 and 5.2.

The mechanical properties of an improved MWK fabric structure (Fig. 5.4) for composite reinforcement were reported by Zhou Rongxing *et al.* (2004). The MWK structure with double-loop pillar stitch was used in this study and showed better mechanical properties than structures using other stitches. The tensile properties of different MWK structures in the weft and warp directions are presented in Fig. 5.4 and test result data are summarized in Table 5.3.

The above study showed that MWK structures with double-loop pillar stitch have better mechanical properties than the common MWK structure with tricot stitches. It can be seen that the breaking force for MWK structures with double-loop pillar stitch is about 5–7% higher than for MWK structures with tricot stitch, in both weft and warp directions. This result confirms that the MWK structure with double-loop pillar stitch exhibits better mechanical properties. However, the increased breaking force depends on the test direction. The increase in the weft direction was a little higher than that in the warp direction. This phenomenon was explained by the fact that even if the underlaps in the double-loop pillar stitches were more oriented in the weft and warp directions than in the tricot stitch, their contribution to the breaking forces in the weft direction was more important than in the warp direction. The results also showed that the stitch yarn linear density had an obvious influence on the breaking force. This is normal because the stitch yarn with higher linear density can undertake higher yarn-breaking force.

The effects of the basic stitches on the breaking elongation were not obvious, however. The differences in the breaking elongation of the improved MWK structure and the common MWK structure in all test directions were very small. This result indicates that the MWK structures are stable and their breaking elongations are independent of the basic loop structures.

Furthermore, the tensile properties of the MWK structures were visibly regular in different test directions. As illustrated in Fig. 5.4, the tensile breaking force of all the specimens in the warp yarn direction was a little higher than those in the weft yarn direction. There are two reasons for this.

Table 5.1 Elastic properties of multiaxial warp-knitted fabrics

Fabric	Angle	V_f	Young's modulus E (GPa)				Poisson's ratio v			
			Exp.	Standard deviation	Theor.	Exp./theor.	Exp.	Standard deviation	Theor.	Exp./theor.
Glass-epoxy										
LIBA	0°	51.2%	16.2	0.6	17.63	92%	0.30	0.03	0.30	102%
	90°	51.2%	17.4	1.3	17.63	99%	0.33	0.01	0.30	110%
	67.5°	51.2%	17.6	0.5	17.42	101%	0.32	0.03	0.31	103%
Stitched multiaxial	0°	45.0%	16.4	0.3	15.63	105%	0.33	0.00	0.30	112%
	90°	45.0%	16.8	0.7	15.63	107%	0.35	0.02	0.30	116%
	67.5°	45.0%	15.2	0.1	15.44	99%	0.35	0.02	0.31	114%
Carbon-epoxy										
LIBA	0°	52.6%	41.7	1.3	42.34	99%	0.34	0.01	0.27	124%
	90°	52.6%	43.3	2.4	42.34	102%	0.32	0.05	0.27	117%
	67.5°	52.6%	43.9	1.1	40.99	107%	0.37	0.05	0.29	126%
Stitched multiaxial	0°	40.8%	34.6	1.7	33.25	104%	0.35	0.03	0.28	127%
	90°	40.8%	33.2	1.7	33.25	100%	0.34	0.02	0.28	123%
	67.5°	40.8%	34.4	1.1	32.22	107%	0.34	0.02	0.30	114%

Source: adapted from Pattyn *et al.*, 1999.

Table 5.2 Strength properties of multiaxial warp-knitted fabrics

Fabric	Angle	V_f	*S* (MPa)			
			Exp.	Standard deviation	Theor. (LPF)	Exp./theor.
Glass-epoxy						
LIBA	0°	51.2%	319	15	334	96%
	90°	51.2%	359	13	334	108%
	67.5°	51.2%	301	4	330	91%
Stitched multiaxial	0°	45.0%	320	5	256	125%
	90°	45.0%	361	15	256	141%
	67.5°	45.0%	329	15	175	188%
Carbon-epoxy						
LIBA	0°	52.6%	548	27	585	94%
	90°	52.6%	573	30	585	98%
	67.5°	52.6%	354	15	560	63%
Stitched multiaxial	0°	40.8%	547	25	476	115%
	90°	40.8%	538	16	476	113%
	67.5°	40.8%	394	20	468	84%

Source: adapted from Pattyn *et al.*, 1999.

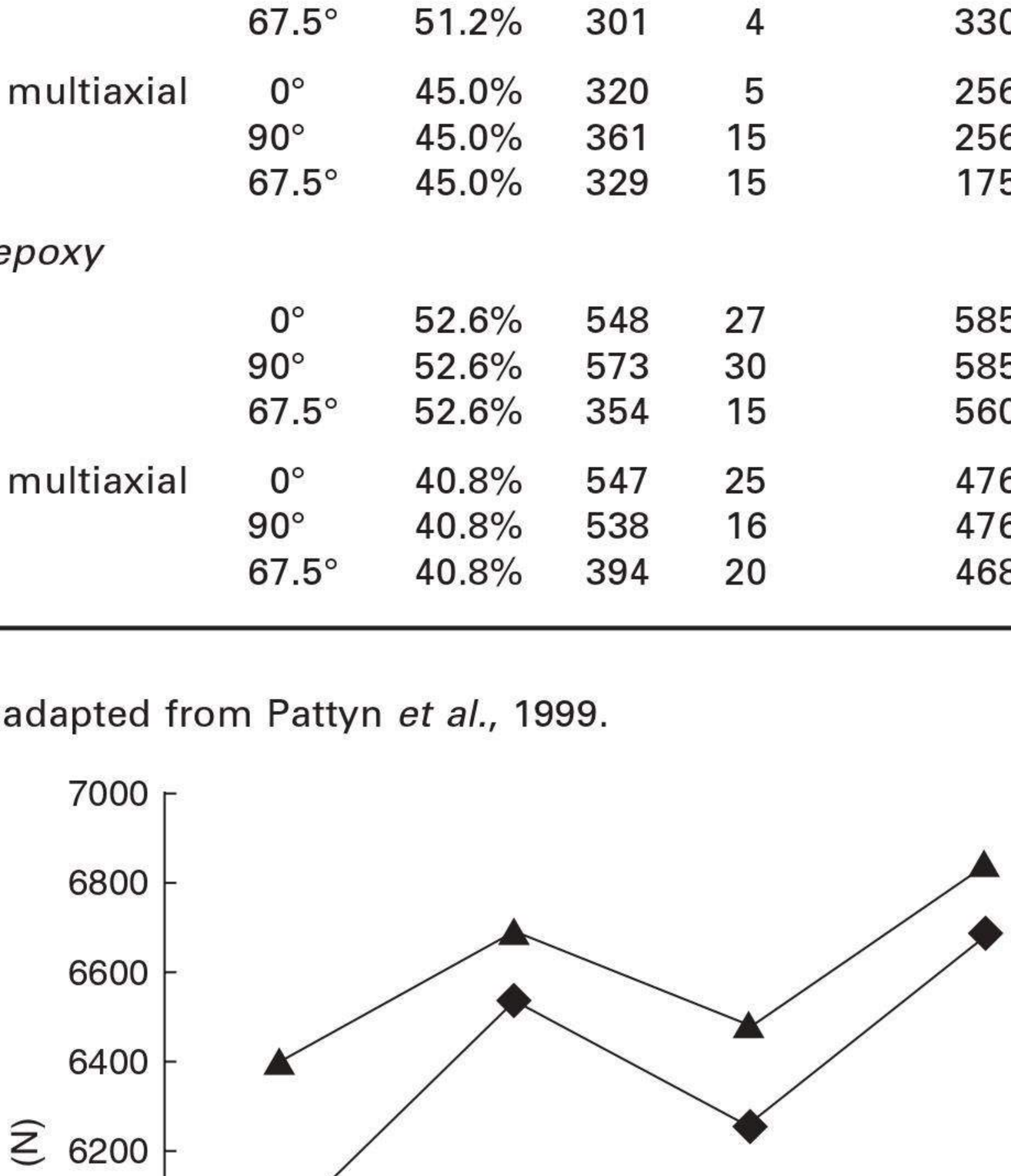

5.4 Tensile properties of different MWK structures in the weft and warp directions.

Table 5.3 Tensile data on MWK fabrics

	Specimen	Stitch yarn, dtex			
		75		150	
		Testing direction		Testing direction	
		0°	90°	0°	90°
Breaking force, N	EQt	6217.6	6402.7	6258.2	6486.5
	EQd	6538.1	6691.2	6693.1	6849.4
Increase of breaking force, %	–	5.15%	4.51%	6.95%	5.59%
Breaking elongation, mm	EQt	7.49	7.12	6.98	7.11
	EQd	7.58	7.71	6.20	6.14

Source: adapted from Zhou Rongxing *et al.*, 2004.

Firstly, the yarn densities of the insertion yarns in different directions are slightly different due to the setup requirements of the knitting machine; and secondly, the weft yarns are subjected to more damage than the warp yarns when the needles go through the fabric during the knitting process.

In addition, the tensile strength of the improved MWK structure depends on the direction. Improvement in the weft direction was better than that in the warp direction. The basic stitches had no influence on the breaking strength and elongation. The tensile properties of the MWK structure in a direction are governed by those of the yarns inserted in that direction.

5.3 Modelling tensile properties of multiaxial warp-knitted fabrics

Unlike traditional woven fabrics, MWK fabric does not possess an interlaced structure. Each inserting system has a series of uncrimped parallel yarns, which account for some intrinsic advantages of these fabrics, such as fast response to stress, which means a higher initial Young's modulus and a high percentage of the usable yarn potential (Chou and Ko, 1989).

Many researchers have studied MWK fabrics, but very few have attempted to model their mechanical properties. A meso-modelling approach for coupled drape and failure simulation of a biaxial non-crimp fabric with tricot stitch was carried by Creech and Pickett (2006).

There are probably three major reasons for the little use of modelling approaches. Firstly, since the inserting yarns are not interlaced with one

another as in woven structures, slippage between yarns occurs very easily and is always accompanied by yarn rotation. This will obviously make any analysis complex and difficult. Particularly when the force method (Kawabata *et al.*, 1973) is used, the stress distribution on a single inserting yarn in the deformed state is nearly impossible to determine if both the frictional force and the interaction between the inserting yarns and stitching loops are considered. In addition, Kilby's trellis method (Kilby, 1963) cannot be applied here since the assumptions made in his paper are impossible for MWK fabrics.

Secondly, incorporating a stitching yarn system such as chain or tricot provides MWK fabrics with the properties of both woven and knitted fabrics to some degree. It is thus very difficult to measure the effect of the stitching yarn system. Thirdly, the non-uniform deformation of different geometric unit cells, meaning that different unit cells will deform differently, is an unavoidable problem in modelling the mechanical properties of MWK fabrics. This is illustrated in Fig. 5.5 (after deformation, the line p–p is changed into p*–p*). The deformations of cells 1, 2 and 3 are different, so there is extra complexity with the unit cell method (Du and Ko, 1996).

In this chapter, a macroscopic approach is developed, dealing with fabric structure under uniaxial tensile deformation, in order to tackle the above-mentioned difficulties. A model for uniaxial tensile deformation is obtained, which is justified by Instron 4466 tensile testing. In addition, a formula for calculating the tensile modulus of the fabric in any direction is presented.

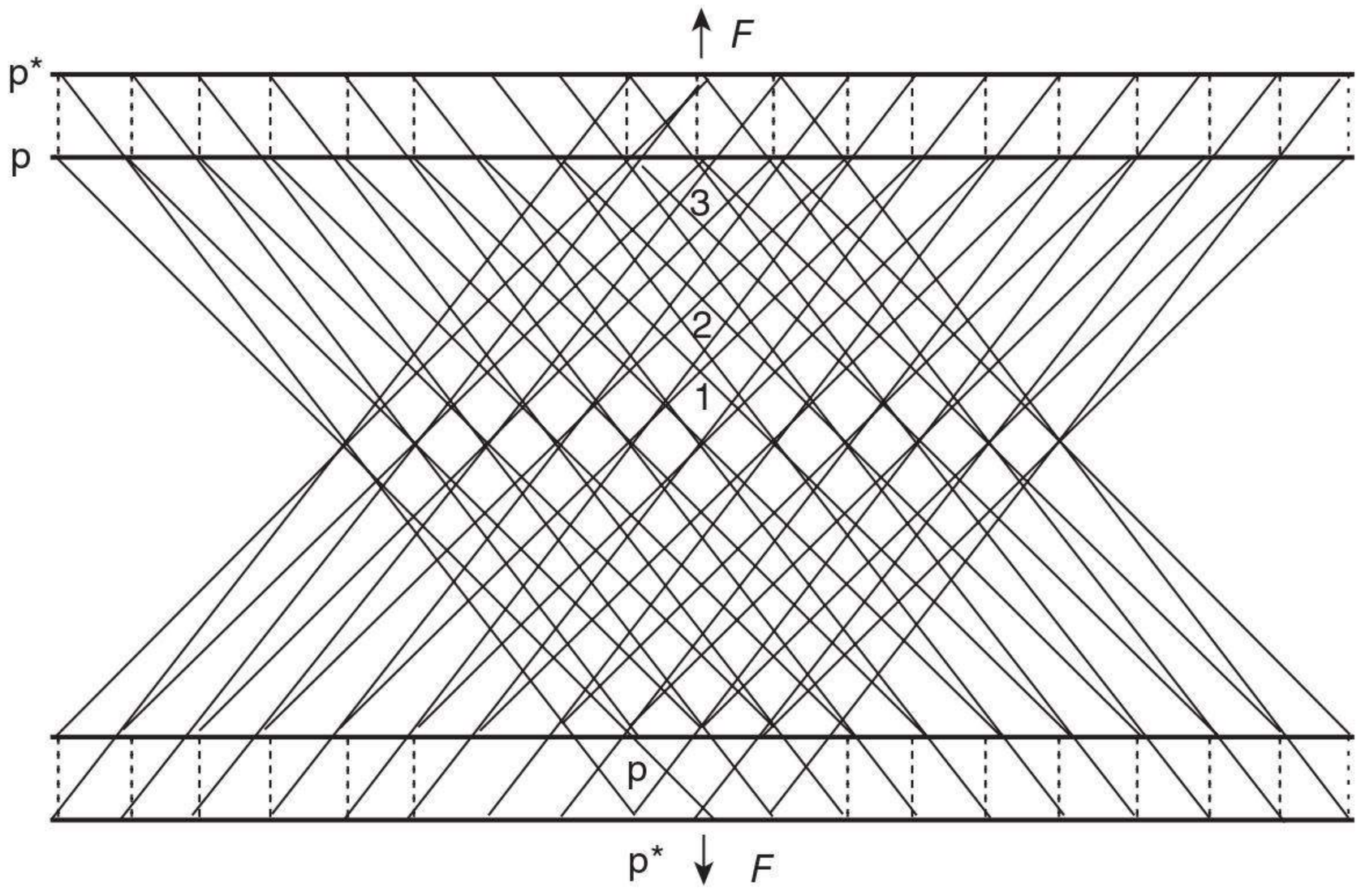

5.5 Different deformations of different unit cells in an MWK fabric under uniaxial stretch.

5.3.1 Theory

The modelling of the tensile stress–strain relationship of MWK fabrics is illustrated in this section. The following notations are valid throughout this chapter:

Subscript i (i = 1–4), where 1 = warp yarn, 2 = weft yarn, 3 = bias yarn ($+\theta$) and 4 = bias yarn ($-\theta$)
E = tensile modulus of the fabric, kg/cm
E_L = tensile modulus of a single inserting yarn, kg/cm
F = tensile force exerted on unit length of fabric, kg/cm
F_{is} = resultant of forces along the axis of a single inserting yarn (i = 1–4), kg
F_{isR} = tensile force exerted on a single inserting yarn in the stretching direction (i = 1–4), kg
F_L = tensile force exerted on unit length of tricot fabric, kg/cm
$f_i(\ )$ = function of the stress–strain relationship of a single inserting yarn (i = 1–4)
f_{is} = resultant frictional forces along the axis of a single inserting yarn (i = 1–4), kg
L_0 = sample length in the undeformed state, cm
L_0' = fabric length in the deformed state, cm
L_i = yarn length in the undeformed state, cm
L_i' = yarn length in the deformed state, cm
ΔL = elongation of the fabric after deformation, cm
n_i = number of yarns per unit length of fabric along the direction perpendicular to the yarn's axis, /cm
n_i' = number of yarns per unit length of fabric along the direction perpendicular to the stretching direction, /cm
W_0 = sample width, cm
ε = strain of the fabric after deformation, %
ε_i = strain of inserting yarns after deformation, %
θ = angle between the warp yarn axis and the tensile force direction along the clockwise direction, arc
$\pm\theta_0$ = angle between the bias yarn axis and the warp yarn axis, arc (the plus sign represents the angle from the warp yarn axis to the bias yarn axis along the clockwise direction, and minus is along the counterclockwise direction)
$\Delta\theta_i$ = angle of an inserting yarn's rotation after deformation, arc

5.3.2 Basic assumptions and approximations

In order to proceed, it is necessary to make four assumptions to simplify the analysis. First, the fabric is in a small planar strain state; second, the

yarns in each inserting system remain straight and parallel to one another, both before and after deformation; third, $\Delta\theta_i$ values are small enough to permit the neglect of the second-order and higher terms when expanding the related functions into Taylor's series; and fourth, one can neglect the possible waviness of inserting yarns.

5.3.3 Modelling of uniaxial tensile deformation

The model of a tensile stress–strain relationship is based on the simplified fabric structure in Fig. 5.6. A macroscopic approach, rather than a unit cell structure, is used for the analysis. For clarity, stitching loops in MWK fabrics are also omitted. In Fig. 5.6, the bold lines represent inserting yarns in the deformed state, while the fine lines represent those in the undeformed state.

Relationships between ε and ε_i

According to Fig. 5.6, it is easy to obtain the following equation:

$$\varepsilon = \frac{\frac{1}{2}\Delta L + \frac{1}{2}\Delta L}{L_0} = \Delta L / L_0 \qquad 5.1$$

In order to determine the relationship between ε and ε_i (i = 1–4), we take the warp inserting yarn as an example, as shown in Fig. 5.7. The relationship between ε and ε_i belongs to the scope of a plane-strain transformation (from

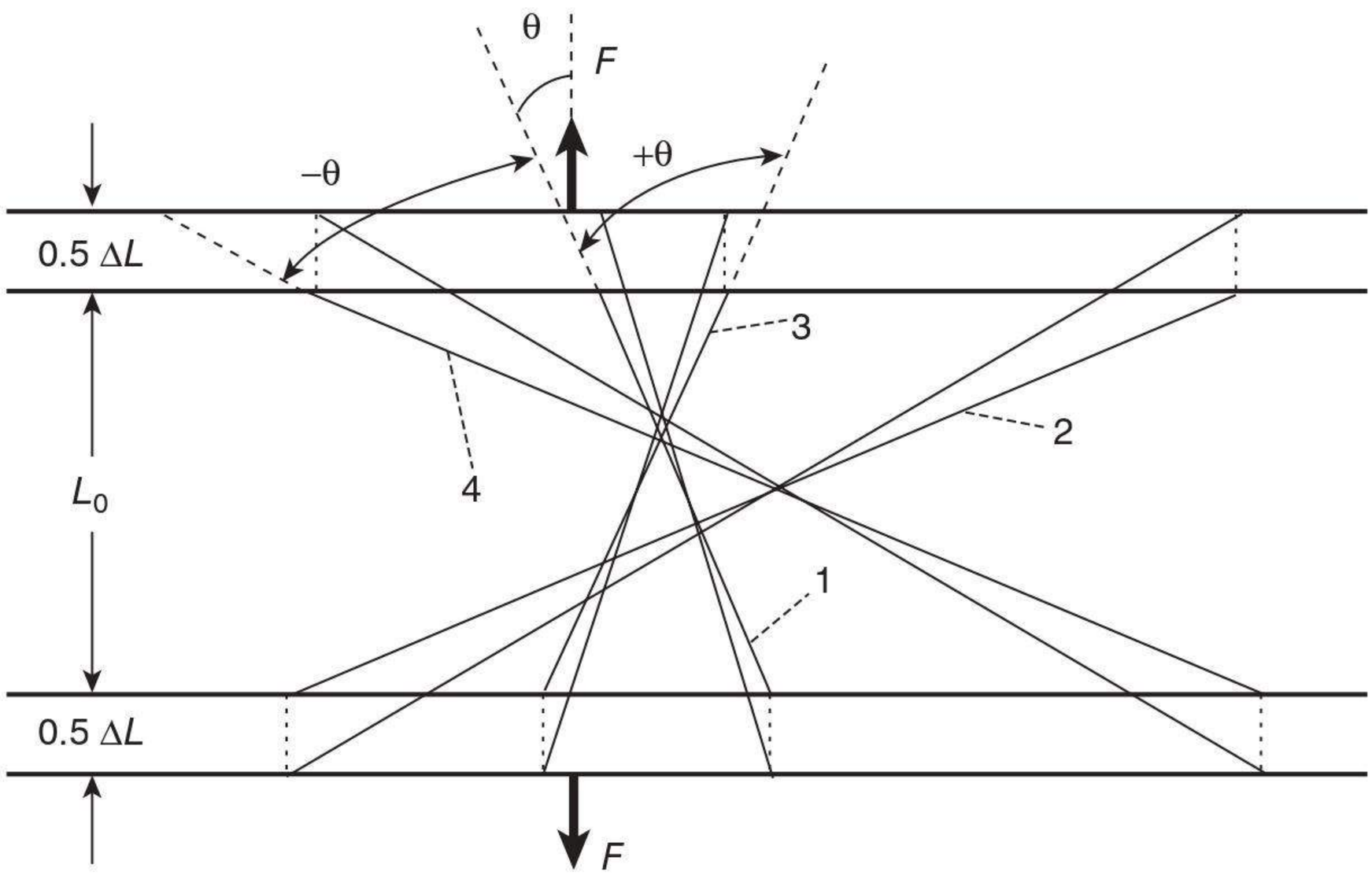

5.6 Uniaxial tensile deformation of an MWK fabric.

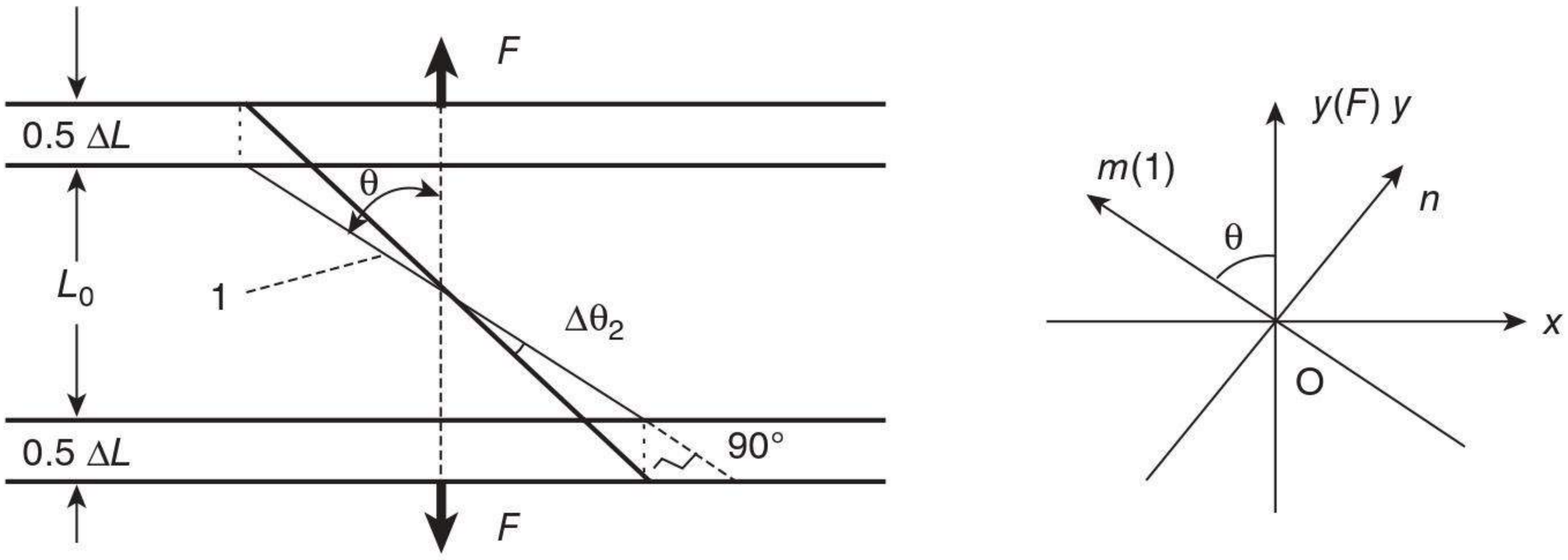

5.7 Tensile deformation of a single warp inserting yarn.

off-axis to on-axis) in elasticity. The formula for transformation is as follows (see the coordinates in Fig. 5.7):

$$\begin{bmatrix} \varepsilon_m \\ \varepsilon_n \\ \frac{1}{2}\gamma_{mn} \end{bmatrix} = [T] \begin{bmatrix} \varepsilon_x \\ \varepsilon_y \\ \frac{1}{2}\gamma_{xy} \end{bmatrix} \quad 5.2$$

where γ is a constant and

$$[T] = \begin{bmatrix} \cos^2\theta & \sin^2\theta & 2\sin\theta\cos\theta \\ \sin^2\theta & \cos^2\theta & -2\sin\theta\cos\theta \\ -\sin\theta\cos\theta & \sin\theta\cos\theta & \cos^2\theta - \sin^2\theta \end{bmatrix}$$

For uniaxial tensile deformation (low strain), Equation 5.2 can be simplified into Equation 5.3, in which the Poisson's ratio and shear strain are ignored both off-axis and on-axis, and only the tensile strain along the yarn's axis is particularly emphasized:

$$\begin{bmatrix} \varepsilon_m \\ 0 \\ 0 \end{bmatrix} = [T] \begin{bmatrix} \varepsilon_x \\ 0 \\ 0 \end{bmatrix} \quad 5.3$$

According to Fig. 5.8 and Equation 5.3, we can obtain Equation 5.4:

$$\varepsilon_1 = \varepsilon\cos^2\theta \quad 5.4$$

Similarly, we can work out the following equations:

$$\varepsilon_2 = \varepsilon\cos^2(\theta - \pi/2) \quad 5.5$$

$$\varepsilon_3 = \varepsilon\cos^2(\theta_0 - \theta) \quad 5.6$$

$$\varepsilon_4 = \varepsilon\cos^2(\theta_0 + \theta) \quad 5.7$$

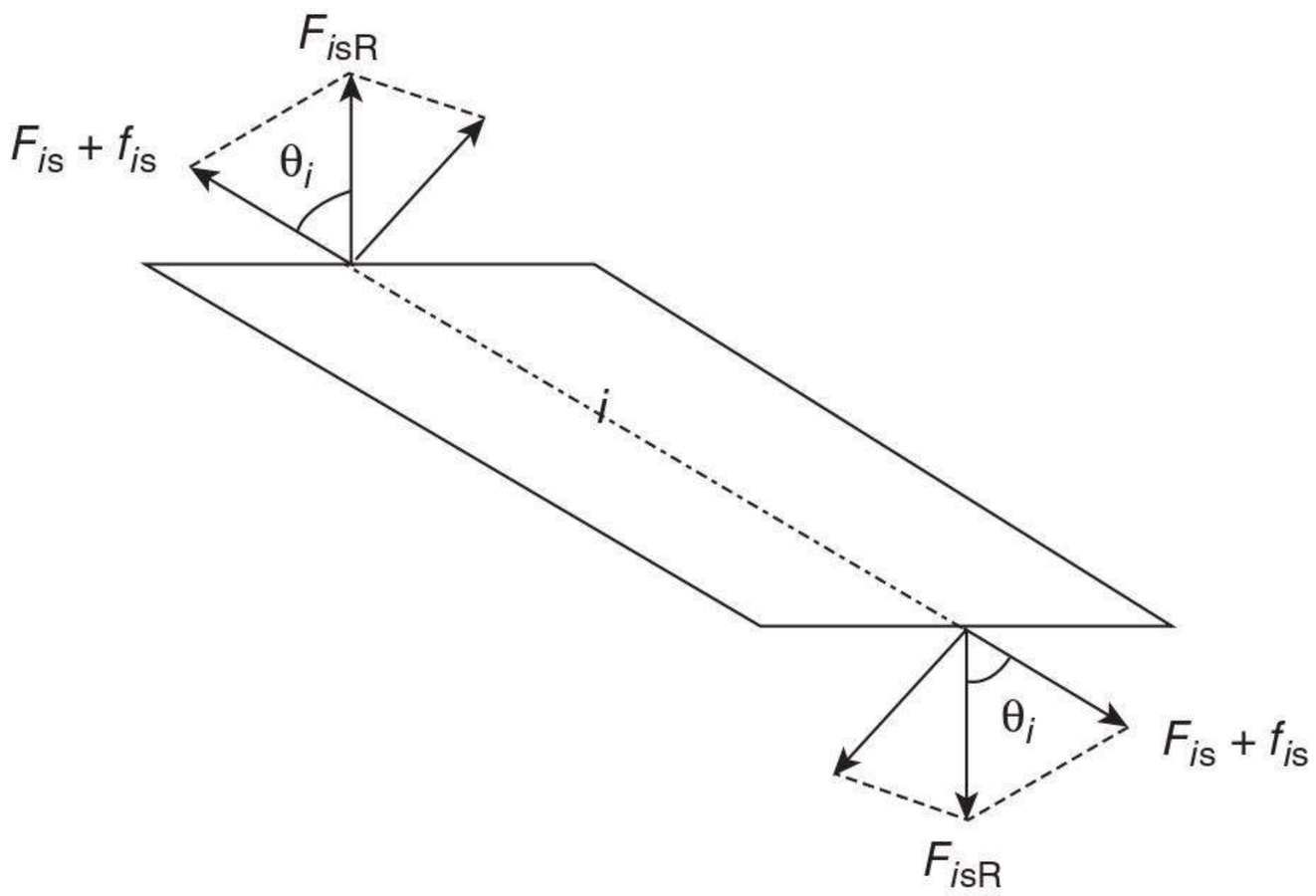

5.8 Forces exerted on a single inserting yarn.

Then Equations 5.4–5.7 can be written into one equation:

$$\varepsilon_i = \varepsilon \cos^2 \theta_i \quad (i = 1\text{–}4) \tag{5.8}$$

The stress–strain relationship of a multiaxial warp-knitted fabric under uniaxial stretch

When an MWK fabric is subjected to a uniaxial stretch, the forces exerted on a single inserting yarn are illustrated in Fig. 5.8. Here, we limit our consideration to the resultant force along the neutral line of a single yarn. From Fig. 5.9, we can obtain Equation 5.9:

$$\begin{aligned} F_{is} &= F_{isR} \cos\ _i - f_{is} \\ F_{isR} &= (F_{is} + f_{is})/\cos\ _i \quad (i = 1\text{–}4) \end{aligned} \tag{5.9}$$

Through a simple geometrical relationship, it is easy to obtain Equation 5.10:

$$n_i' = n_i \cos\theta_i \ (i = 1\text{–}4) \tag{5.10}$$

The load–elongation relationship of a single inserting yarn can be represented by Equation 5.11:

$$F_{is} = f_i(\varepsilon_i) \ (i = 1\text{–}4) \tag{5.11}$$

From Figs 5.7 and 5.9, we can obtain Equation 5.12:

$$F = \frac{1}{W_0} \sum_{i=1}^{4} n_i' F_{isR}(W_0 - L_0 \tan\theta_i) + F_L(\varepsilon) \tag{5.12}$$

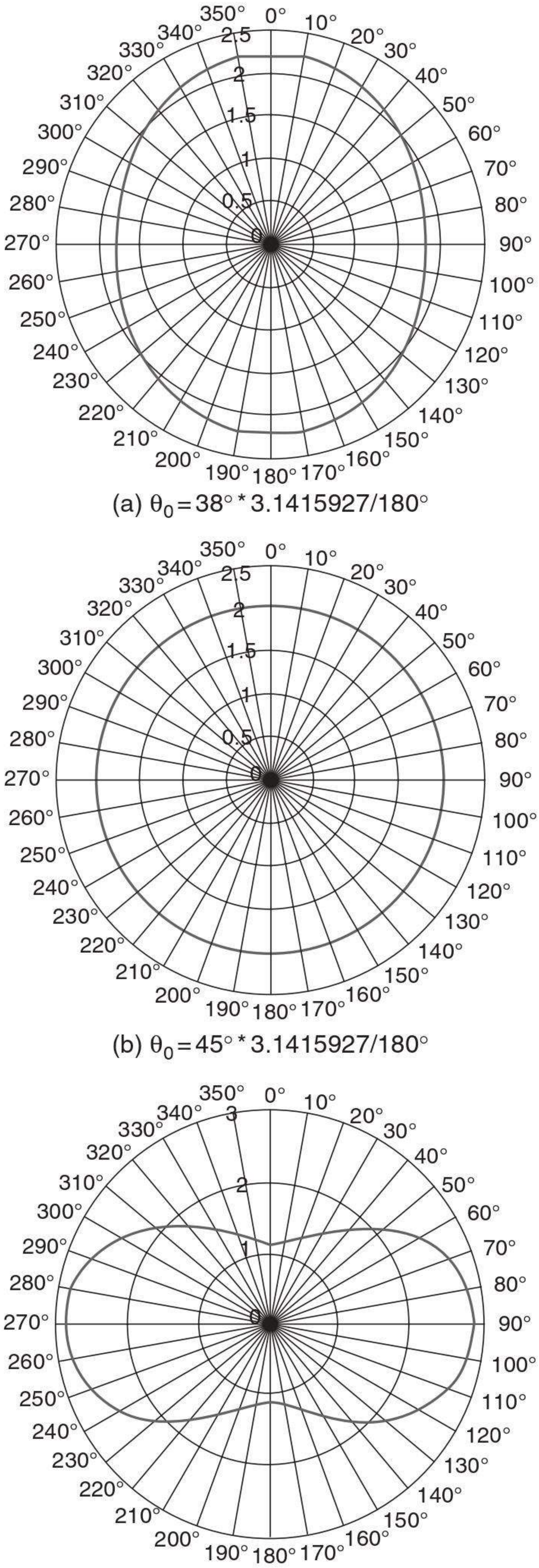

(a) $\theta_0 = 38° * 3.1415927/180°$

(b) $\theta_0 = 45° * 3.1415927/180°$

(c) $\theta_0 = 75° * 3.1415927/180°$

5.9 Tensile moduli in different directions of an MWK fabric.

We then apply Equations 5.9, 5.10 and 5.11 to Equation 5.12, in order to obtain Equation 5.13:

$$F = \frac{1}{W_0}\sum_{i=1}^{4} n_i[f_i(\varepsilon_i) + f_{is}(\varepsilon_i)](W_0 - L_0 \tan\theta_i) + F_L(\varepsilon) \qquad 5.13$$

In Equation 5.13, n_i and ε_i stand for the structural parameters of an MWK fabric; $f_i(\ )$ and $F_L(\ )$ stand for the inserting yarns' mechanical properties and the behaviour of the stitching system respectively; and $f_{is}(\ )$ stands for the interactions between inserting yarn systems. On the right-hand side of Equation 5.13, all the terms can be determined from simple tests, except for $f_{is}(\ )$, which is very difficult to evaluate, even though the frictional coefficient between glass fibre yarns can be obtained.

Formulation of the tensile modulus

Equation 5.8 can be rewritten as Equation 5.14 when $W_0 >> L_0$, as follows:

$$F = \sum_{i=1}^{4} n_i[f_i(\varepsilon_i) + f_{is}(\varepsilon_i)] + F_L(\varepsilon) \qquad 5.14$$

Generally speaking, when the fabric is only subjected to a small planar strain, the terms $f_{is}(\ )$ and $F_L(\ )$ may be neglected. If the four inserting yarn systems have exactly the same density (n) and tensile modulus (E_L), and the terms $f_{is}(\ )$ and $F_L(\ )$ are neglected, then Equation 5.14 can be rewritten as Equation 5.15:

$$F = nE_L\sum_{i=1}^{4}\varepsilon_i \qquad 5.15$$

We can then substitute Equation 5.8 in 5.15 to obtain Equation 5.16:

$$F = nE_L\varepsilon\sum_{i=1}^{4}\cos^2\theta_i \qquad 5.16$$

From Equation 5.16, we can obtain Equation 5.17:

$$E = nE_L\sum_{i=1}^{4}\cos^2\theta_i \qquad 5.17$$

Substituting Equations 5.4–5.7 into Equation 5.17, and letting $dE/d\theta = 0$, we can get θ values for E_{max} (maximum) and E_{min} (minimum):

$$\sin 2\theta \cos 2\theta_0 = 0 \qquad 5.18$$

$$E = \begin{cases} E_{max}, \text{ when } \quad \theta = \begin{cases} 0, & \pi/6 < \theta_0 < \pi/4 \\ \pi/2, & \pi/4 < \theta_0 < \pi/2 \end{cases} \\ E_{min}, \text{ when } \quad \theta = \begin{cases} 0, & \pi/4 < \theta_0 < \pi/2 \\ \pi/2, & \pi/6 < \theta_0 < \pi/4 \end{cases} \end{cases} \qquad 5.19$$

$$E = 2nE_{\mathrm{L}}\ (\theta_0 = \pi/4) \tag{5.20}$$

According to Equation 5.20, we can conclude that the fabric is nearly isotropic when $\theta_0 = \pi/4$. Three polar diagrams for Equation 5.17 are given in Fig. 5.9, which will be of great value in the design and application of MWK fabrics. Note that the real value for the tensile modulus is equal to the product of nE_{L} and the radius coordinate value.

5.4 Experimental methods and validation

The specifications of the samples used in the present research are listed in Table 5.4. The inserting yarns are all glass filaments and the tricot yarns are polyester filaments. The sample size is 3 cm (L_0) × 6 cm (W_0). Uniaxial tensile testing of samples is done along four directions (warp, weft and bias ±45°) on an Instron 4466. Single yarn load–elongation curves are obtained as shown in Fig. 5.10.

Table 5.4 Specifications of samples ($\theta_0 = \pi/4$)

Direction	Tex	n_i
Warp – 1	900	4.6
Weft – 2	70	2.5
Bias (+45°) – 3	300	6.8
Bias (–45°) – 4	300	6.8
Tricot loops – 5	9	5

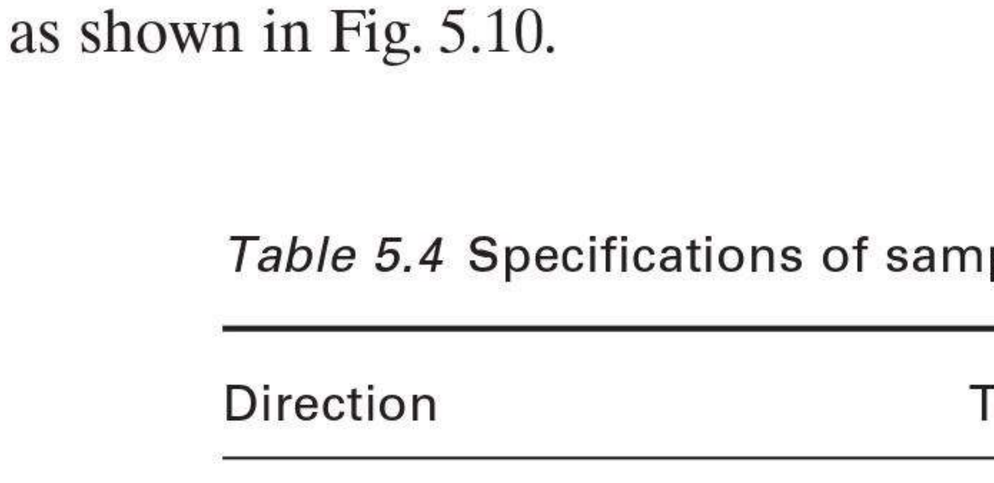

(a) The warp yarn's tensile behaviour

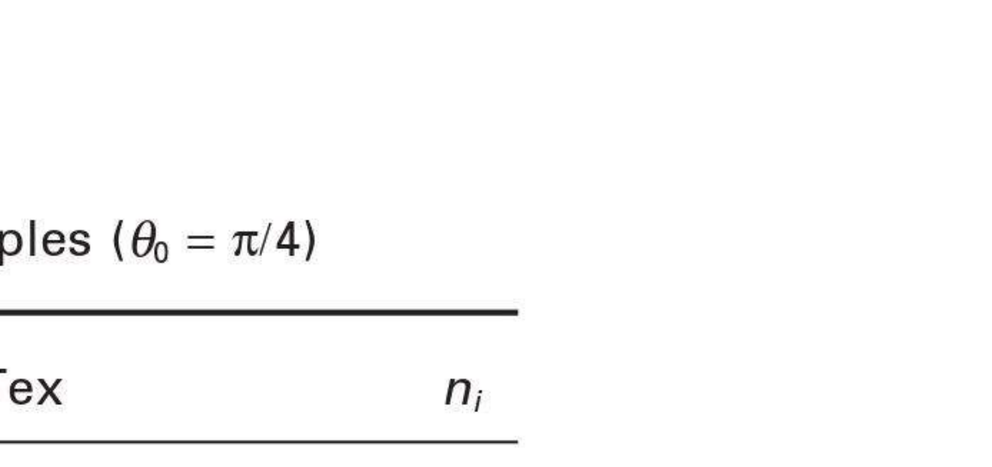

(b) The weft yarn's tensile behaviour

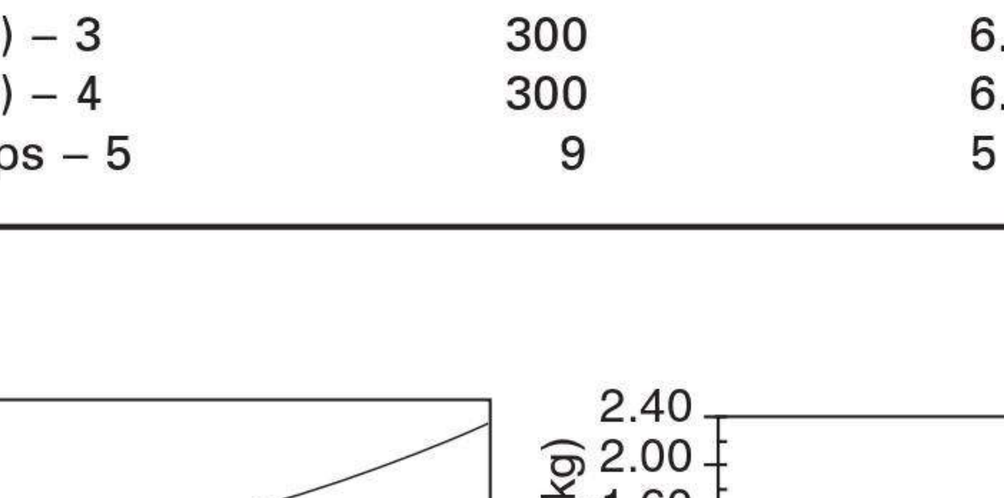

(c) The bias yarn's tensile behaviour

5.10 Tensile behaviour of an inserting yarn.

5.4.1 Validation of the model

In order to verify the accuracy of the model established above, comparison was made between the theoretical and tested results. In practical calculation, the effective width of sample for every inserting system should be $W_0 - L_0\tan\theta_i$, since the aspect ratio of the sample is not infinite. In Tables 5.5–5.7, $f_{is}(\varepsilon_i)$ and $F_L(\varepsilon)$ are neglected, which proves to be acceptable. The theoretical calculations are listed in Tables 5.5–5.7 where the input data include ε and f_{is} and output results of the calculation are ε_i and F^*.

Three sets of stress–strain curves are presented in Fig. 5.11, according to the theoretical calculations in Tables 5.5–5.7. The experimental curves are also shown for the sake of comparison. For simplicity, the curves for $\theta = -\pi/4$ are not given since they are basically the same as those for $\theta = +\pi/4$. Obviously, the two sets of results are in good agreement. According to Fig. 5.11, it can also be noted that the experimental curves are always below the theoretical ones. This is different from the relationship indicated by

Table 5.5 Theoretical calculations for warp directional stretch ($\theta = 0$)

ε	1		2		3		4		F^* (see note)
	ε_1	$n_1 f_{1s}$	ε_2	$n_2 f_{2s}$	ε_3	$n_3 f_{3s}$	ε_4	$n_4 f_{4s}$	
0	0	0.00	0	0	0	0.00	0	0.00	0.00
0.001	0.001	1.84	0	0	0.0005	0.82	0.0005	0.82	2.66
0.002	0.002	5.52	0	0	0.0010	1.36	0.0010	1.36	6.88
0.003	0.003	9.66	0	0	0.0015	2.45	0.0015	2.45	12.11
0.004	0.004	14.26	0	0	0.0020	3.54	0.0020	3.54	17.80
0.005	0.005	17.94	0	0	0.0025	4.90	0.0025	4.90	22.84
0.006	0.006	21.62	0	0	0.0030	6.53	0.0030	6.53	28.15
0.007	0.007	24.84	0	0	0.0035	8.02	0.0035	8.02	32.86
0.008	0.008	28.06	0	0	0.0040	9.32	0.0040	9.32	37.38
0.009	0.009	30.36	0	0	0.0045	11.02	0.0045	11.02	41.38
0.010	0.010	32.66	0	0	0.0050	12.24	0.0050	12.24	44.90
0.011	0.011	35.42	0	0	0.0055	13.53	0.0055	13.53	48.95
0.012	0.012	36.80	0	0	0.0060	15.03	0.0060	15.03	51.83
0.013	0.013	39.10	0	0	0.0065	15.98	0.0065	15.98	55.08
0.014	0.014	41.86	0	0	0.0070	17.61	0.0070	17.61	59.47
0.015	0.015	44.16	0	0	0.0075	18.56	0.0075	18.56	62.72
0.016	0.016	46.92	0	0	0.0080	19.86	0.0080	19.86	66.78
0.017	0.017	50.14	0	0	0.0085	21.42	0.0085	21.42	71.56
0.018	0.018	52.90	0	0	0.0090	22.85	0.0090	22.85	75.75
0.019	0.019	56.12	0	0	0.0095	24.21	0.0095	24.21	80.33
0.020	0.020	58.88	0	0	0.0100	25.30	0.0100	25.30	84.18

Note: $$F^* = \frac{1}{W_0}\sum_{i=1}^{4} n_i f_i(\varepsilon_i)(W_0 - L_0\tan\theta_i)$$

Table 5.6 Theoretical calculations for weft directional stretch ($\theta = \pi/2$)

ε	1		2		3		4		F^* (see note)
	ε_1	$n_1 f_{1s}$	ε_2	$n_2 f_{2s}$	ε_3	$n_3 f_{3s}$	ε_4	$n_4 f_{4s}$	
0	0	0	0	0.00	0	0.00	0	0.00	0.00
0.001	0	0	0.001	0.15	0.0005	0.82	0.0005	0.82	0.97
0.002	0	0	0.002	0.25	0.0010	1.36	0.0010	1.36	1.61
0.003	0	0	0.003	0.35	0.0015	2.45	0.0015	2.45	2.80
0.004	0	0	0.004	0.55	0.0020	3.54	0.0020	3.54	4.09
0.005	0	0	0.005	0.78	0.0025	4.90	0.0025	4.90	5.67
0.006	0	0	0.006	1.05	0.0030	6.53	0.0030	6.53	7.58
0.007	0	0	0.007	1.33	0.0035	8.02	0.0035	8.02	9.35
0.008	0	0	0.008	1.65	0.0040	9.32	0.0040	9.32	10.97
0.009	0	0	0.009	1.90	0.0045	11.02	0.0045	11.02	12.92
0.010	0	0	0.010	2.20	0.0050	12.24	0.0050	12.24	14.44
0.011	0	0	0.011	2.53	0.0055	13.53	0.0055	13.53	16.06
0.012	0	0	0.012	2.80	0.0060	15.03	0.0060	15.03	17.83
0.013	0	0	0.013	3.08	0.0065	15.98	0.0065	15.98	19.06
0.014	0	0	0.014	3.35	0.0070	17.61	0.0070	17.61	20.96
0.015	0	0	0.015	3.60	0.0075	18.56	0.0075	18.56	22.16
0.016	0	0	0.016	3.88	0.0080	19.86	0.0080	19.86	23.73
0.017	0	0	0.017	4.13	0.0085	21.42	0.0085	21.42	25.55
0.018	0	0	0.018	4.40	0.0090	22.85	0.0090	22.85	27.25
0.019	0	0	0.019	4.68	0.0095	24.21	0.0095	24.21	28.88
0.020	0	0	0.020	4.88	0.0100	25.30	0.0100	25.30	30.17

Note: $$F^* = \frac{1}{W_0}\sum_{i=1}^{4} n_i f_i(\varepsilon_i)(W_0 - L_0 \tan\theta_i)$$

Equation 5.13, where the solid (experimental) curves should be higher than the broken (theoretical) ones when $f_{is}(\ )$ and $F_L(\ )$ are ignored. There are three possible reasons for this discrepancy: firstly, when the sample is clamped for testing, it does not stay in a perfect straight state; secondly, the inserting yarns do not deform uniformly even in the same system; and lastly, slippage may occur during stretch.

5.5 Conclusions

There are many difficulties in modelling the mechanical properties of MWK fabrics. This chapter presents a simplified method of dealing with deformation using the macroscopic structure of MWK fabrics, in which a uniaxial tensile model is established and a formula worked out for calculating tensile moduli in any direction. Comparison of the model and experimental results demonstrates that the model is justified, and the results obtained from the theoretical calculation and experiments show good agreement with each other.

Table 5.7 Theoretical calculations for bias directional stretch ($\theta = +\pi/4$)

ε	1		2		3		4		F^* (see note)
	ε_1	$n_1 f_{1s}$	ε_2	$n_2 f_{2s}$	ε_3	$n_3 f_{3s}$	ε_4	$n_4 f_{4s}$	
0	0	0.00	0	0.00	0	0.00	0	0	0.00
0.001	0.0005	1.15	0.0005	0.08	0.001	1.36	0	0	1.97
0.002	0.0010	1.84	0.0010	0.15	0.002	3.54	0	0	4.53
0.003	0.0015	3.91	0.0015	0.23	0.003	6.53	0	0	8.60
0.004	0.0020	6.30	0.0020	0.25	0.004	9.32	0	0	12.59
0.005	0.0025	8.05	0.0025	0.28	0.005	12.24	0	0	16.40
0.006	0.0030	9.66	0.0030	0.35	0.006	15.03	0	0	20.03
0.007	0.0035	12.19	0.0035	0.43	0.007	17.61	0	0	23.92
0.008	0.0040	14.26	0.0040	0.55	0.008	19.86	0	0	27.26
0.009	0.0045	16.01	0.0045	0.70	0.009	22.85	0	0	31.20
0.010	0.0050	17.94	0.0050	0.83	0.010	25.30	0	0	34.68
0.011	0.0055	19.55	0.0055	0.95	0.011	27.88	0	0	38.13
0.012	0.0060	21.62	0.0060	1.05	0.012	30.26	0	0	41.60
0.013	0.0065	23.46	0.0065	1.20	0.013	32.64	0	0	44.97
0.014	0.0070	24.84	0.0070	1.33	0.014	35.70	0	0	48.78
0.015	0.0075	26.68	0.0075	1.48	0.015	38.28	0	0	52.36
0.016	0.0080	28.06	0.0080	1.65	0.016	40.53	0	0	55.38
0.017	0.0085	29.50	0.0085	1.78	0.017	42.36	0	0	58.00
0.018	0.0090	30.36	0.0090	1.90	0.018	43.86	0	0	59.99
0.019	0.0095	31.51	0.0095	2.05	0.019	45.36	0	0	62.14
0.020	0.0100	32.66	0.0100	2.20	0.020	46.78	0	0	64.21

Note: $$F^* = \frac{1}{W_0}\sum_{i=1}^{4} n_i f_i(\varepsilon_i)(W_0 - L_0 \tan\theta_i)$$

On the basis of the foregoing analysis, it may be concluded that the deformation of different unit cells is quite different, as is shown in Fig. 5.6. As a result, the unit cell approach (Du and Ko, 1996) is difficult to apply when modelling the tensile properties of MWK fabrics. The basic assumption of Kilby's trellis method (Kilby, 1963) is that the woven yarns pivot together at the intersections. This cannot be applied to MWK fabrics, where the inserting yarns tend to slip very easily and this is always accompanied by the rotation of the yarn.

The force method often begins with a chosen unit cell, as in Kawabata's study (Kawabata *et al.*, 1973). However, it is very difficult – and indeed nearly impossible – to determine the forces exerted on a single inserting yarn when an MWK fabric is under tensile force, since this will involve many unexpected force moments (e.g. the frictional force moment), as well as many additional forces, such as frictional and shear forces. Thus, the equilibrium equation is too complex to solve easily.

According to the results obtained, the macroscopic approach that deals with fabric structure under tensile deformation is workable. It is reasonable

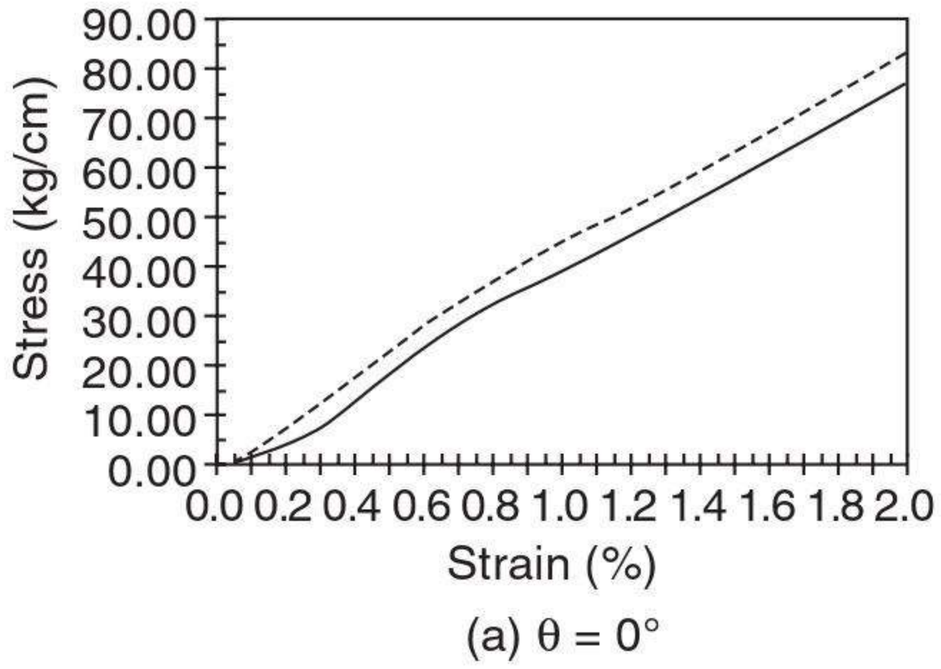

(a) θ = 0°

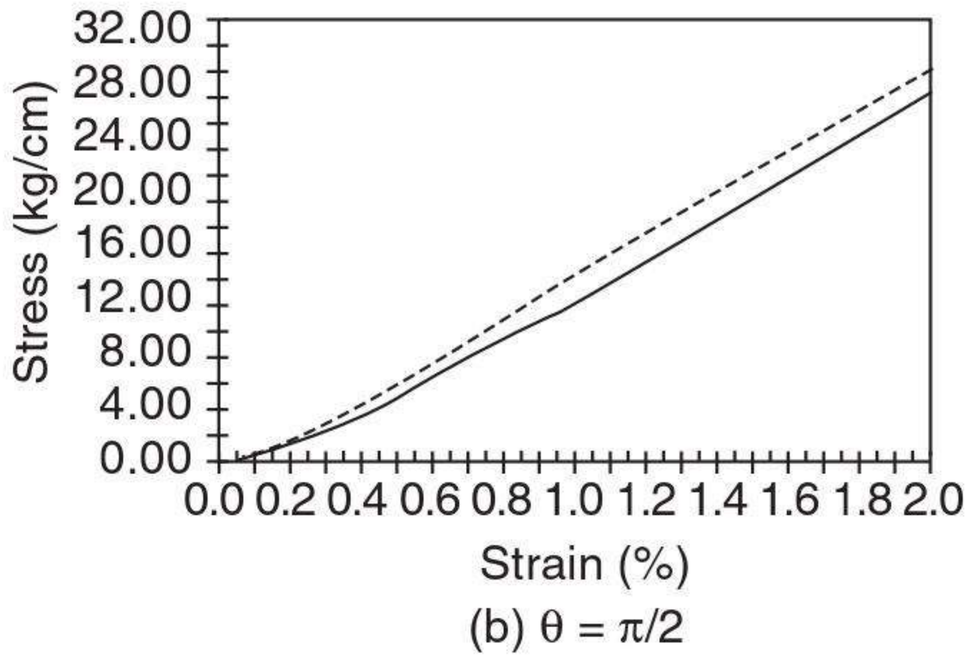

(b) θ = π/2

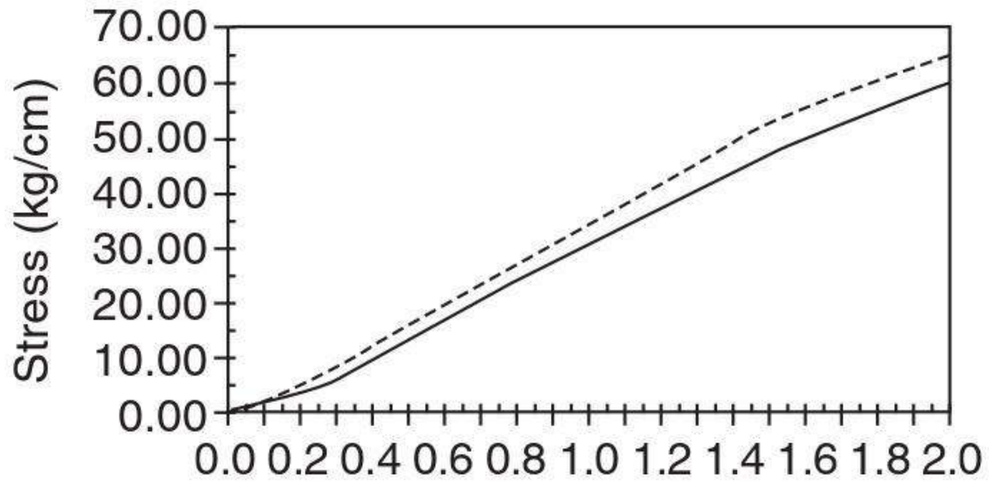

(c) θ = + π/4

5.11 The stress–strain curves of MWK fabrics (the broken line is from the model, the solid line from experimental).

to neglect the effect of frictional force and the stitching system in predicting the uniaxial in-plane tensile properties of MWK fabrics. The model for the uniaxial stress–strain relationship and the formula for tensile modulus are of great value in designing and engineering applications for MWK fabrics.

5.6 References

Chen Nanliang (2001), Research on the tensile property of the composite reinforced with multiaxial warp-knitted fabrics (in Chinese), *Journal of Donghua University*, **27**, 2, April, 99–101.

Chen Nanliang (2002), Effect of the materials and structures of the warp-knitted ground on the tensile strength of the composite reinforced with multiaxial warp-knitted fabrics (in Chinese), *Journal of Donghua University*, **28**, 1, February, 105–106.

Chou T-W and Ko F K (eds) (1989), *Textile Structural Composites* 3, Elsevier, New York, 29–169.

Creech G and Pickett A K (2006), Meso-modelling of non-crimp fabric composites for coupled drape and failure analysis, *Journal of Material Science*, **41**, 6725–6736.

Dexter H B and Hasko G H (1996), Mechanical properties and damage tolerance of multiaxial warp-knit composites, *Composites Science and Technology*, **56**, 3, 367–380.

Du G-W and Ko F (1996), Analysis of multiaxial warp-knit preforms for composite reinforcement, *Composites Science and Technology*, **56**, 3, 253–260.

Kaufmann J R (1991), Industrial applications of multiaxial warp knit composites, Chapter 5 in *High-Tech Fibrous Materials* (ed. Tyrone L Vigo and Albin F Turbak), American Chemical Society, Washington, DC, 81–89.

Kawabata S, Niwa M and Kawai H (1973), The finite-deformation theory of plain weave fabrics, Part I: The biaxial-deformation theory; Part II: The uniaxial-deformation theory; Part III: The shear-deformation theory, *Journal of Textile Institute*, **64**, 21, 47, 62.

Kilby W F (1963), Planar stress–strain relationships in woven fabrics, *Journal of the Textile Institute*, **54**, T9–27.

Ko F K, Bruner J, Pastore A and Scardino F (1980), Development of multi-bar weft insertion warp-knit fabric for industrial applications, *ASME Paper No. 90-TEXT-7*, October.

Ko F K, Krauland K and Scardino F (1982), Weft insertion warp-knit for hybrid composites, in *Progress in Science and Engineering of Composites*, *ICCM-V*, *Fourth International Conference on Composites*, 982–987.

Ko F K, Fang P and Pastore C (1985), Multilayer multidirectional warp-knit fabrics for industrial applications, *Journal of Industrial Fabrics*, **4**, 2, 4–12.

Ko F K, Pastore C, Yang J M and Chou T W (1986), Structure and properties of multilayer multidirectional warp-knit fabric reinforced composites, in *Proc. 3rd US–Japan Conf. on Composites*, Tokyo, 21–28.

Kong H, Mouritz A P and Paton R (2004), Tensile extension properties and deformation mechanisms of multiaxial non-crimp fabrics, *Composite Structures*, **66**, 249–259.

Lomov S V, Verpoest I, Barburski M and Laperre J (2003), Carbon composites based on multiaxial multiply stitched preforms, Part 2. KES-F Characterisation of the deformability of the preforms at low loads, *Composites, Part A*, **34**, 359–370.

Pattyn H, Verpoest I, Ivens J and Villalon E (1999), Comparison of warp-knitted and stitched non-crimp fabrics, *Duracosys 99, Proc. 4th Int. Conf. on Durability Analysis of Composite Systems*, Brussels, Belgium, 11–14 July, 435–440.

Shen Wei (2002), Research on tensile property of bi-axial warp-knitted structure (in Chinese), *Journal of Donghua University*, **28**, 6, December, 105–110.

Zhou Rongxing, Hu Hong, Chen Nanliang and Feng Xunwei (2004), A study on the tensile properties of the MWK structures for composite reinforcement, *Journal of Donghua University (Eng. Ed.)*, **21**, 6, 121–123.

6

Bending properties of multiaxial warp-knitted fabrics

Abstract: The bending properties of fabrics govern many aspects of fabric performance, such as hand and drape, and they are an essential part of the complex fabric deformation analysis. To understand the behaviour of multiaxial warp-knitted (MWK) fabrics in general under bending is very important, since their functional properties are closely related to their mechanical properties, such as bending, shear and tensile. The main concern in this chapter is to establish a predictive model for assessing the bending behaviour of MWK fabrics. In addition, an elaborate description and interpretation of the bending properties of MWK fabrics are presented, based on many bending hysteresis curves obtained from KES-FB-2.

Key words: multiaxial warp-knitted (MWK) fabrics, bending behaviour of MWK fabrics, modelling bending behaviour of MWK fabrics, KES-FB-2, bending hysteresis.

6.1 Introduction

The bending properties of fabrics govern many aspects of fabric performance, such as hand and drape, and they are an essential part of the complex fabric deformation analysis. Like other mechanical properties, the bending behaviour of a woven fabric directly influences its performance. It is well known that fabric bending rigidity, along with its shear rigidity, determines the drapeability of a fabric. Research results show that fabric bending rigidity is also an important contributor to the fabric's formability, handle, buckling behaviour, wrinkle resistance and crease resistance. In the case of industrial fabrics, such as air-supported structures or fabric-reinforced flexible-composite conveyor belts, the bending behaviour of the fabrics is critically important.

Thus the bending of woven fabrics has received considerable attention in the literature. A substantial amount of literature is available on woven fabrics, especially on plain weaves. Bending of fabrics, however, is generally non-linear. Woven fabrics are made of large numbers of fibres that may have considerable freedom of motion, relative to each other, within the fabric structure. As a result, the fibre strains which develop during bending are considerably lower than those which develop in bending of corresponding solid sheet materials. With this mobility, the potential

flexibility of the fibres can be realized and the fabric structure will, in turn, have a low bending rigidity. The inter-fibre friction associated with the fibre movement is believed to be the major cause of fabric non-linear bending behaviour. Computational models for solving large-deflection elastic problems from theoretical models have been applied to specific fabric engineering and apparel industry problems, for example the prediction of the robotic path for controlling the laying of fabric onto a work surface (Brown *et al.*, 1990; Clapp and Peng, 1991). The non-linear bending behaviour of woven fabrics can be separated into two components: a non-linear component due to friction and a linear component. The bending resistance is made up of three components: (i) the bending resistance of the threads lying in the direction of bending, (ii) the interaction between the threads, and (iii) a frictional restraint. A typical bending hysteresis curve of plain weaves is given in Fig. 6.1, which is basically symmetrical about the origin O and regular (like a leaf) for both warp-wise and weft-wise bending.

To understand the behaviour under bending of knitted fabrics in general is very important, since their functional properties are closely related to their mechanical properties, such as bending, shear and tensile. For example, the drape properties of fabrics are affected by both bending and shear properties. An increase in bending and shear parameters, such as bending and shear rigidity, and hysteresis of bending, results in a decrease in the drape structure of the fabric, something undesirable in most cases (Gaucher and King, 1983). Another example of the importance of the bending of knitted fabrics involves their handle properties. Handle is the sum total of sensations of the physical and mechanical properties of fabric when it is handled by touching, flexing by the fingers, smoothing, etc. In most cases, lower bending and shear parameters and lower roughness for knitted fabrics

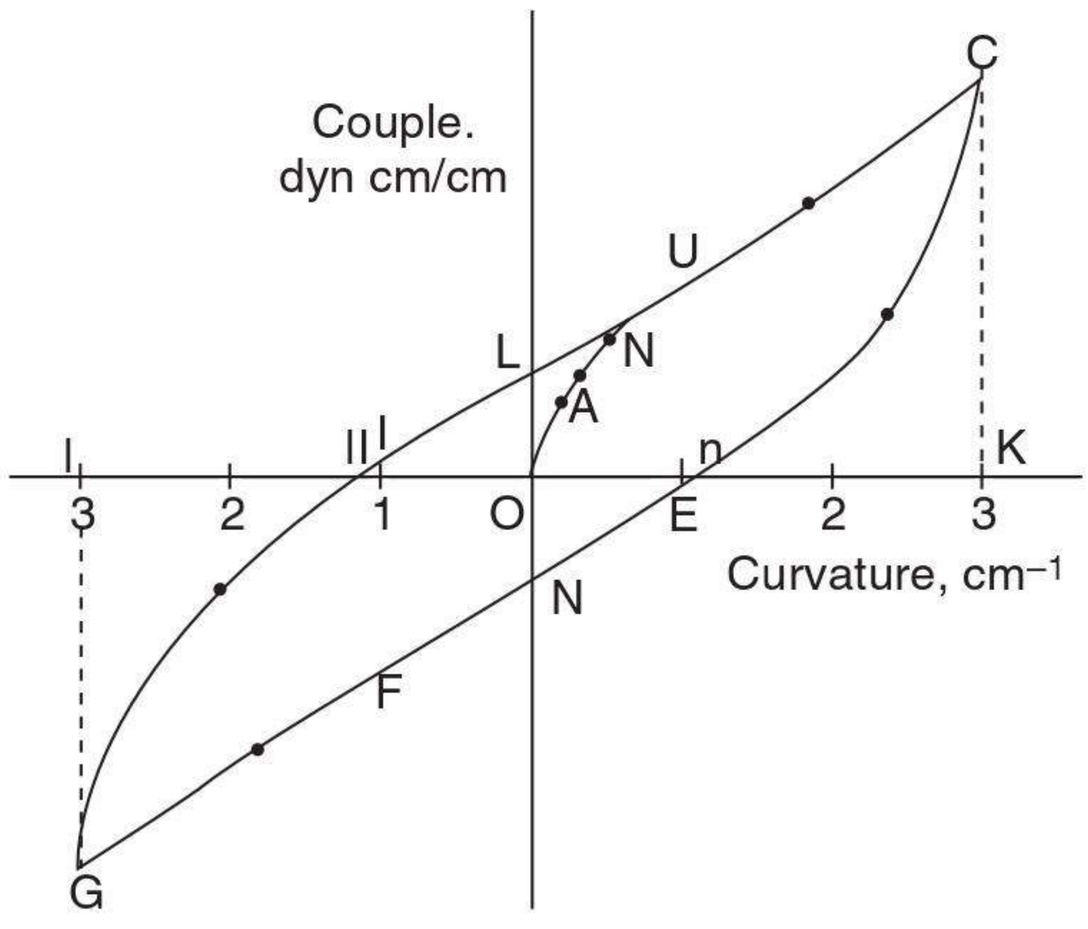

6.1 Typical bending-hysteresis curve for woven fabrics.

are necessary for the best handle (Chen *et al.*, 1992). Many examples exist showing the relationship between a fabric's functional properties and its bending properties.

In this chapter, an elaborate description and interpretation of the bending properties of MWK fabrics are presented, based on many bending hysteresis curves obtained on KES-FB-2. Further, a predictive bending model to assess the MWK fabrics based on KES-F experiments (Kawabata, 1980) in different bending directions is described. In the modelling process, an important finding is that the bending paths of non-orthogonally bent yarn systems follow different cylindrical helices. In addition, the theoretical model is derived directly from the structural parameters of the fabric, and the bending properties of its constituent inserting yarns can be used to calculate all the bending hysteresis curves of an MWK fabric in different bending directions. Furthermore, the bending rigidity at an arbitrary curvature can also be calculated with this model.

6.2 Bending properties of multiaxial warp-knitted fabrics

The bending behaviour of MWK fabrics is quite different from that of plain weaves and other apparel materials. From the experimental analysis, it may be understood that the bending properties of MWK fabrics are dependent not only on bending directions (such as warp-wise, weft-wise and bias-wise) but also on bending sequences, which means that which of the two sides of an MWK fabric is bent inwards or outwards first will lead to different bending results even if the bending direction (say, in the warp-wise direction) remains unchanged. According to the bending hysteresis curves obtained from KES-FB-2 (Kawabata's evaluation system), MWK fabric bending involves not only the spreading of filaments in inserting yarns, but also the buckling of inserting yarns, which accounts for the more remarkable irregularity and non-symmetry of MWK fabric bending hysteresis curves compared with those of plain weaves. A simple procedure for measuring the bending properties of fabrics is explained here. In order to measure the bending properties of the fabric the sample is bent between the curvatures –2.5 and 2.5 cm^{-1}, the radius of the bend being 1/curvature as shown in Fig. 6.2. The bending moment required to give this curvature is continuously monitored to give the curve shown in Fig. 6.3. The following quantities are measured from this curve:

Bending rigidity B = slope of the bending moment–curvature curve
Moment of hysteresis $2HB$ = hysteresis width of the curve

Furthermore, the inserting yarns not completely parallel to the applied bending moment direction will undergo both bending and torsional

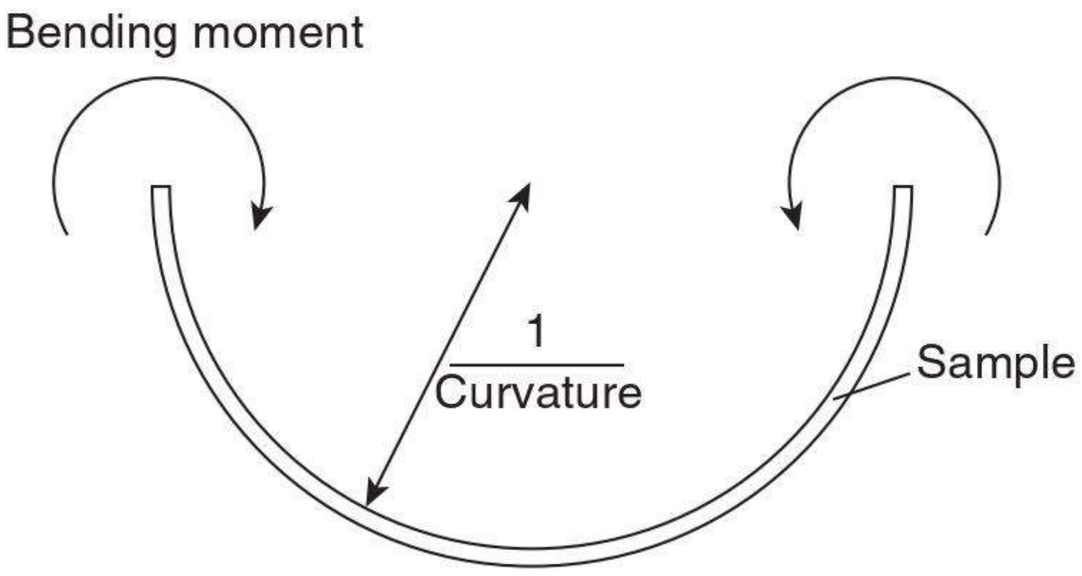

6.2 Forces involved in fabric bending.

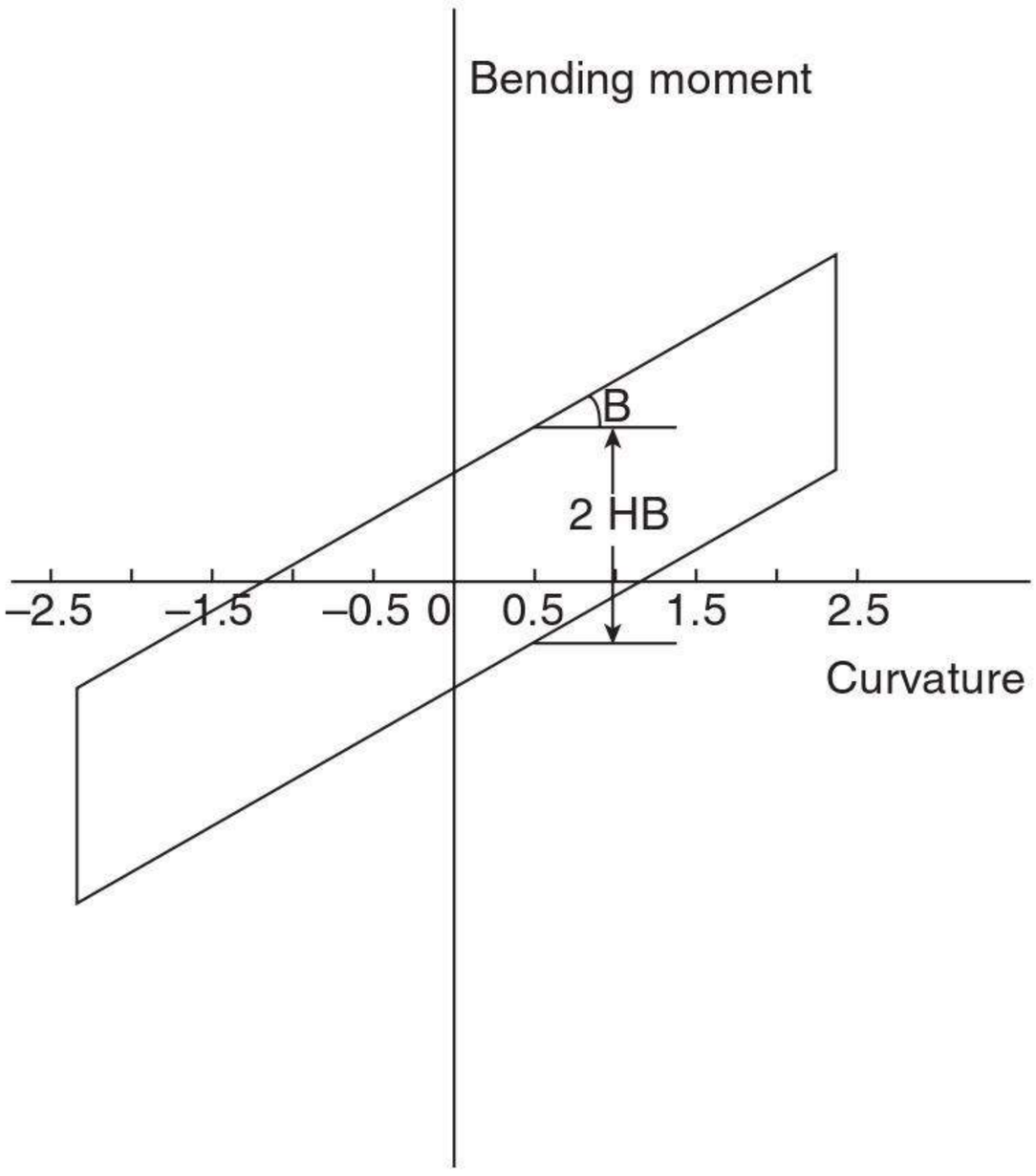

6.3 Plot of bending moment against curvature.

deformation during a bending cycle. Experimental observation and theoretical study have shown that the bending paths of those non-orthogonally bent yarn systems follow different cylindrical helices.

There is no elaborate theory and modelling method currently available as far as bending properties of MWK fabrics are concerned, but a thorough and systematic research approach in this direction is needed in product design, especially composite design (in the moulding process, the conformability of the fabric will depend to a great degree on the bending properties). Davies and Owen, 1971; Delaney, 1981a,b; Gibson and Postle, 1978; Ko *et al.*, 1986; Vigo and Turbak, 1991 and other authors (Cooper, 1960; Livesey and Owen, 1964; Grosberg, 1966; Grosberg and Swani, 1966; Owen, 1968) made a considerable contribution to the study of bending properties of plain weaves; unfortunately, these works are less helpful when studying MWK fabrics, which are more complex than plain weaves.

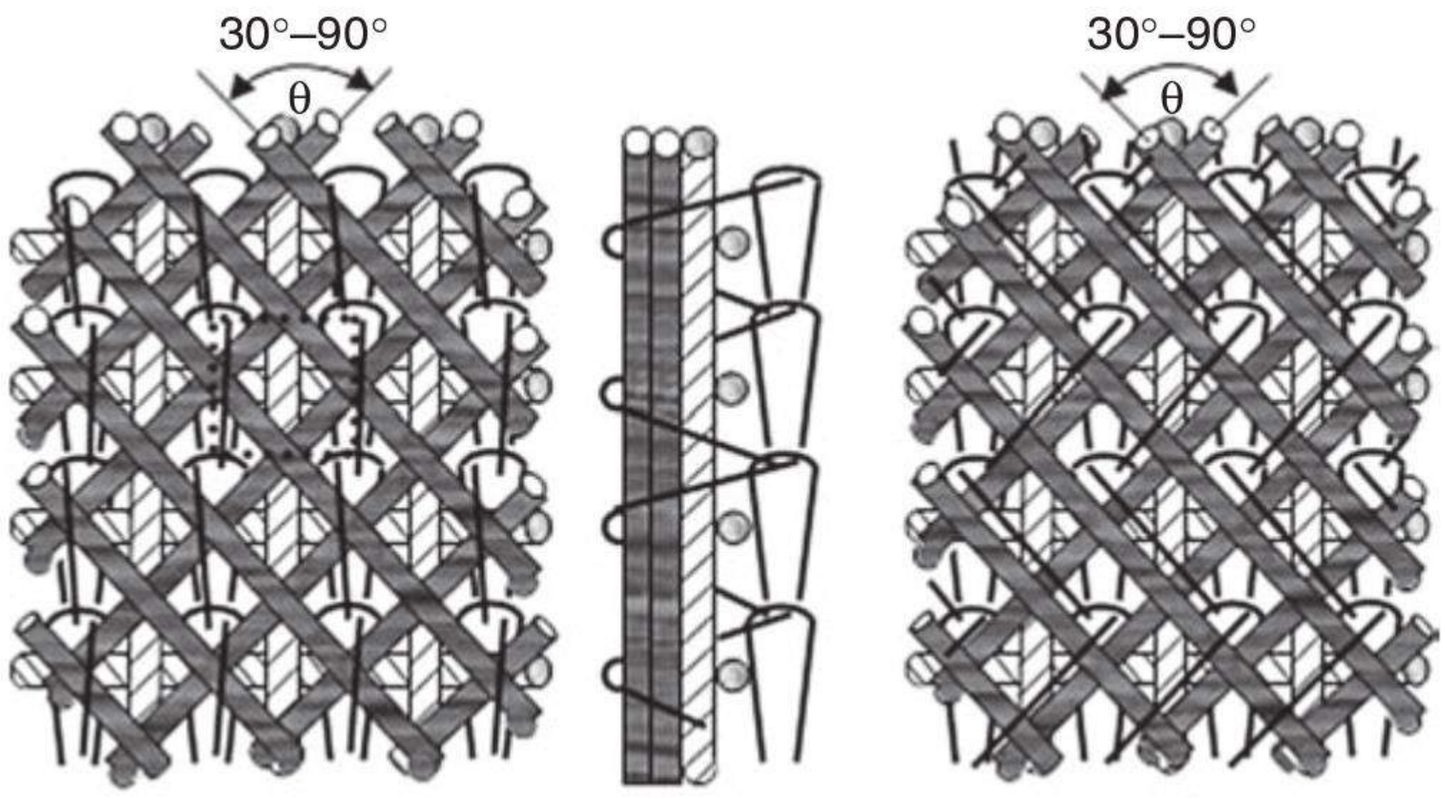

(a) Chain structure (b) Tricot structure

6.4 Typical structure of an MWK fabric.

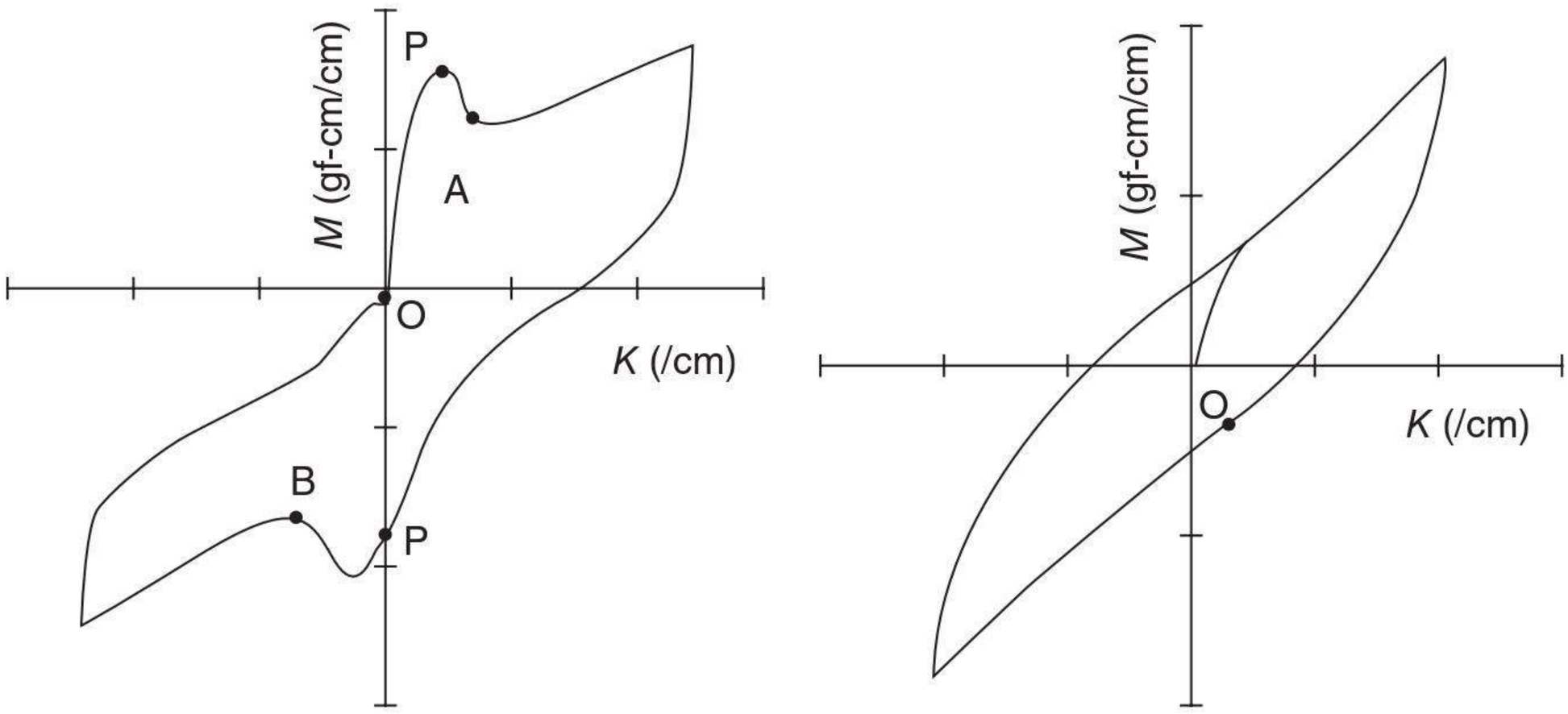

(a) MWK fabric (b) Plain weave

6.5 Comparison of typical bending hysteresis curves of an MWK fabric and a plain weave.

Figure 6.4 shows typical structures of MWK fabrics (Du and Ko, 1996) with two categories of stitching systems – tricot structure and chain loops. Structure (b) using glass filament yarns as the inserting system is chosen for modelling, the results of which can be applied to other MWK fabric structures.

The bending properties of MWK fabrics are characterized by KES-FB-2, and are quite different from those of plain weaves. Figure 6.5 shows typical bending hysteresis curves of an MWK and a plain weave. It can be observed that the bending hysteresis curve of an MWK fabric looks more irregular and non-symmetrical (about the origin O) than that of a plain weave. Two points, A and B, are particularly worth noting because they indicate the

special bending characteristics of MWK fabrics with glass filament yarns as inserting systems.

With the aid of KES-FB-2, experiments on bending properties were carried out using three kinds of MWK fabrics. The inserting yarns are all glass filament yarns, and the tricot loops are polyester yarns. The details of the sample fabrics are as follows:

- **Sample 1.** Biaxial warp-knitted fabric (Karl Mayer type)
  There are two inserting yarn systems, weft and warp respectively, which are held together by tricot loops. Density: 5.0 threads/cm for weft, the same for warp. The yarn count is 618 Tex for weft inserting yarn, 596 Tex for warp inserting yarn, and 9 Tex for stitching yarns (tricot loops).
- **Sample 2.** Triaxial warp-knitted fabric (LIBA type)
  There are three inserting yarn systems, one for warp and the other two for bias (30° to the warp direction), held together by tricot loops. Density: 4.1 threads/cm for warp, four yarns, 1100 Tex for warp and 9 Tex for stitching yarns.
- **Sample 3.** Multiaxial warp-knitted fabric (as shown in Fig. 6.4)
  There are four inserting yarn systems, one for warp, one for weft and the other two for bias (45° to the warp direction), also held together by tricot loops. Density: 4.6 threads/cm for warp, 2.5 threads/cm for weft and 6.8 threads/cm for bias. The yarn count is 300 Tex for bias yarns, 900 Tex for warp, 70 Tex for weft and 9 Tex for stitching yarns. The sample size is 10 cm (length) × 3 cm (width).

6.2.1 Results of experiments

In interpreting the bending properties of MWK fabrics, one thing must be pointed out first. The inserting yarns employed in MWK fabrics in most cases are glass fibre yarns since they are generally used as industrial and engineering materials. Polyester yarns, especially with high strength and high modulus, can also be used as inserting yarns. For the purpose of a typical study, however, MWK fabrics with glass filament bundles as inserting yarns were chosen for research.

Glass filament yarns are quite different from those made of polymer filaments in mechanical behaviour. They possess no viscosity but perfect elasticity within a tensile strain of about 23%. As a result, for bending hysteresis curves of this kind of fabric, only the frictional effect between filaments, between inserting yarn systems, and between inserting yarns and tricot loops at the contact regions, will contribute to the hysteresis, and the viscosity has no effect.

In the following analysis, the effect of the stitching system has not been considered, since the count of stitching yarns is far smaller than that of

inserting yarns. The tricot loops, however, determine the maximum slipping distance of inserting yarns and relate to motional friction within fabrics.

6.3 Bending hysteresis curves of multiaxial warp-knitted fabrics

In Fig. 6.6, typical bending hysteresis curves of MWK fabrics are given, of which (a) is the most typical according to the experiments. It is quite different from that of a plain weave. Compared with the curve for plain weave in Fig. 6.1, it can be seen that the bending hysteresis curve of an MWK fabric presents even more remarkable irregularity and non-symmetry (about the origin O). For convenience, here we divide the curve in Fig. 6.6(a) into six segments, marked OA, AB, BC, CD, DE and EO.

Figure 6.6 shows that the shape of segments OA and AB is basically the same for all the curves (a) to (d). For segment OA, no slippage occurs and the high initial Young's modulus is due to the combined contribution of the high bending rigidity of glass yarns (bundle of filaments, being bent as an unseparated integrity) and the static friction between filaments and between yarn systems. The bending curvature at point A is very small, nearly equal to zero. This segment possesses good linearity.

After point A, small relative slippage at regions with low frictional restraint begins to occur. With the bending process under way, the slippage phenomenon becomes more and more visible till point B. It can be seen from Fig. 6.6(a) that segment AB also presents a substantial linearity, although no better than that of segment OA. Here, we call the motional friction occurring in segment AB the 'stable motional friction', which is quite different from that in segment BC.

The experiment shows that a very special phenomenon occurs in segment BC (at point P), that the filaments in the inserting yarns are spread laterally at the bending point, and that the cross-section of these yarns is changed from the shape of 'race track' to 'a thin piece' (a series of filaments nearly lined up). This is illustrated in Fig. 6.7, which may account for the sharp decrease of bending moment at point P.

It can be understood from Fig. 6.6(a) and (c) that the motional friction in segment BC is very unstable and segment BC shows a remarkable non-linearity, which may be due to the spread of filaments to a great degree. However, this conclusion is not always true. Referring to Fig. 6.6(b), it can be found that the corresponding segment is basically linear, which is caused by the higher density and higher count of the inserting yarns being bent. In this situation, the effect of the spread of filaments plays only a secondary role.

The shape of segments CD and EO is just analogous to those of plain weaves (Fig. 6.1). However, it can also vary a lot according to different

(a) Sample 1, weft-wise bending

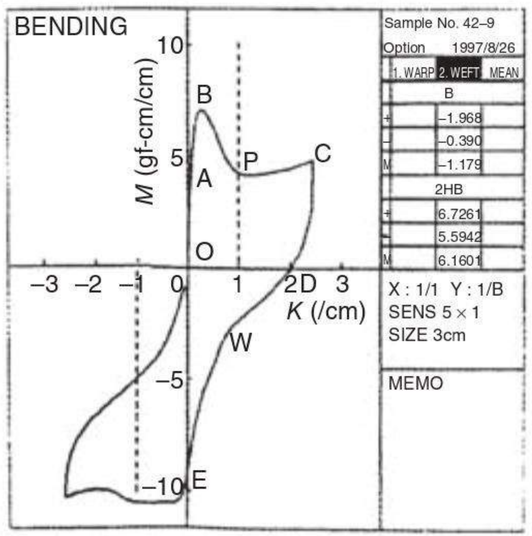

(b) Sample 3, warp-wise bending

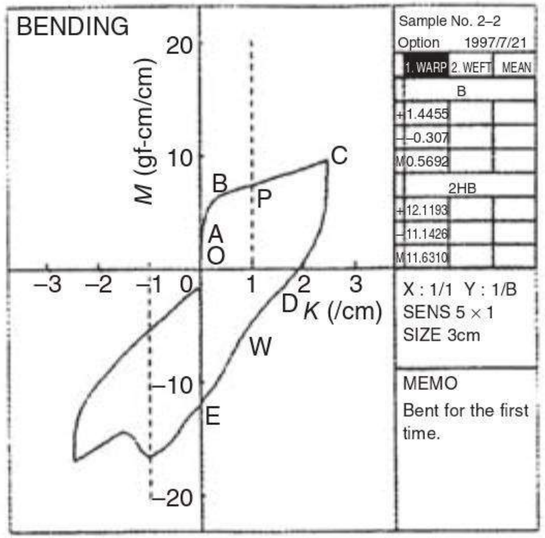

(c) Sample 1, warp-wise bending

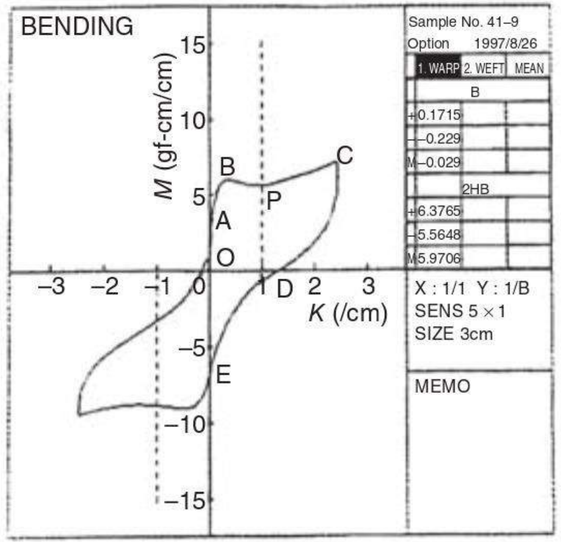

(d) Sample 2, weft-wise bending

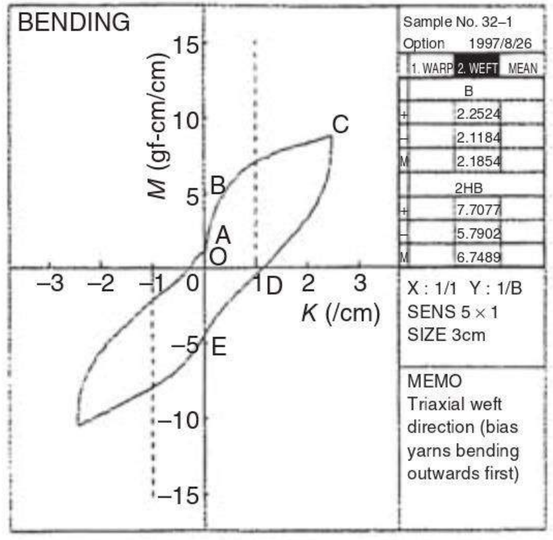

6.6 Typical bending hysteresis curves for MWK fabrics.

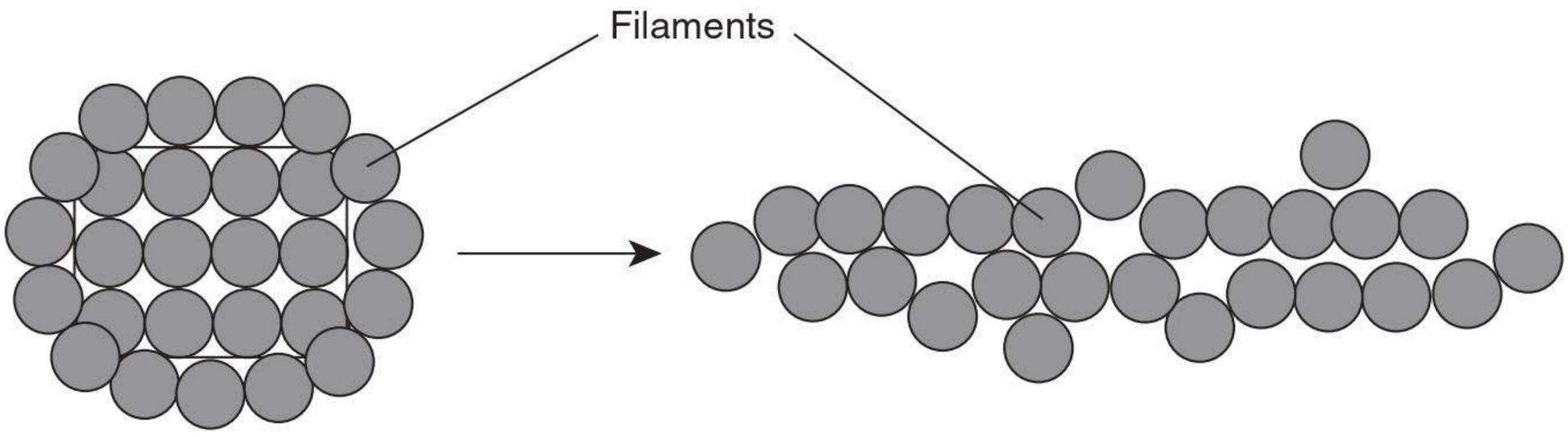

6.7 Spread of filaments in a bent yarn at the bending point.

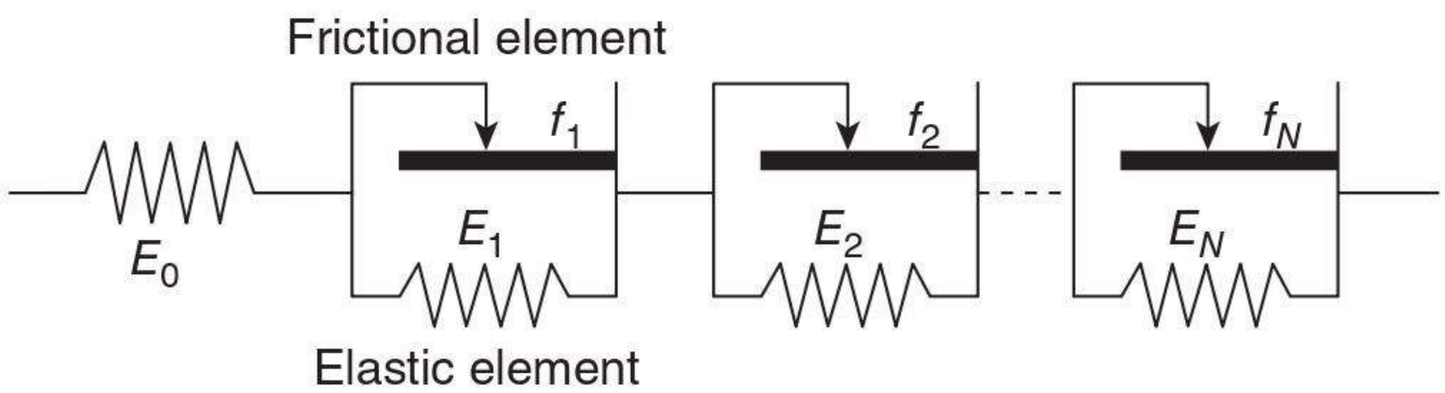

6.8 A modified Olofsson's model.

fabric parameters and different bending conditions. Here, observations show that point S is most interesting, where the inserting yarns being bent are still in a bent state even though the bending curvature here is zero. This will lead to the succeeding buckling phenomenon in segment DE (Fig. 6.6(a) and (b), point W), which will be analyzed in detail later.

As far as the bending process of segments OA and AB is concerned, a modified Olofsson's model of assembly of frictional and elastic elements may be applied here to give a clearer description. As shown in Fig. 6.8, an extra elastic element (E_0) is connected in series with the original model. The elements in Fig. 6.6 are arranged in the sequence below:

$$\sigma(E_0) < \sigma(f_1) < \sigma(f_2) < \ldots < \sigma(f_N), \quad E_0 > E_N > E_{N-1} > \ldots > E_2 > E_1$$

For segment OA, it is an elastic and static frictional bending, in which only E_0 takes effect and all frictional elements do not move. With the increase of bending curvature (from point A to point B), the frictional element f_1 first begins to move, then f_2, f_3, etc., till f_N. In this segment, however, the shape of the cross-section of inserting yarns hardly changes, which accounts for the good linearity of segment AB.

In Fig. 6.6(d), the curve is visibly different from the others, being more like the bending hysteresis curve of a plain weave (Fig. 6.1). The sample for Fig. 6.6(d) is triaxial warp-knitted fabric, LIBA type, in which the inserting yarns (except warp yarns) are penetrated randomly by the tricot loops. Compared with Karl Mayer type fabrics, the LIBA type fabric is a little

looser in structure. As a result, the frictional effect is less remarkable, which leads to the lower initial Young's modulus and comparatively regular shape of the bending hysteresis curve.

In summary, it can be seen from Fig. 6.6 that the shape of the bending hysteresis curves of an MWK fabric is quite like a 'dog's bone'.

6.4 Buckling of the bent-inserting yarns

The outstanding characteristic of the bending properties of MWK fabrics is the buckling of bent-inserting yarns, which can account for the special shape of segment DE in Fig. 6.6(a). This phenomenon is very complex and dependent on many factors, such as the yarn count, the interaction between the filaments (which is related to the surface finishing of the filaments) and the frictional effect between yarn systems, as well as the pressure exerted by the two clamps of the KES device.

For the curve in Fig. 6.6(a), the warp yarns do not become straight at point S, though the bending curvature here is zero. In Fig. 6.9, a schematic diagram of this state is illustrated. The buckles B_1, B_2 and B_3 are kept in their shapes by the frictional restraint resulting from the two clamps (C_1 and C_2) and the interaction between yarn systems. When the bending process reaches point D (where the bending moment becomes large enough to overcome the frictional restraint), the buckles will disappear suddenly, resulting in the sharp decrease in bending moment at point W. This may also account for the non-symmetry of the bending hysteresis curve to some degree.

6.5 Effect of bending sequence on bending hysteresis curves

According to experiments, it was found that when the bending direction keeps unchanged, the bending hysteresis curves present differences in terms of different bending sequences. This phenomenon is even more visible in biaxial warp-knitted fabrics. As shown in Fig. 6.10, two curves are obtained from sample 1, both being bent warp-wise but in inverse bending sequence.

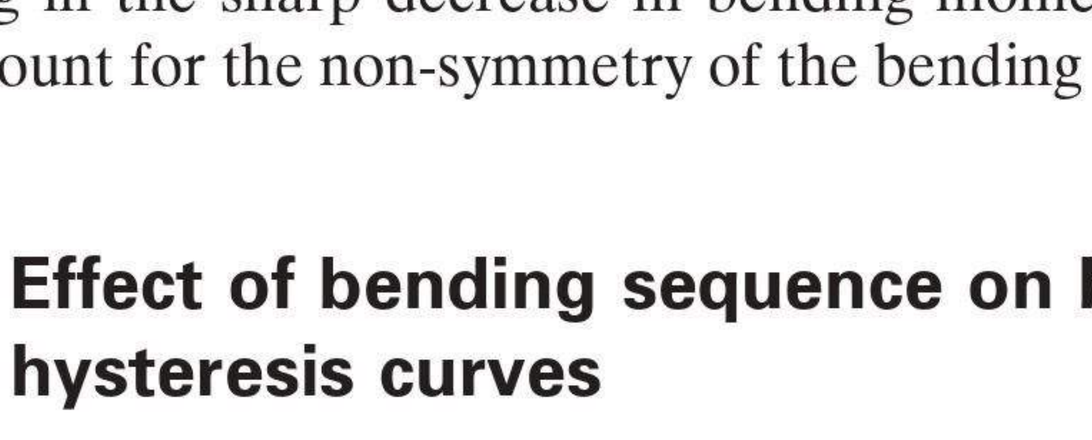

6.9 A schematic diagram of buckling (exaggerated).

(a) Sample 1, warp-wise bending
(Warp yarns are bent outwards first)

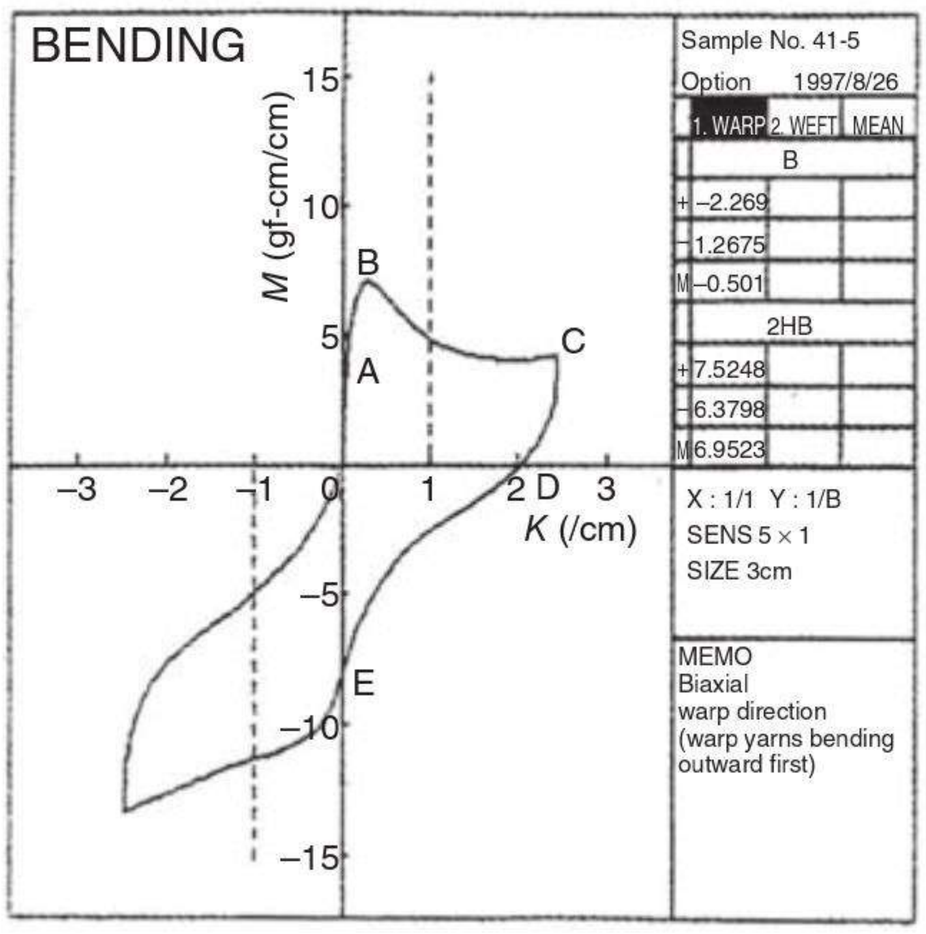

(b) Sample 1, warp-wise bending
(Warp yarns are bent inwards first)

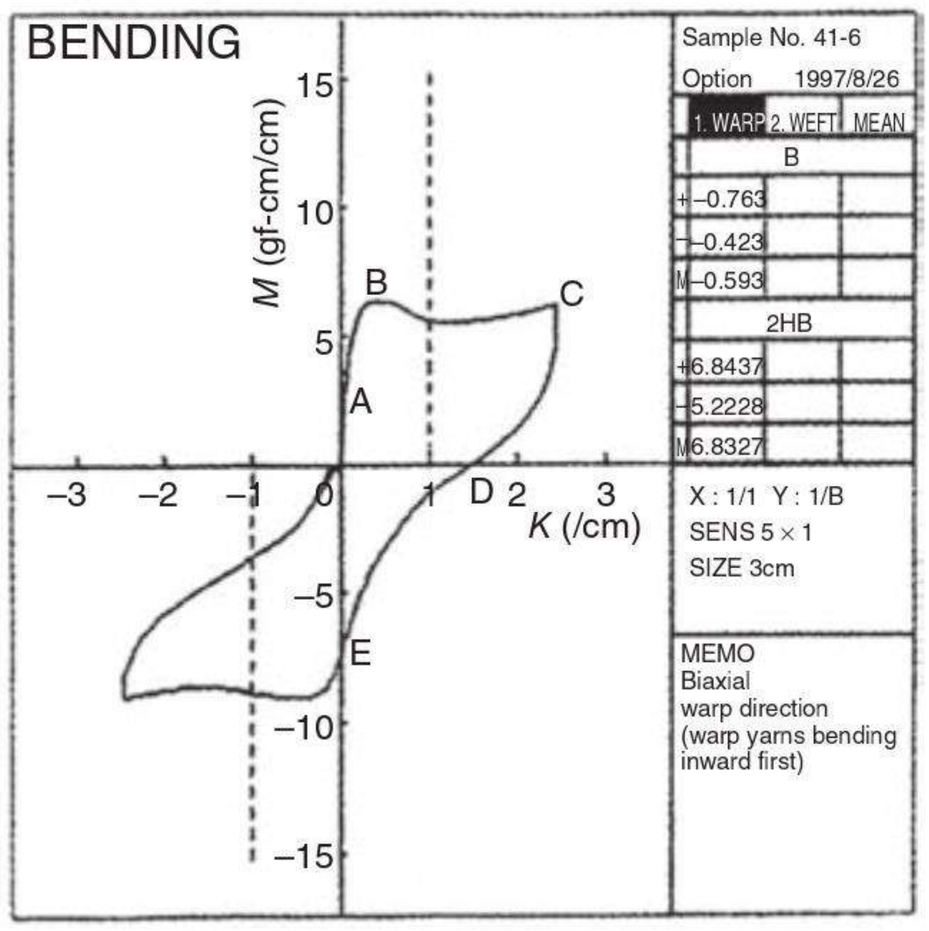

6.10 The effect of bending sequence on the bending hysteresis curves.

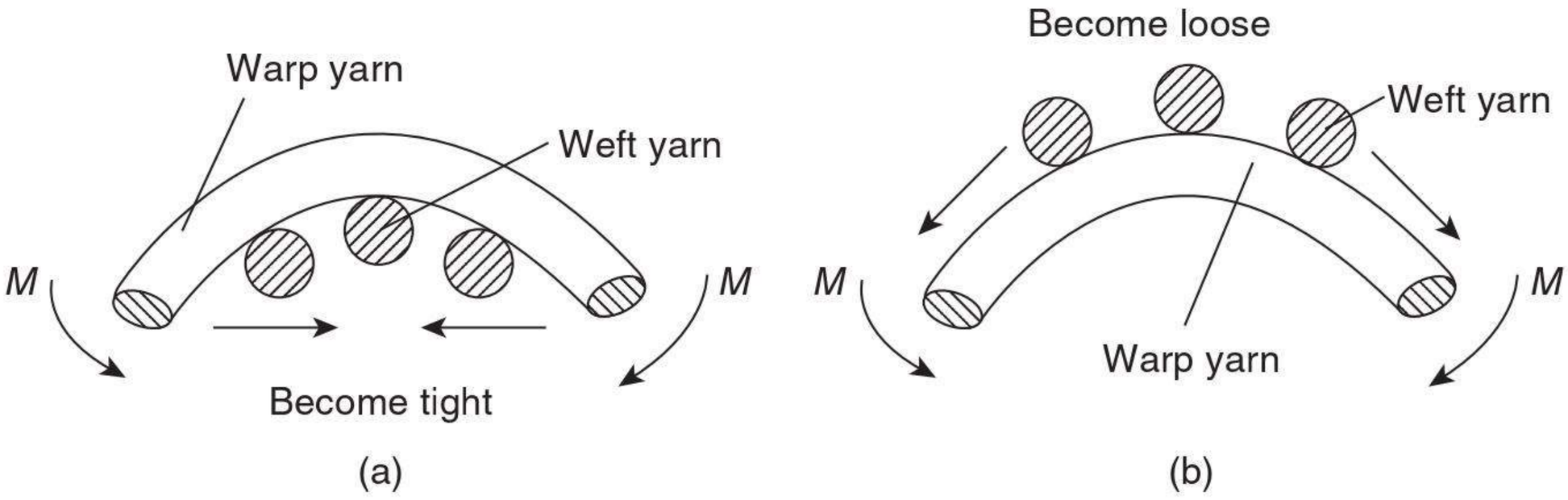

6.11 A schematic diagram of different bending sequences.

It can be noted that the two curves are different in shape, especially for segments BC and DE. This phenomenon may be explained by Fig. 6.11 as follows. It is the different frictional effect in Fig. 6.11(a) and (b), resulting from the different slippage of non-bent yarns, which leads to the different bending hysteresis curves. This must be considered in product design, especially in moulding. It should be pointed out that the slippage of inserting yarns depends on the size and density of tricot loops to a great degree.

6.6 Cyclic bending

Although the bending hysteresis curves of MWK fabrics look irregular and non-symmetrical, they tend to become regular and symmetrical after cyclic bending, as shown in Fig. 6.12. It can be deduced from these curves

(a) Bending for the first time

(b) Bending for the fourth time

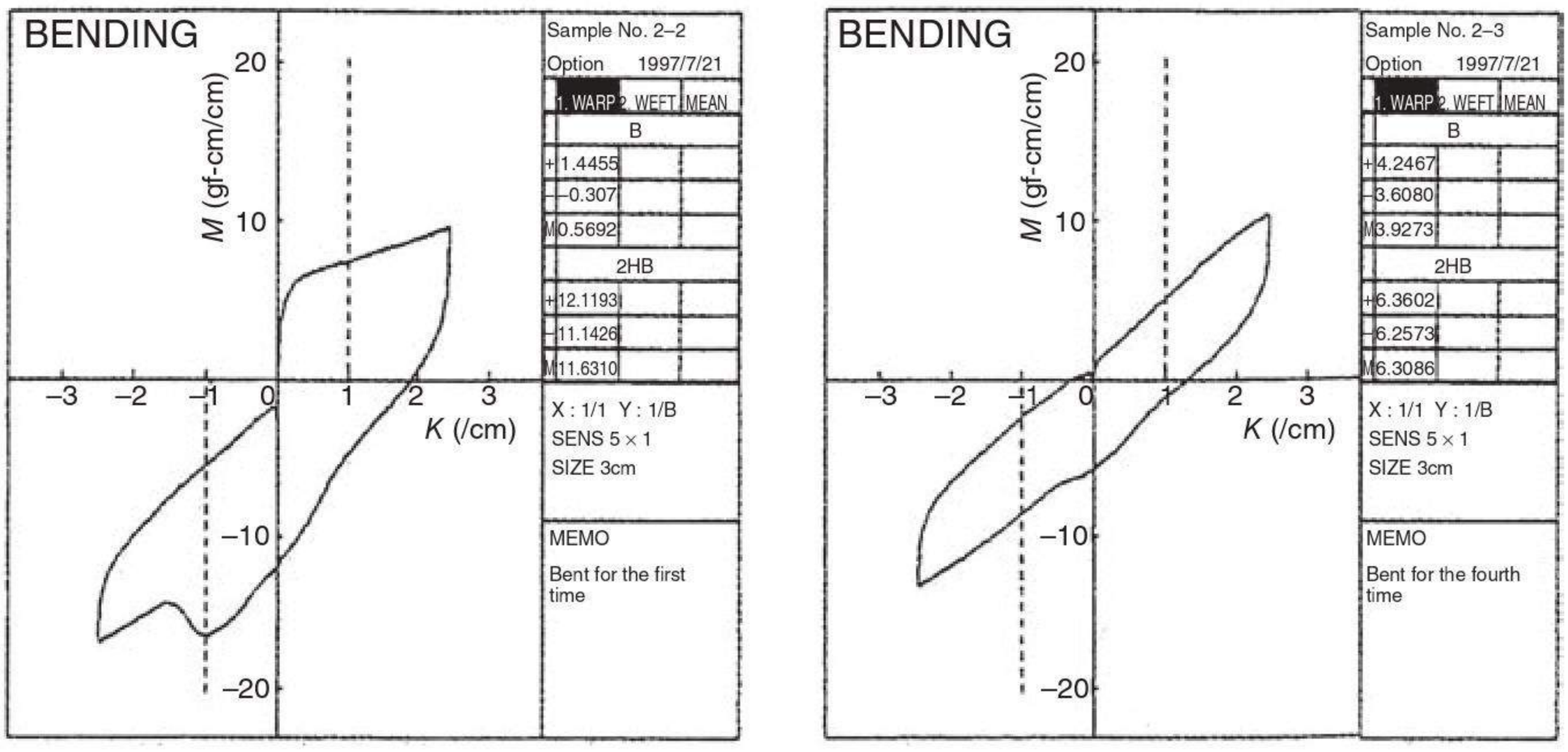

6.12 Sample 3, warp-wise bending.

that the final shape of the bending hysteresis curve of an MWK fabric is very close to a parallelogram, as shown in Fig. 6.12(b) (the broken lines). In fact, the static friction within an MWK fabric will become smaller and smaller, and the fabric structure will become looser and looser after cyclic bending.

As a result, the non-linear component will decrease and the buckling phenomenon will disappear. The final 'parallelogram' may be of more practical value, since it represents a relatively stable state quite different from the situation in the first bending which is easily influenced by contingent factors. From this point of view, the bending with unstable bending results can be regarded as 'mechanical conditioning'. How many cycles an MWK fabric will need to be mechanically conditioned obviously relates to the different structural parameters of the fabric, different yarn finishes and different yarn materials.

6.7 Modelling bending properties of multiaxial warp-knitted fabrics

From experimental observations, it is found that point A in Fig. 6.6(a) is produced by the spreading of glass filaments in inserting yarns at the bending point, as illustrated in Figure 6.7. However, to what degree the moment value at point A will go down with respect to the peak point P_o depends on different structures of MWK fabrics, although this kind of spreading occurs in all situations. Generally, the thicker the bent inserting

yarns are, the smaller the degree to which this spreading will influence the shape of the hysteresis curve, since the larger bending moment of the thicker yarns will be dominant in determining the magnitude of the final bending moment.

The other point (B) comes from the common contribution of both the aforesaid spreading of glass filaments and the buckling of bent inserting yarns, and the buckling phenomenon dominates the moment magnitude of point B to a great degree. This kind of buckling is illustrated in Fig. 6.9. Actually, when the bending process reaches point P, the fabric does not really become completely straight, despite the vanishing of bending curvature at this point. The buckles B_1, B_2, and B_3 keep their shapes from the frictional restraint in the two clamps (C_1 and C_2) and the interaction of the yarn systems. After point P, when the bending moment becomes large enough to overcome this frictional restraint, the buckles disappear suddenly at point B, which may account for the sharp decrease of bending moment at this point.

The main concern in this chapter is to establish a predictive model for assessing the bending behaviour of MWK fabrics. As the analysis above shows, it is very difficult to consider both the spreading and buckling phenomena in the model. Fortunately, however, the bending behaviour of a single inserting yarn is quite analogous to that of an MWK fabric, which also shows the two special characteristics – the spreading of glass filaments and the buckling phenomenon – as shown in Fig. 6.13.

Based on the previous discussion, according to the experimental results from the bending of single inserting yarns and the structural parameters of the fabric, we have developed a predictive model for calculating the entire bending hysteresis curve of an MWK fabric being bent in an arbitrary direction, using the following notation:

1 = warp yarn
2 = weft yarn
3 = bias yarn ($+\theta_0$)
4 = bias yarn ($-\theta_0$)
K = bending curvature of the fabric, /cm
K_i = bending curvature of an inserting yarn system (i = 1–4), /cm
L_0 = sample length, cm
M = bending moment exerted on the fabric, gf·cm/cm
M_i = bending moment exerted on a single inserting yarn (i = 1–4), gf·cm
$M_L(K)$ = bending moment of the stitching system, gf (gram force)·cm/cm
$M_S(K)$ = frictional moment between yarn systems, gf·cm/cm
n_i = number of yarns per unit length of fabric along direction perpendicular to corresponding yarn's axis (i = 1–4), /cm

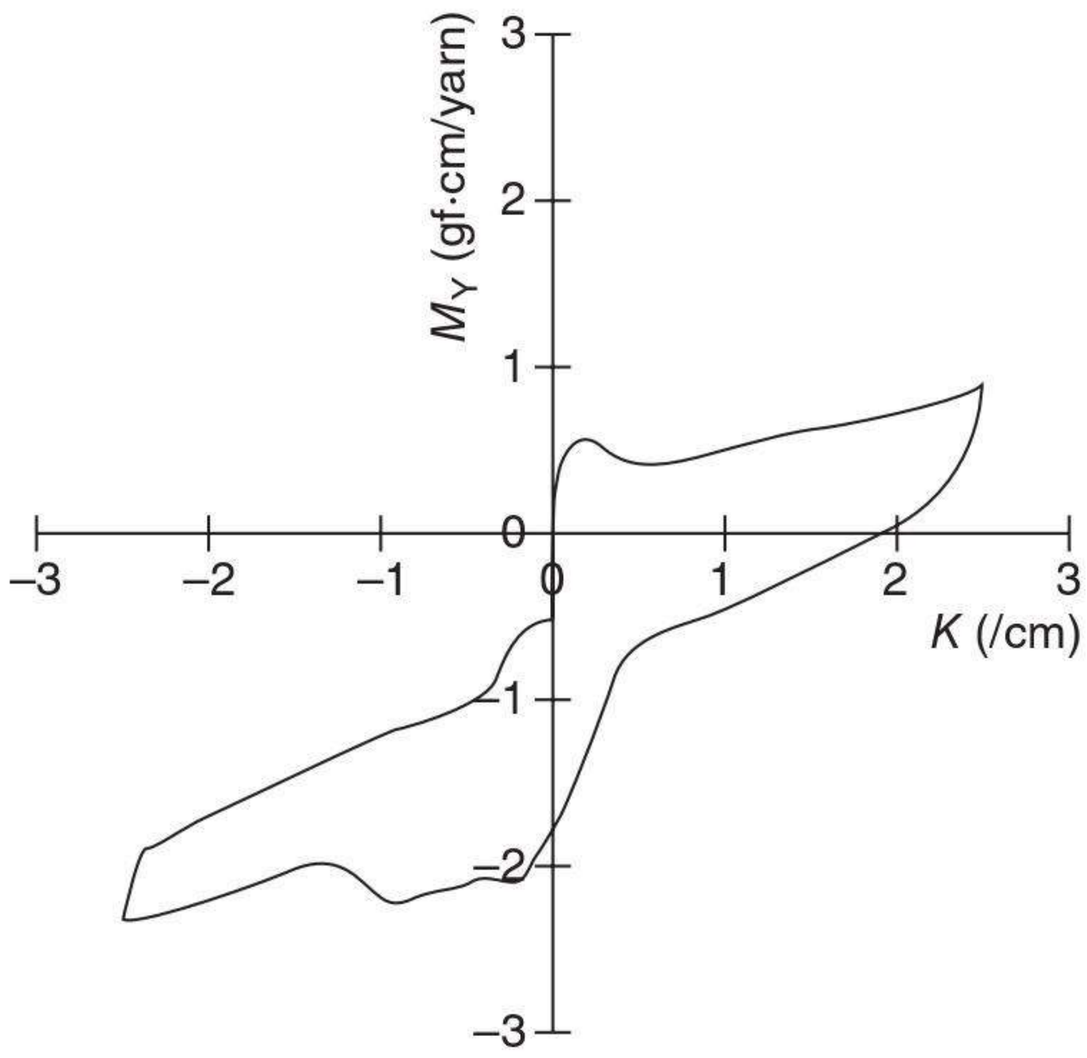

6.13 Typical bending hysteresis curve of a single glass filament yarn (900 Tex).

n'_i = number of yarns per unit length of fabric along direction perpendicular to bending moment direction (i = 1–4), /cm
W_0 = sample width, cm
θ = clockwise angle from bending moment direction to warp yarn axis
$\pm\theta_0$ = angle between bias yarn axis and warp yarn axis (the plus sign represents the angle from the warp yarn axis to the bias yarn axis along the clockwise direction, and the minus indicates the counterclockwise direction)

As far as the bending properties of fabrics are concerned, perhaps the biggest difficulty in modelling is the introduction of frictional restraint, which should account for most of the deviation. To model the bending behaviour of plain weaves, two methods are available to determine the frictional restraint: one is the cantilever method (Grosberg and Swani, 1966), which requires many experiments and is therefore tedious, and the other is the parallel plates method (Grosberg, 1966), which requires the frictional coefficient μ and the internal pressure force V. From the viewpoint of practical application, neither method can be readily applied. For MWK fabrics with glass filament yarns as inserting systems, the frictional restraint can be separated into two components: the frictional interaction between glass filaments within single inserting yarns, and the frictional interaction between yarn systems. The first component has been contained in our model. For the second, it is reasonable to ignore the acceptable deviation as far as our model is concerned. The modelling is described in the foregoing section.

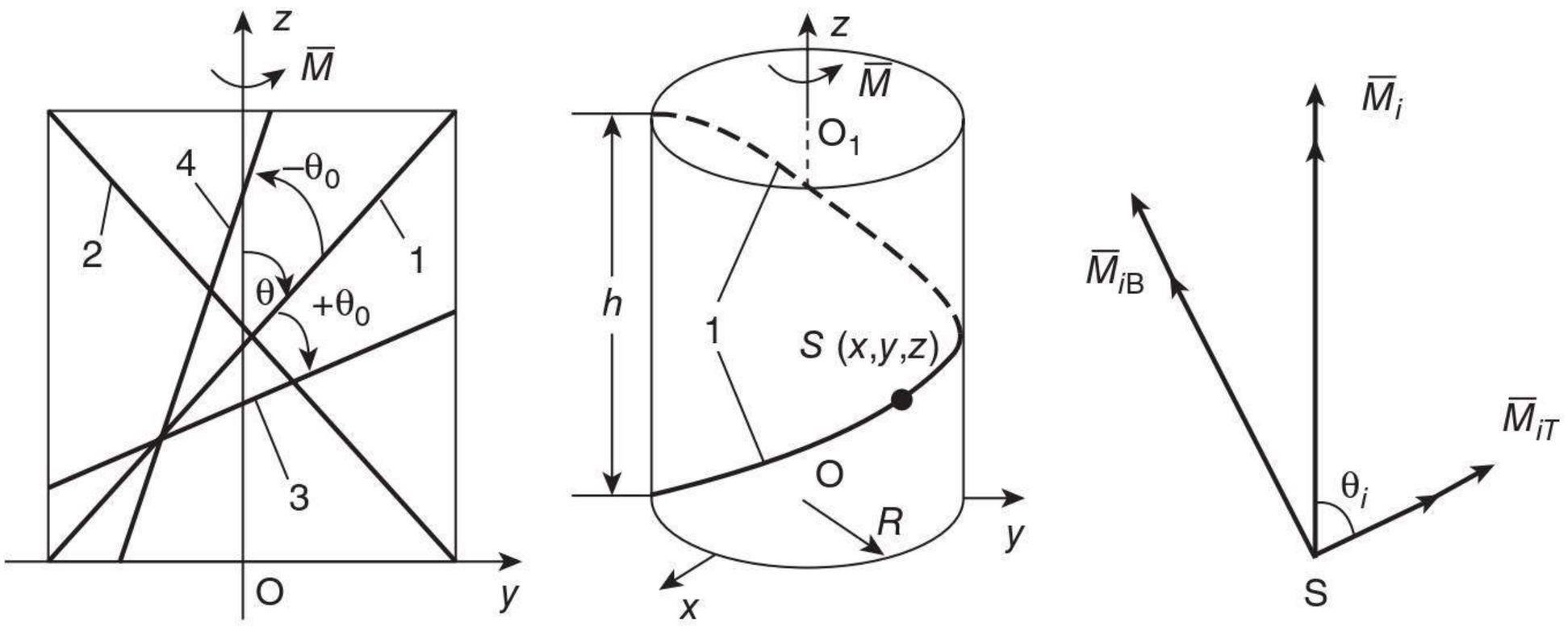

6.14 Bending of an MWK fabric along an arbitrary direction.

From Fig. 6.6, it is obvious that when an MWK fabric is bent along an arbitrary direction, the inserting yarns non-orthogonal to the bending moment direction will undergo both bending and torsional moment. According to our experimental study and mathematical analysis, the bending path of these yarns follows a cylindrical helix, as illustrated in Fig. 6.14. The parametric equation of the cylindrical helix can be written as:

$$S(x, y, z): \begin{cases} x = R\cos t \\ y = R\sin t \\ z = Ct \end{cases} \tag{6.1}$$

where C is a constant and t is the parameter. Using Equation 6.1, we can obtain two other equations:

$$\tan(\pi/2 - \theta) = h/(2\pi R) \tag{6.2}$$

and

$$C = h/2\pi \tag{6.3}$$

From Equations 6.2 and 6.3 we have:

$$C = R\tan^{-1}\theta \tag{6.4}$$

According to Equations 6.1 and 6.4, the curvature of an arbitrary point S on the helix can be obtained as follows:

$$K_S = \sqrt{\frac{(\dot{x}^2 + \dot{y}^2 + \dot{z}^2)(\ddot{x}^2 + \ddot{y}^2 + \ddot{z}^2) - (\dot{x}\ddot{x} + \dot{y}\ddot{y} + \dot{z}\ddot{z})}{(\dot{x}^2 + \dot{y}^2 + \dot{z}^2)^3}} = \frac{\sin^2\theta}{R} \tag{6.5}$$

Based on the mathematical derivation above, we have

$$K_i = K\sin^2\theta_i \quad (i = 1, 2, 3, 4) \tag{6.6}$$

where

$$K = \frac{1}{R}, \quad \theta_1 = \theta, \quad \theta_2 = \theta + \frac{\pi}{2},$$
$$\theta_3 = \theta + \theta_0, \quad \theta_4 = \theta - \theta_0. \tag{6.7}$$

In addition, the bending moment exerted on a single yarn can be decomposed into two components – the bending moment $M_{i\mathrm{R}}$ and the torsional moment $M_{i\mathrm{T}}$ (Fig. 6.14):

$$\begin{aligned} M_{i\mathrm{R}} &= M_i \sin\theta_i \\ M_{i\mathrm{T}} &= M_i \cos\theta_i \end{aligned} \quad (i = 1\text{–}4) \tag{6.8}$$

From Equation 6.8, the magnitude of the moment exerted on a single inserting yarn can be calculated as

$$M_i = \frac{M_{i\mathrm{B}}}{\sin\theta_i} \tag{6.9}$$

Figure 6.15 illustrates how a sample fabric is clamped in KES testing. For convenience, only warp yarns are drawn here.

It is very easy to derive the relationship between n_i and n_i' from Fig. 6.15:

$$n_i' = n_i \sin\theta_i \tag{6.10}$$

Also, the effective bending length should be the length of PQ, which relates to the corresponding inserting yarn system. Here 'effective' means that both ends of the inserting yarns being bent are held by the clamps. PQ can be obtained from Equation 6.11 as follows:

$$|\mathrm{PQ}|_i = L_0 - W_0 |\tan^{-1}\theta_i| \tag{6.11}$$

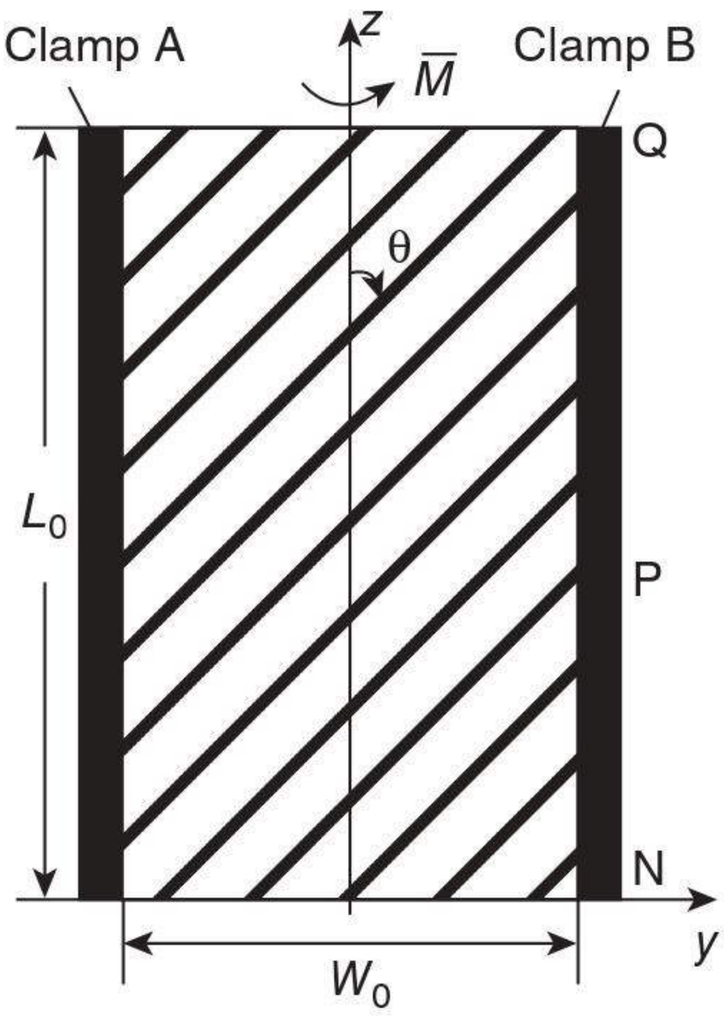

6.15 Illustration of a clamped sample fabric.

Table 6.1 Specifications of samples ($\theta_0 = 45°$)

Direction	Tex	n_i
Warp – 1	900	4.6
Weft – 2	70	2.5
Bias (+45°) – 3	300	6.8
Bias (–45°) – 4	300	6.8
Tricot loops – 5	9	5

According to Equations 6.9, 6.10, and 6.11, the bending moment exerted on an MWK fabric can be calculated as:

$$M = \sum_{i=1}^{4} n_i' M_i \frac{|\mathrm{PQ}|_i}{L_0} + M_\mathrm{S}(K) + M_\mathrm{L}(K) \tag{6.12}$$

Equation 6.12 can be rewritten as Equation 6.13:

$$M = \sum_{i=1}^{4} n_i M_{i\mathrm{R}}\left(1 - \lambda\left|\tan^{-1}\theta_i\right|\right) + M_\mathrm{S}(K) + M_\mathrm{L}(K), \quad \lambda = \frac{W_0}{L_0} \tag{6.13}$$

We tested the sample fabrics (Fig. 6.4(b)) along four bending directions (warp, weft and bias $\pm\theta_0$) on the KES-FB-2. The specifications of samples used in our research are listed in Table 6.1, and the sample size is 3 cm (L_0) $\times$ 1 cm (W_0). We also tested the bending behaviour of single inserting yarns at the same time. Fig. 6.16 presents three sets of bending hysteresis curves obtained on KES. Here, only the bias +45° bending is given, since the other bias bending (–45°) is analogous.

6.8 Model validation

As far as the model given by Equation 6.13 is concerned, the most difficult term to determine is $M_\mathrm{S}(K)$, which denotes the frictional restraint between yarn systems. As analyzed earlier, this kind of restraint is very complex and relates to many parameters, such as the number of inserting systems, the density and pattern of the stitching system, the inserting yarn count, the finishing of glass filaments, and the bending direction. Actually, it is very difficult to represent $M_\mathrm{S}(K)$ directly by an analytical function with an acceptable deviation. The term $M_\mathrm{S}(K)$, however, can be neglected to a great degree as far as a relatively open MWK structure is concerned, and the open condition is basically always satisfied by MWK fabrics in view of their industrial applications. Furthermore, it is clear from Fig. 6.17 that the model without $M_\mathrm{S}(K)$ is in good agreement with the experiments.

The other term to consider is $M_\mathrm{L}(K)$, which denotes the bending of the stitching system. Since the stitching yarns are much finer than the inserting yarns, $M_\mathrm{L}(K)$ can also be neglected in order to simplify the predictive

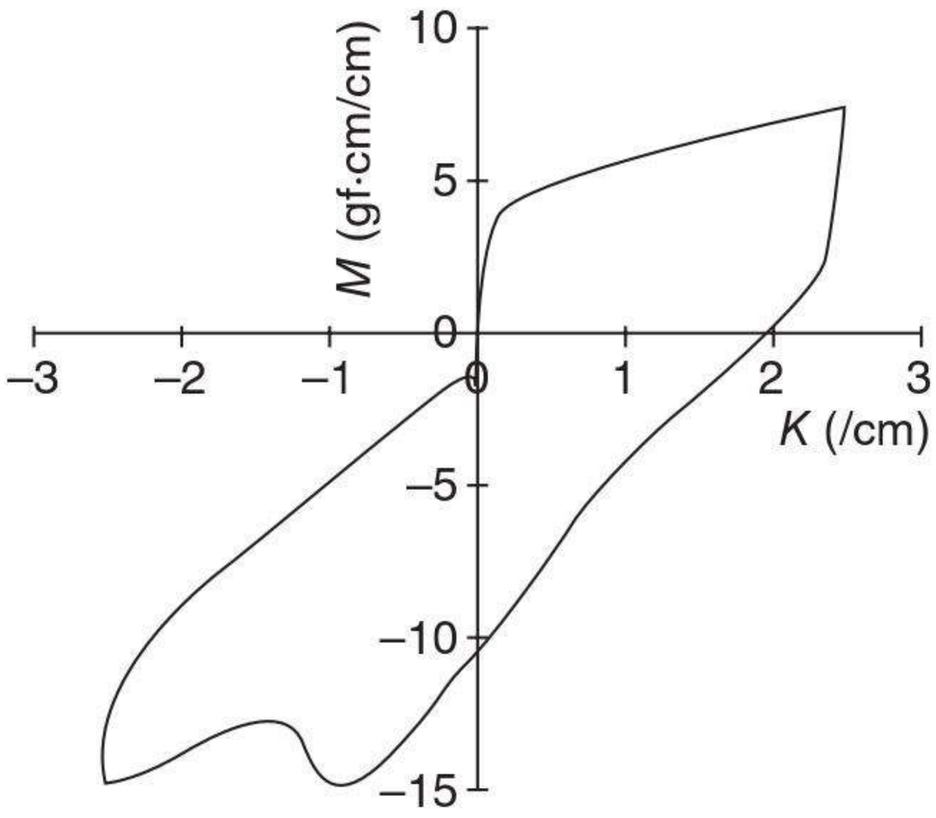

(a1) Warp-wise bending of the fabric

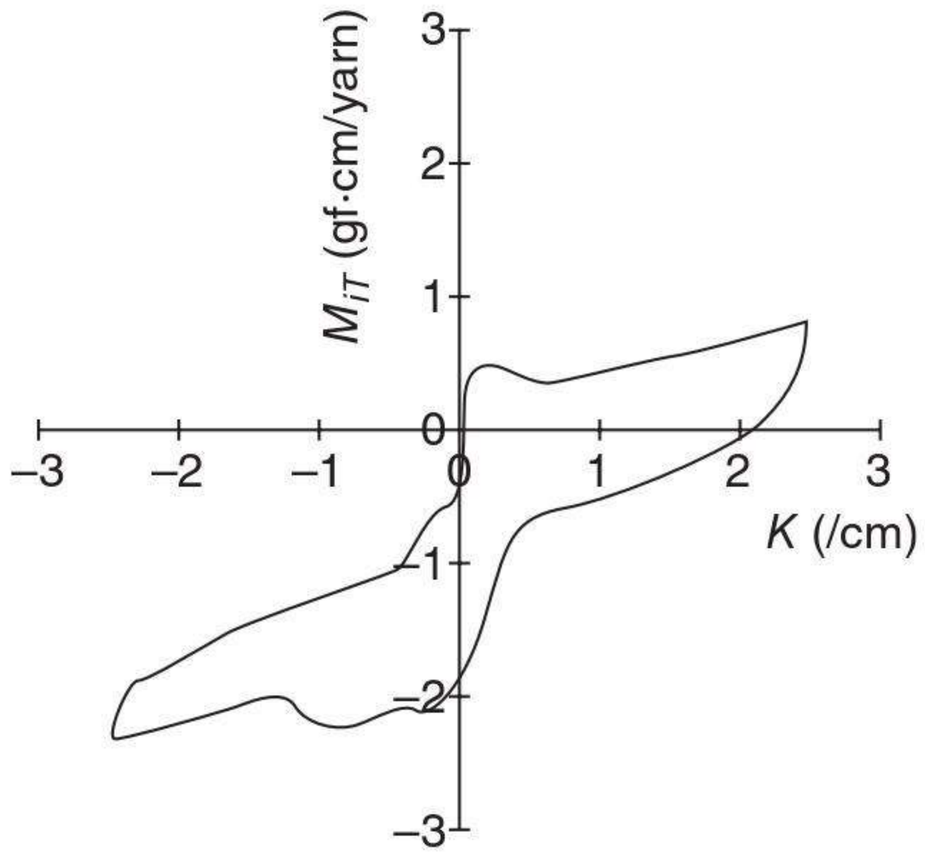

(a2) Bending of a single warp yarn

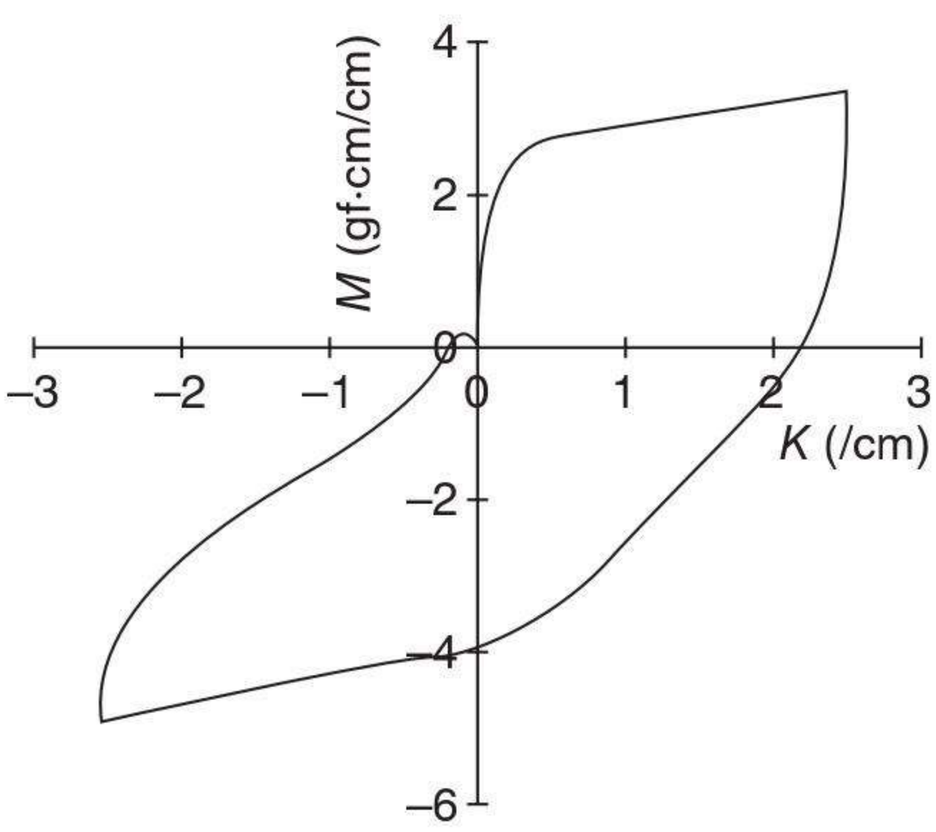

(b1) Weft-wise bending of the fabric

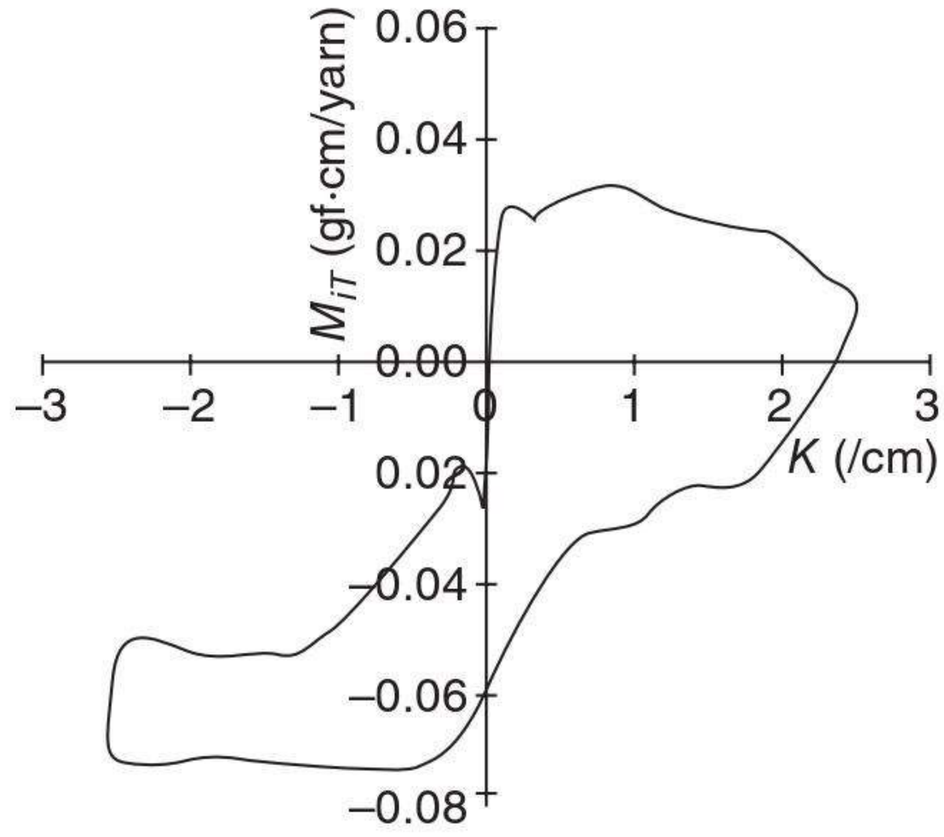

(b2) Bending of a single weft yarn

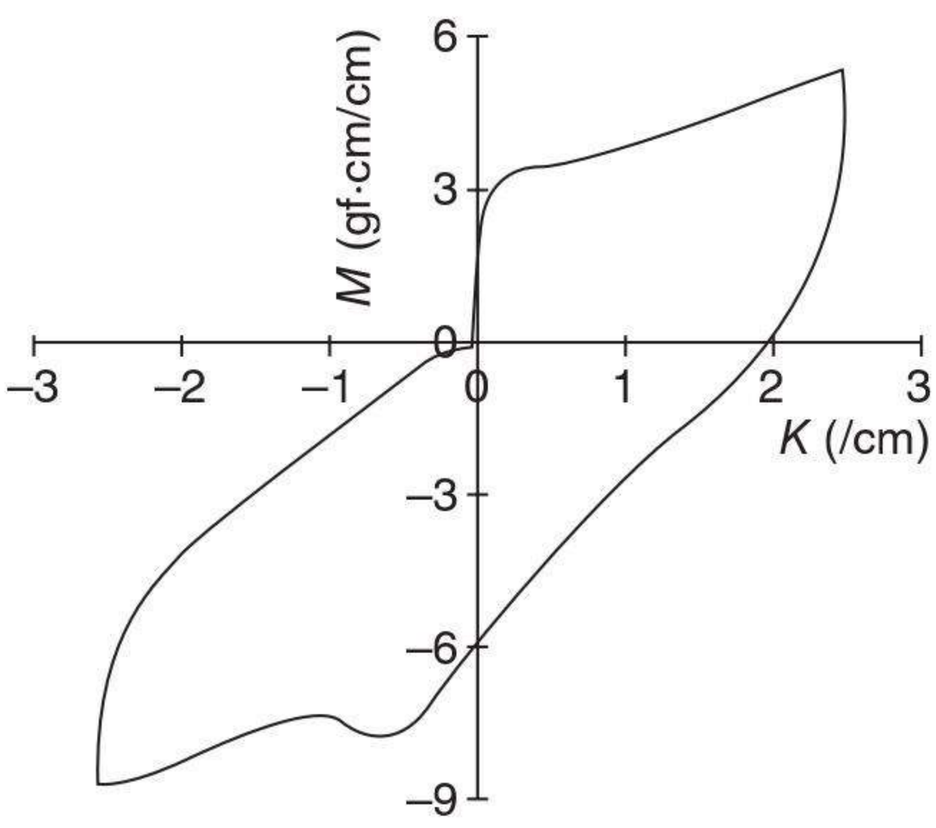

(c1) Bias-wise bending (+ 45°) of the fabric

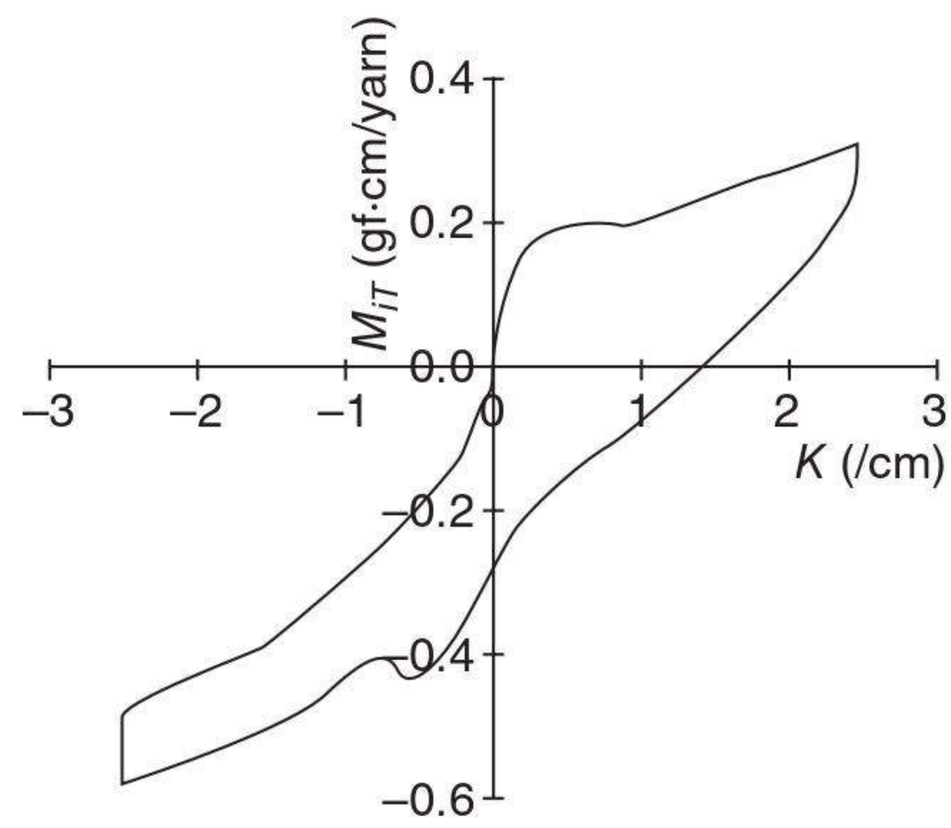

(c2) Bending of a single bias yarn (+ 45°)

6.16 Experimental bending hysteresis curves of an MWK fabric and its single inserting yarns.

model. Of course, this term can be introduced very easily only if the bending properties of the stitching system are tested.

According to the analysis above, Equation 6.13 can be simplified into the form of Equation 6.14 as:

$$M = \sum_{i=1}^{4} n_i M_{i\mathrm{B}}\left(1 - \lambda\left|\tan^{-1}\theta_i\right|\right), \quad \lambda = \frac{W_0}{L_0} \qquad 6.14$$

Based on Equation 6.14, calculations are made along three bending directions (warp-wise, weft-wise and bias-wise ($+\theta_0$)). The comparison of the calculated results and experimental data is given in Fig. 6.17, which shows that the model set forth earlier (Equation 6.13) is in good agreement with the experiments.

6.9 Conclusions

This chapter presents the bending properties of MWK fabrics and their modelling to describe the bending behaviour. The bending properties of MWK fabrics are quite different from those of traditional wovens and apparel materials, and the bending hysteresis curves are not only irregular but non-symmetrical. This presents more complexity and variability. The bending process involves both the slippage of non-bent-inserting yarns and the buckling of bent-inserting yarns, and different bending sequences will lead to different bending hysteresis curves. The shape of the bending hysteresis curve is liable to be affected by many factors, which leads to difficulty in modelling. Generally, the bending hysteresis curve of an MWK fabric obtained in the first bending cycle is quite like a 'dog's bone' and close to a parallelogram after cyclic bending. As far as the frictional restraint between inserting yarn systems is concerned, it is more difficult to determine even if the frictional coefficient (which should be some function of the frictional direction) between the glass filament yarns can be obtained. Actually, this kind of frictional restraint may not be represented directly by an analytical function, but it can be ignored to a great degree as far as a basic estimation is concerned, which seems reasonable from Fig. 6.17.

The following conclusions can be drawn from this chapter. The bending process of MWK fabrics involves two special deformation phenomena, i.e. spreading of the glass filaments in inserting yarns and buckling of inserting yarns being bent. The spreading and buckling of single inserting yarns can reflect those of an MWK fabric consisting of these yarns. The bending path of a non-orthogonally bent inserting yarn follows a cylindrical helix. The frictional restraint between yarn systems can be ignored to a great degree for a basic estimation of the bending behaviour of MWK fabrics. The whole bending hysteresis curve of an MWK fabric being bent in an arbitrary

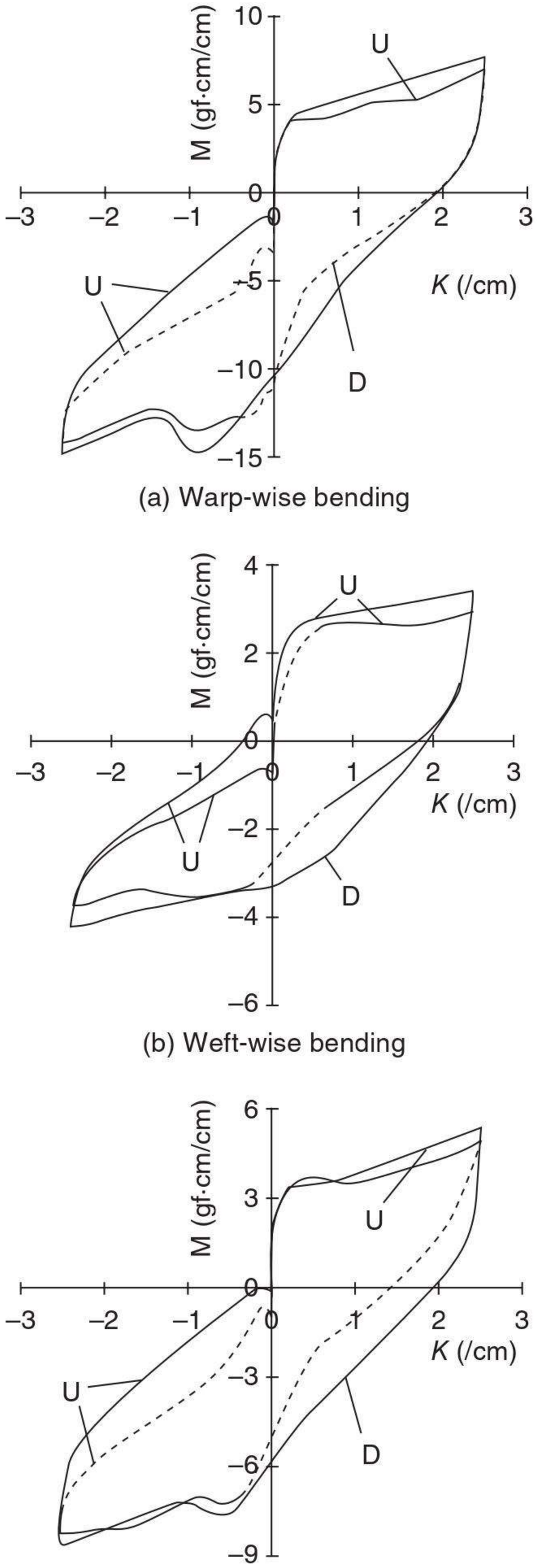

(a) Warp-wise bending

(b) Weft-wise bending

(c) Bias-wise bending (+θ)

6.17 Comparison of calculated results and experimental data.

direction can be calculated through the model established in this chapter. The prediction seems consistently off in the unloading portion of the bending hysteresis curves, which could be improved by including the frictional component.

6.10 References

Brown III P R, Buchanan D R and Clapp T G (1990), Large deflection bending of woven fabric for automated material handling, *Journal of the Textile Institute*, **81**, 1.

Chen P L, Barker R L, Smith G W and Scruggs B (1992), Handle of weft knit fabrics, *Textile Research Journal*, **83**, 200–210.

Clapp T G and Peng H (1991), A comparison of linear and non-linear bending methods for predicting fabric deformation in automated handling, *Journal of the Textile Institute,* **82**, 341.

Cooper D N E (1960), The stiffness of woven textiles, *Journal of the Textile Institute*, **51**, T317.

Davies I and Owen J D (1971), The bending behaviour of warp-knitted fabrics, *Journal of the Textile Institute*, **6**, 42, 181.

Delaney P (1981a), The bending properties of some plain and twill weave wool fabrics, *SAWTRI Tech. Rep. no. 480*, September.

Delaney P (1981b), The bending properties of some punto-di-roma wool fabrics, *SAWTRI Tech. Rep. no. 489*, November.

Du G-W and Ko F (1996), Analysis of multiaxial warp-knit preforms for composite reinforcement, *Composites Science and Technology*, **56**, 3, 253–260.

Gaucher M L and King M W (1983), Predicting the drape coefficient of knitted fabrics, *Textile Research Journal*, **53**, 297–303.

Gibson V L and Postle R (1978), An analysis of the bending and shear properties of woven, double-knitted, and warp-knitted outerwear fabrics, *Textile Research Journal*, **48**, 14.

Grosberg P (1966), The mechanical properties of woven fabrics, Part II: The bending of woven fabrics, *Textile Research Journal*, **36**, 205.

Grosberg P and Swani N M (1966), The mechanical properties of woven fabrics, Part III: The buckling of woven fabrics; Part IV: The determination of the bending rigidity and frictional restraint in woven fabrics, *Textile Research Journal*, **36**, 332, 338.

Kawabata S (1980), *The Standardization and Analysis of Hand Evaluation* (2nd edn), Textile Machinery Society of Japan, Osaka.

Ko F K, Pastore C, Yang J M and Chou T W (1986), Structure and properties of multilayer multidirectional warp knit fabric reinforced composites, in *Proc. 3rd US–Japan Conf. on Composites*, Tokyo, 21–28.

Livesey R G and Owen J D (1964), Cloth stiffness and hysteresis in bending, *Journal of the Textile Institute,* **55**, T516.

Owen J D (1968), The bending behaviour of plain-weave fabrics woven from spun yarns, *Journal of the Textile Institute*, **5**, 3, 391.

Vigo T L and Turbak A F (1991), *High-tech Fibrous Materials: Composites, Biomedical Materials, Protective Clothing, and Geotextiles*, American Chemical Society, Washington, DC, 81–89.